

1 **Response to reviewers for “Secondary organic aerosol formation from in situ OH, O₃, and NO₃**
2 **oxidation of ambient pine forest air in an oxidation flow reactor.”**

3 **B. B. Palm, J. L. Jimenez, et al.**

4 We thank the reviewers for their comments on our paper. To facilitate the review process we have
5 copied the reviewer comments in black text. Our responses are in regular blue font. We have responded
6 to all the referee comments and made alterations to our paper (in bold text).

7 **Anonymous Referee #1**

8 Overview

9 R1.0. This well-written and impressive manuscript summarizes oxidation flow reactor (OFR) experiments
10 aimed at studying in situ SOA formation from ambient pine forest air during the BEACHON-ROMBAS
11 campaign after oxidation by OH, O₃, and NO₃ radicals. Since SOA formation was measured semi-
12 continuously during this study, the authors were able to capture diurnal and daily changes. More SOA
13 was formed from precursors present in nighttime air than in the daytime air for all 3 oxidations.
14 Interestingly, OH oxidation produced ~ 4 times more SOA than NO₃ and O₃ oxidation at all times of day.
15 O:C and H:C ratios of the SOA formed by O₃, NO₃ and several eq. hours of OH oxidation yielded similar
16 oxidation levels of ambient organic aerosol (OA). The authors previously demonstrated that ambient
17 VOC concentrations alone could not explain the amount of SOA formed in the OFR by OH oxidation. This
18 behavior was likely due to SOA being formed from semivolatile/intermediate volatility organic
19 compounds (S/IVOCs) that entered the OFR. However, for SOA formed from O₃ and NO₃ oxidation, the
20 measured VOCs were found in the present study to be sufficient in explaining the amount of SOA
21 formed in the OFR. More specifically, this means that for O₃ and NO₃ oxidation of ambient S/IVOCs does
22 not yield appreciable SOA amounts. The difference between the OH and O₃/NO₃ OFR experiments
23 provides some support for their hypothesis that ambient S/IVOCs generally lacking double bonds in their
24 structures (especially since double bonds in VOCs emitted upwind of the site are likely already oxidized
25 before they enter the OFR). Using ambient mixtures in this study provides important insights into SOA
26 formation potential and chemical evolution in the real atmosphere, and thus, this work will be of high
27 interest to the larger atmospheric chemistry community. I only have a few minor comments below that I
28 kindly ask the authors to address before publication. As a result, I recommend that this manuscript be
29 accepted with minor revisions noted below.

30 R1.1. My biggest comment is related to timescales in the OFR for multi-phase chemical processes. Since
31 the authors appear to justify that their OFR experiments can produce similar oxidation states (O:C
32 ratios) in OA found in the atmosphere, my question is this a result of the "correct" processes that
33 actually occur in the atmosphere? Besides for heterogeneous oxidation (through OH oxidation), what
34 about aqueous-phase processes such as accretion or decomposition reactions of epoxides and or
35 hydroperoxides? There is a lot of work published now by the Caltech, UNC, Oberlin College, and other
36 groups that have shown epoxides are really important in aqueous-phase chemical processes. Recently,
37 the Harvard (Martin) and UNC groups have shown that multi-phase chemical reactions of
38 hydroperoxides could be important as well (Liu et al., 2016, PCCP; Riva et al., 2017, Atmos. Environ.).
39 There is evidence from this site that even MBO oxidation products can undergo aqueous-phase
40 reactions within aerosol to yield organosulfates (Zhang et al., 2012, ES&T). I'm not sure authors can
41 really address this issue now, but I think some discussion needs to be included that acknowledges that

42 these processes may explain some part of ambient oxidation states, which can't be reflected on the
43 reaction timescales of the OFR.

44 We thank the reviewer for pointing out this caveat. We have included the following text as a new
45 paragraph starting after page 16, line 22:

46 **“While these two vectors describe the possible oxidation processes in the OFR, there may be other**
47 **vectors (e.g., from condensed phase chemistry or reactive uptake) occurring in the atmosphere. As**
48 **documented in Hu et al. (2016), SOA formation processes that require reactive uptake or within-**
49 **particle non-radical chemistry (such as uptake of isoprene epoxydiols to form IEPOX-SOA) on time**
50 **scales longer than the several minute residence time in the OFR are not captured with the OFR**
51 **method used in this work. This is because the rate of reactive uptake and non-radical particle-phase**
52 **chemistry do not speed up proportionally to increased OH and HO₂ (or O₃ or NO₃). However, to our**
53 **knowledge the only precursor for which reactive uptake of epoxides has been shown to be a major**
54 **pathway is isoprene, which was a very minor precursor at this site (Karl et al., 2012). The formation of**
55 **epoxides during MBO oxidation has been proposed to play a role during BEACHON-RoMBAS (Zhang**
56 **et al., 2012). However, recent results suggest that formation of epoxides during MBO oxidation is not**
57 **important in the atmosphere (Knap et al., 2016). Thus, at this time it is not clear whether any**
58 **important SOA-forming processes in this environment are missed by the OFR setup, and this question**
59 **should be investigated in future studies.”**

60 R1.2. In section 2.2 of the experimental methods section, can the authors provide more information or
61 clarify on how the ambient might or might not change upon entering the OFR? Specifically, is it drier in
62 the OFR compared to the ambient RH? If the RHs aren't the same, how might this affect the
63 interpretation of the results?

64 To address this comment, we have added the following text to the experimental methods section at
65 page 5, line 16:

66 **“The OFR was located on top of the measurement trailer in order to sample ambient air directly**
67 **without using an inlet. Therefore the temperature and RH inside the OFR were the same as ambient**
68 **conditions, with the exception of minor heating from the UV lamps mounted inside the OH-OFR (up to**
69 **~2°C heating at the highest lamp settings, and ~0.5°C at the settings producing the most SOA; Li et al.,**
70 **2015). No heating occurred during O₃ or NO₃ modes. Thus RH within the OFR was the same or slightly**
71 **lower than ambient, depending on the operating mode.”**

72 R1.3. I'm curious if the authors know how hydroperoxides behave in their OFR? Do they photolyze quite
73 easily due to the UV radiation you are using? How might this affect the interpretation of the results?

74 Non-OH chemistry, such as photolysis of hydroperoxides, has indeed been investigated via modeling in
75 Peng et al. (2016). That investigation concluded that for a wide variety of gases and for OH-OFR
76 conditions in BEACHON-RoMBAS, reactions with OH dominated over other possible reactions, including
77 O(¹D), O(³P), O₃, and photolysis at 185 nm or 254 nm. This was also the case for OH oxidation at other
78 field campaigns where ambient air was oxidized in the OFR. Peng et al. (2016) illustrated that non-OH
79 reactions can become significant under certain circumstances, such as very low RH, high external OH
80 reactivity, or when the gases involved are particularly reactive towards a non-OH pathway. However,
81 these conditions are more commonly found in laboratory studies, where they can also be avoided by

82 carefully designing such experiments. Peng et al. (2016) also investigated photolysis of SOA, and found
83 that while photolysis could affect a small but non-negligible percentage of SOA, photolysis of SOA across
84 the lifetime of particles in the atmosphere would play a much larger role.

85 To address this comment, we have moved the sentence “The gas-phase HO_x/O_x chemistry inside the OFR
86 has also been investigated with kinetic modeling (Li et al., 2015; Peng et al., 2015, 2016).” from page 5,
87 lines 12-13, to page 5, line 25, and altered it to read:

88 **“The gas-phase HO_x/O_x chemistry and possible non-OH chemistry inside the OFR was investigated**
89 **with kinetic modeling (Li et al., 2015; Peng et al., 2015, 2016). For the wide variety of compounds**
90 **investigated in Peng et al. (2016), reactions with OH dominated over other possible reactions,**
91 **including O(¹D), O(³P), O₃, and photolysis at 185 nm or 254 nm, under the conditions of OH oxidation**
92 **in the OFR during this campaign.”**

93

94 **Anonymous Referee #2**

95 Overview

96 R2.0. This work describes the first field observations of in-situ OH, O₃, and NO₃ exposures to ambient air
97 using an oxidative flow reactor. This is highly important work in the field of atmospheric chemistry
98 today, with extensive field and lab studies being performed to better understand the chemical
99 mechanisms and potential to form (or fragment) secondary organic aerosol. Observations here are
100 conducted in a forested environment with biogenic precursor gases (monoterpene dominant) and
101 highlight the dominance of OH oxidation chemistry, but show potential for O₃ and NO₃ reactions with
102 C=C bond VOC species at night. Several studies have been performed using a similar method since the
103 2011 BEACON-RoMBAS study described here, making the analysis and results of this study very relevant
104 for upcoming manuscripts for this research team and others. In-situ NO₃ chemistry and modeling is
105 especially novel. Specific comments to be addressed:

106 R2.1. Pg. 4, Line 22: Discussing MT's here, but haven't defined how these are measured, if cumulative
107 MT's by PTR, or summed by GC/MS.

108 **We have changed the sentence starting at page 4, line 21, to: "VOC concentrations at the site**
109 **(quantified using proton-transfer-reaction time-of-flight mass spectrometry; PTR-TOF-MS) varied on a**
110 **diurnal cycle..."**

111 R2.2. Pg. 5, Line 5: Please provide average concentration increases for "moderate increases" of NO_x, CO,
112 and anthro VOCs. Also, what anthro VOCs?

113 **We have changed the text at page 5, line 5 to: "...leading to moderate increases in NO_x (up to ~5 ppbv**
114 **from ~2 ppbv), CO (up to ~140 ppbv from ~100 ppbv), and anthropogenic VOCs (e.g., benzene up to**
115 **~50 pptv from ~20 pptv, and toluene up to ~150 pptv from ~50 pptv) during the late afternoon and**
116 **evening (Fry et al., 2013; Ortega et al., 2014)."**

117 R2.3. Pg. 5, Line 20: Are periods with very high local winds excluded from the analysis?

118 **We have added the following text to the manuscript at page 5, line 20:**

119 **"The data were not screened for high local wind speeds. However, periods of high wind speeds were**
120 **infrequent during the campaign, and the influence of local winds was likely tempered by the fact that**
121 **the OFR was located within the canopy of the forest."**

122 R2.4. Pg. 6: The thorough explanation of NO₃ exposure estimates here and in supplemental material is
123 appreciated. It seems worth considering how representative one equivalent day of NO₃ aging would be
124 of atmospheric conditions. Given the typical diel pattern of NO₃, and relatively low concentrations,
125 would it ever be expected that a whole day's worth of oxidation could occur prior to further oxidation
126 from OH?

127 **The reviewer touches on a very important point, which is that NO₃ concentrations in the atmosphere are**
128 **much more variable than those of OH or O₃. This means that the eq. NO₃ ages calculated assuming an**
129 **average of 1 pptv of NO₃ in this work need to be interpreted in the context of that assumption, which is**
130 **only strictly applicable to this research site. Other sites may have much more or less average ambient**
131 **NO₃. We had already made this point in the paragraph starting on page 6, line 24. To more strongly**

132 make the point that, even for a given location, the NO₃ concentrations can be variable from one night to
133 the next, we have altered the text starting on page 7, line 3 to read:

134 **“Estimated eq. NO₃ ages from this study are therefore shown simply for a common metric of**
135 **comparison for all of the data during this study, interpretable in terms of the average chemistry**
136 **occurring at the BEACHON site. Interpretation of measurements at other sites would need to be**
137 **adjusted to local NO₃ concentrations.”**

138 R2.5. Pg.8, Line 22: Can further argument be provided for the assumption in this modeled correction (of
139 no fragmentation for O₃ or NO₃ reaction LVOC products)? I’m wondering to what extent does the
140 assumption drive conclusions? Figure 5 suggests lower OA concentrations at 2-3 days NO₃ eq. aging
141 compared to 1 day eq. aging.

142 To address this comment, we have added the following text to page 8, line 24:

143 **“This assumption is reinforced by the fact that for the highest O₃ and NO₃ eq. ages achieved in this**
144 **work, no net decrease of OA was observed when SOA-forming gases were not present (see Sect. 3.2.1**
145 **and Fig. 5). If fragmentation reactions in the gas phase (or from heterogeneous oxidation) were**
146 **important for the range of eq. ages studied here, observations would show a net loss of OA at the**
147 **highest eq. ages when SOA-forming gases (e.g., MT) were not present.”**

148 Regarding the lack of SOA formation observed at the highest NO₃ ages in Fig. 5, those data points were
149 coincident with low ambient MT concentrations (all blue on the MT concentration color bar), so little to
150 no SOA formation was expected. This comment is also addressed by our response to R2.14 below.

151 R2.6. Pg. 9, line 1: The acronym for sesquiterpene (SQT) has not yet been defined.

152 We thank the reviewer for catching this mistake. We have changed the page 9, line 1 instance of SQT to
153 **“sesquiterpenes (SQT)”**.

154 R2.7. Pg. 10, line 15: The negative values in Figure 2d for the fraction of monoterpenes reacted, along
155 with the instances of OFR output MT concentrations that exceed ambient levels shown in Figure S7,
156 should be mentioned. Can this be attributed to instrument uncertainty, or are there other factors at play
157 that give these apparent MT generation events?

158 To address this comment, we have added the following text at page 10, line 15:

159 **“The scatter in the measurements is thought to be due mainly to incomplete and/or variable mixing of**
160 **the injected N₂O₅ flow into the sampled ambient air (see Sect. S1 for more details), with some**
161 **contribution from measurement variability at low ambient MT concentrations.”**

162 We have also added the following text to the end of the Fig. S7 caption:

163 **“Note that the ambient MT were sampled through a separate inlet within the canopy, several meters**
164 **from the OFR. Short periods of higher MT concentrations measured through the OFR (at low O₃**
165 **exposures) may be due to spatial heterogeneity in ambient MT concentrations within the canopy.”**

166 R2.8. Pg. 10, line 24: Change “didn’t” to “did not”.

167 Done.

168 R2.9. Pg. 12, Line 6: please provide average daytime MT+SQT concentration and average nighttime
169 MT+SQT concentration here.

170 We have changed the text at page 12, line 6 to:

171 **“This is consistent with the general increase in MT and SQT (average of 1.1 and 0.04 ppbv in the**
172 **canopy during nighttime, and 0.4 and 0.03 ppbv during daytime, respectively) and related precursor**
173 **concentrations in the shallower nighttime boundary layer.”**

174 We have also clarified the related text in Sect. 2.1. The VOC concentrations quoted in the original text
175 referred to the measurements at 25 m, above the forest canopy. As shown in Palm et al. (2016), the in-
176 canopy concentrations were higher, and those are the concentrations that are relevant to this analysis.
177 Therefore, the text on page 4, line 24 was changed to:

178 **“During BEACHON-RoMBAS, the concentration of MBO+isoprene in the forest canopy ranged from**
179 **about 2 ppb during daytime to 0.4 ppb at nighttime (see Palm et al., 2016).”**

180 The text at page 5, line 2 was changed to:

181 **“MT concentrations in the canopy spanned from 0.4 ppb during the day to 1.1 ppb at night, on**
182 **average.”**

183 R2.10. Pg. 12, line 19: In Figure 6, there is an uptick in OA enhancement with the highest level of O₃
184 oxidation for the nighttime air. However, in Figure S7 it appears that the MTs are largely depleted prior
185 to reaching this extent of aging. Would this suggest that something beyond the measured
186 monoterpenes is contributing to SOA formation from O₃ oxidation at these highest levels of aging?

187 The apparent uptick in OA enhancement at the highest O₃ eq. ages is most likely a result of
188 measurement variability due to the limited number of measurements in each eq. age bin. To address the
189 possibility that the O₃ ages used in this study were not high enough to lead to SOA formation from non-
190 VOC precursors, we have changed the text at page 12, line 19 to read:

191 **“Such molecules would typically not react appreciably with O₃ or NO₃ over the range of eq. ages**
192 **achieved in this work, but will still react with OH and may lead to SOA formation. Future O₃ and NO₃**
193 **oxidation studies should include higher eq. age ranges in order to investigate if additional SOA could**
194 **be formed from ambient precursors at higher ages.”**

195 R2.11. Pg. 13, Line 11: abstract says factor of 3.4. Here it states factor of 4.4. Are these numbers
196 referring to the same discrepancy?

197 We have clarified the relationship between these two numbers by changing the text at page 13, line 10
198 to:

199 **“This is in contrast to the analysis for OH oxidation in Palm et al. (2016), where a factor of 4.4 times**
200 **more SOA was formed from OH oxidation than could be explained by measured VOC precursors. As**
201 **shown in that analysis, the additional SOA-forming gases in ambient air were likely S/IVOCs, where**
202 **the SOA formation from S/IVOCs was 3.4 times larger than the source from VOCs. This conclusion was**
203 **supported by unspiciated measurements of total S/IVOC concentrations (classified by volatility).”**

204 R2.12. Pg. 18, line 24: Change “formed from primary VOCs” to “formed from reaction with primary
205 VOCs”.

206 We have changed this text to read:

207 **“formed from reaction with primary VOCs.”**

208 R2.13. Pg. 20, line 13: Please explain further where 620 g mol⁻¹ is coming from.

209 We have clarified this point by changing the text at page 20, line 11 to:

210 **“To put this in context, if every SOA molecule formed in the OFR contained a single –ONO₂ group (with
211 its mass of 62 g mol⁻¹), then the molecular mass of the full pRONO₂ molecules would be an average of
212 620 g mol⁻¹ (giving the slope of 62 g mol⁻¹ / 620 g mol⁻¹ = 0.10 in Fig. 13).”**

213 R2.14. Figure 5: This method of binning seems to limit comparison of low and high monoterpene
214 conditions at the same levels of oxidation. Particularly for NO₃, why are there not average values for the
215 high monoterpene case at high levels of NO₃ eq. age?

216 The range of eq. NO₃ ages achieved in the OFR was strongly influenced by ambient temperature, which
217 controlled the equilibrium between N₂O₅ and NO₂+NO₃ from the injected N₂O₅. During nighttime (when
218 MT concentrations were higher) it was colder and less NO₃ exposure was realized in the OFR. During
219 daytime (with lower MT concentrations), warm ambient temperatures led to more NO₃ exposure. To
220 make this clearer, we have added the following text on page 11, line 21:

221 **“As seen in Fig. 5 (and in Fig. 6 below), lower eq. NO₃ ages were achieved when MT concentrations
222 were higher, and higher eq. NO₃ ages were achieved when MT concentrations were lower. This was
223 because the higher MT concentrations occurred during nighttime, when lower ambient temperatures
224 shifted the equilibrium towards N₂O₅ and away from NO₂+NO₃ (from the injected N₂O₅), meaning
225 lower NO₃ exposures were realized in the OFR.”**

226 Due to the data limitations, we did not bin data by multiple MT concentrations for day or night;
227 however, the non-binned data points are shown as well (and colored by MT) in order to give a sense of
228 the relationship between SOA formation and MT concentrations for similar oxidation levels. That
229 relationship is also borne out in the measured vs. modeled discussion in Section 3.2.2 and Fig. 7.

230 Supplemental Information:

231 R2.15. Fig S3: Should reiterate in figure caption that these fractional fates are modeled, not measured.
232 Additionally, it seems that the fraction of LVOCs condensing on the aerosol will decrease slightly at
233 higher NO₃ exposures. Would this be due to a greater frequency of fragmentation reactions occurring as
234 opposed to functionalization?

235 We have changed the first line of the Fig. S3 caption from “Fractional fates” to **“Modeled fractional
236 fates”** as suggested. The slightly lower apparent fraction that condenses on particles at higher eq. NO₃
237 ages is a result of the slightly lower condensational sink (i.e., lower aerosol concentrations) during the
238 daytime when those high eq. ages were achieved (see also response to comment R2.14). Fragmentation
239 at high exposures was not included in the model, as described in Sect. 2.3 and in response to comment
240 R2.5.

241 R2.16. Fig S6: why higher NO₃ exposures on the limited data points on Aug9-10?

242 We have changed the last sentence of the Fig. S6 caption to read:

243 **“For these examples, the amount of injected N₂O₅ was held roughly constant (with a higher constant**
244 **value injected on Aug. 9–10).”**

245 R2.17. Fig S8: Which quantile averages are being shown by the black trace?

246 We have changed the last sentence of the Fig. S8 caption to read:

247 **“Quantile averages of OA enhancement per ppbv MT are shown for each oxidant, with error bars**
248 **corresponding to the standard error of the mean of each quantile.”**

249 R2.18. Table S2: revisit for formatting.

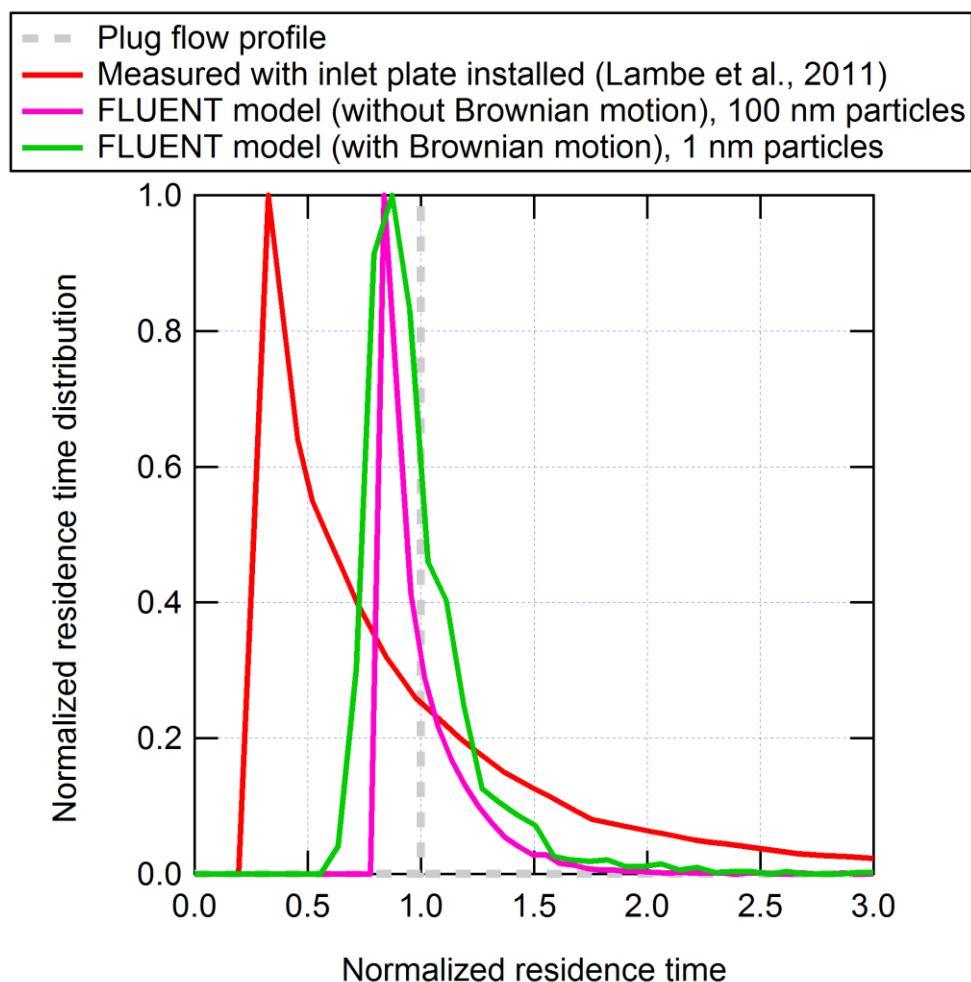
250 We thank the reviewer for pointing out the issue with the formatting of line numbers. It has been fixed.

251 [Other Changes:](#)

252 1: On page 7, line 20, we changed the typo “Scanning Particle Mobility Analyzer” to “**Scanning Mobility**
253 **Particle Sizer**”.

254 2: The author list in the Supplemental Information was changed to match the author list in the main
255 paper.

256 3: We have corrected Fig. S1 to reflect a small change in the FLUENT model results. The new figure is
257 presented here:



258

259 **Fig. S1. Normalized residence time distributions in the OFR as a function of normalized residence time**
260 **(1 = avg. residence time of each distribution). The FLUENT model was used to calculate residence**
261 **times for 1 nm particles (with Brownian motion) and 100 nm particles (without Brownian motion) for**
262 **the OFR configuration without the inlet plate to represent conditions used during BEACHON-RoMBAS.**
263 **These distributions are compared to the bis(2-ethylhexyl) sebacate (BES) particle residence time**
264 **distribution measured with the inlet plate installed in Lambe et al. (2011) and to the ideal plug flow**
265 **distribution (where all particles have equal residence time calculated as the OFR volume divided by**

266 the total flow rate through the OFR). The residence time distribution without the inlet plate is much
267 narrower than with the plate and is close to plug flow, although local winds may at times create a
268 broader distribution than the model shows.

269 **References**

- 270 Fry, J. L., Draper, D. C., Zarzana, K. J., Campuzano-Jost, P., Day, D. A., Jimenez, J. L., Brown, S. S., Cohen,
271 R. C., Kaser, L., Hansel, A., Cappellin, L., Karl, T., Hodzic Roux, A., Turnipseed, A., Cantrell, C., Lefer, B. L.
272 and Grossberg, N.: Observations of gas- and aerosol-phase organic nitrates at BEACHON-RoMBAS 2011,
273 *Atmos. Chem. Phys.*, 13, 8585–8605, doi:10.5194/acp-13-8585-2013, 2013.
- 274 Hu, W., Palm, B. B., Day, D. A., Campuzano-Jost, P., Krechmer, J. E., Peng, Z., de Sá, S. S., Martin, S. T.,
275 Alexander, M. L., Baumann, K., Hacker, L., Kiendler-Scharr, A., Koss, A. R., de Gouw, J. A., Goldstein, A.
276 H., Seco, R., Sjostedt, S. J., Park, J.-H., Guenther, A. B., Kim, S., Canonaco, F., Prévôt, A. S. H., Brune, W. H.
277 and Jimenez, J. L.: Volatility and lifetime against OH heterogeneous reaction of ambient isoprene-
278 epoxydiols-derived secondary organic aerosol (IEPOX-SOA), *Atmos. Chem. Phys.*, 16, 11563–11580,
279 doi:10.5194/acp-16-11563-2016, 2016.
- 280 Karl, T., Hansel, A., Cappellin, L., Kaser, L., Herdinger-Blatt, I. and Jud, W.: Selective measurements of
281 isoprene and 2-methyl-3-buten-2-ol based on NO⁺ ionization mass spectrometry, *Atmos. Chem. Phys.*,
282 12, 11877–11884, doi:10.5194/acp-12-11877-2012, 2012.
- 283 Knap, H. C., Schmidt, J. A. and Jørgensen, S.: Hydrogen shift reactions in four methyl-buten-ol (MBO)
284 peroxy radicals and their impact on the atmosphere, *Atmos. Environ.*, 147, 79–87,
285 doi:10.1016/j.atmosenv.2016.09.064, 2016.
- 286 Lambe, A. T., Ahern, A. T., Williams, L. R., Slowik, J. G., Wong, J. P. S., Abbatt, J. P. D., Brune, W. H., Ng, N.
287 L., Wright, J. P., Croasdale, D. R., Worsnop, D. R., Davidovits, P. and Onasch, T. B.: Characterization of
288 aerosol photooxidation flow reactors: heterogeneous oxidation, secondary organic aerosol formation
289 and cloud condensation nuclei activity measurements, *Atmos. Meas. Tech.*, 4, 445–461,
290 doi:10.5194/amt-4-445-2011, 2011.
- 291 Li, R., Palm, B. B., Ortega, A. M., Hlywiak, J., Hu, W., Peng, Z., Day, D. A., Knote, C., Brune, W. H., de
292 Gouw, J. A. and Jimenez, J. L.: Modeling the Radical Chemistry in an Oxidation Flow Reactor: Radical
293 Formation and Recycling, Sensitivities, and the OH Exposure Estimation Equation, *J. Phys. Chem. A*, 119,
294 4418–4432, doi:10.1021/jp509534k, 2015.
- 295 Ortega, J., Turnipseed, A., Guenther, A. B., Karl, T. G., Day, D. A., Gochis, D., Huffman, J. A., Prenni, A. J.,
296 Levin, E. J. T., Kreidenweis, S. M., DeMott, P. J., Tobo, Y., Patton, E. G., Hodzic, A., Cui, Y. Y., Harley, P. C.,
297 Hornbrook, R. S., Apel, E. C., Monson, R. K., Eller, A. S. D., Greenberg, J. P., Barth, M. C., Campuzano-Jost,
298 P., Palm, B. B., Jimenez, J. L., Aiken, A. C., Dubey, M. K., Geron, C., Offenberg, J., Ryan, M. G., Fornwalt, P.
299 J., Pryor, S. C., Keutsch, F. N., DiGangi, J. P., Chan, A. W. H., Goldstein, A. H., Wolfe, G. M., Kim, S., Kaser,
300 L., Schnitzhofer, R., Hansel, A., Cantrell, C. A., Mauldin, R. L. and Smith, J. N.: Overview of the Manitou
301 Experimental Forest Observatory: site description and selected science results from 2008 to 2013,
302 *Atmos. Chem. Phys.*, 14, 6345–6367, doi:10.5194/acp-14-6345-2014, 2014.
- 303 Palm, B. B., Campuzano-Jost, P., Ortega, A. M., Day, D. A., Kaser, L., Jud, W., Karl, T., Hansel, A., Hunter, J.
304 F., Cross, E. S., Kroll, J. H., Peng, Z., Brune, W. H. and Jimenez, J. L.: In situ secondary organic aerosol
305 formation from ambient pine forest air using an oxidation flow reactor, *Atmos. Chem. Phys.*, 16, 2943–
306 2970, doi:10.5194/acp-16-2943-2016, 2016.
- 307 Peng, Z., Day, D. A., Stark, H., Li, R., Lee-Taylor, J., Palm, B. B., Brune, W. H. and Jimenez, J. L.: HO_x radical
308 chemistry in oxidation flow reactors with low-pressure mercury lamps systematically examined by

309 modeling, *Atmos. Meas. Tech.*, 8, 4863–4890, doi:10.5194/amt-8-4863-2015, 2015.

310 Peng, Z., Day, D. A., Ortega, A. M., Palm, B. B., Hu, W., Stark, H., Li, R., Tsigaridis, K., Brune, W. H. and
311 Jimenez, J. L.: Non-OH chemistry in oxidation flow reactors for the study of atmospheric chemistry
312 systematically examined by modeling, *Atmos. Chem. Phys.*, 16, 4283–4305, doi:10.5194/acp-16-4283-
313 2016, 2016.

314 Zhang, H., Worton, D. R., Lewandowski, M., Ortega, J., Rubitschun, C. L., Park, J.-H., Kristensen, K.,
315 Campuzano-Jost, P., Day, D. A., Jimenez, J. L., Jaoui, M., Offenberg, J. H., Kleindienst, T. E., Gilman, J.,
316 Kuster, W. C., de Gouw, J., Park, C., Schade, G. W., Frossard, A. A., Russell, L., Kaser, L., Jud, W., Hansel,
317 A., Cappellin, L., Karl, T., Glasius, M., Guenther, A., Goldstein, A. H., Seinfeld, J. H., Gold, A., Kamens, R.
318 M. and Surratt, J. D.: Organosulfates as Tracers for Secondary Organic Aerosol (SOA) Formation from 2-
319 Methyl-3-Buten-2-ol (MBO) in the Atmosphere, *Environ. Sci. Technol.*, 46, 9437–9446,
320 doi:10.1021/es301648z, 2012.

321

Secondary organic aerosol formation from in situ OH, O₃, and NO₃ oxidation of ambient forest air in an oxidation flow reactor

Brett B. Palm^{1,2}, Pedro Campuzano-Jost^{1,2}, Douglas A. Day^{1,2}, Amber M. Ortega^{1,3,*}, Juliane L. Fry⁴, Steven S. Brown^{2,5}, Kyle J. Zarzana^{1,2,*}, William Dube^{1,5}, Nicholas L. Wagner^{1,5}, Danielle C. Draper^{4,#}, Lisa Kaser⁶, Werner Jud^{7,^}, Thomas Karl⁸, Armin Hansel⁷, Cándido Gutiérrez-Montes⁹, and Jose L. Jimenez^{1,2}

¹Cooperative Institute for Research in Environmental Sciences, University of Colorado, USA

²Department of Chemistry and Biochemistry, University of Colorado, USA

³Department of Atmospheric and Oceanic Science, University of Colorado, USA

⁴Department of Chemistry, Reed College, USA

⁵NOAA Earth System Research Laboratory, Chemical Sciences Division, Boulder, CO, USA

⁶Atmospheric Chemistry Observations & Modeling Laboratory, National Center for Atmospheric Research, USA

⁷Institute of Ion Physics and Applied Physics, University of Innsbruck, Austria

⁸Institute of Atmospheric and Cryospheric Sciences, University of Innsbruck, Austria

⁹Departamento de Ingeniería, Mecánica y Minería, Universidad de Jaen, Jaen, Spain

*Now at Air Pollution Control Division, Colorado Department of Public Health and Environment, Denver, CO, USA

#Now at NOAA Earth System Research Laboratory, Chemical Sciences Division, Boulder, CO, USA

^Now at Department of Chemistry, University of California, Irvine, USA

^Now at Research Unit Environmental Simulation (EUS), Institute of Biochemical Plant Pathology (BIOP), Helmholtz Zentrum München GmbH, Germany

Correspondence to: Jose L. Jimenez (jose.jimenez@colorado.edu)

Abstract: Ambient pine forest air was oxidized by OH, O₃, or NO₃ radicals using an oxidation flow reactor (OFR) during the BEACHON-RoMBAS (Bio-hydro-atmosphere interactions of Energy, Aerosols, Carbon, H₂O, Organics & Nitrogen–Rocky Mountain Biogenic Aerosol Study) campaign to study biogenic secondary organic aerosol (SOA) formation and organic aerosol (OA) aging. A wide range of equivalent atmospheric photochemical ages was sampled, from hours up to days (for O₃ and NO₃) or weeks (for OH). Ambient air processed by the OFR was typically sampled every 20–30 min, in order to determine how the availability of SOA precursor gases in ambient air changed with diurnal and synoptic conditions, for each of the three oxidants. More SOA was formed during nighttime than daytime for all three oxidants, indicating that SOA precursor concentrations were higher at night. At all times of day, OH oxidation led to approximately 4 times more SOA formation than either O₃ or NO₃ oxidation. This is likely because O₃ and NO₃ will only react with gases containing C=C bonds (e.g., terpenes) to form SOA, but won't react appreciably with many of their oxidation products or any species in the gas phase that lacks a C=C bond (e.g., pinonic acid, alkanes). In contrast, OH can continue to react with compounds that lack C=C bonds to produce SOA. Closure was achieved between the amount of SOA formed from O₃ and NO₃ oxidation in the OFR and the SOA predicted to form from measured concentrations of ambient monoterpenes and sesquiterpenes using published chamber yields. This is in contrast to previous work at this site (Palm et al., 2016), which has shown that a source of SOA from semi- and intermediate-volatility organic compounds (S/IVOCs) 3.4 times larger than the source from measured VOCs is needed to explain the measured SOA formation from OH oxidation. This work suggests that those S/IVOCs typically do not contain C=C bonds. O₃ and NO₃ oxidation produced SOA with elemental O:C and H:C similar to the least oxidized OA observed in local ambient air, and neither oxidant led to net mass loss at the highest exposures, in contrast with OH oxidation. An OH exposure in the OFR equivalent to several hours of atmospheric aging also produced SOA with O:C and H:C values similar to ambient OA, while higher aging (days–weeks) led to formation of SOA with progressively higher O:C and lower H:C (and net mass loss at the highest exposures). NO₃ oxidation led to the production of particulate organic nitrates (pRONO₂), while OH and O₃ oxidation (under low NO) did not, as expected. These measurements of SOA formation provide the first direct comparison of SOA formation potential and chemical evolution from OH, O₃ and NO₃ oxidation in the real atmosphere, and help to clarify the oxidation processes that lead to SOA formation from biogenic hydrocarbons.

1 Introduction

Submicron atmospheric aerosols have important impacts on radiative climate forcing (Myhre et al., 2013) and human health (Pope and Dockery, 2006). A large fraction of submicron particulate mass is composed of organic aerosols (OA), and is produced from a variety of sources (Zhang et al., 2007). Primary OA (POA) is directly emitted as particles (e.g., via fossil fuel combustion, biomass burning), while secondary OA (SOA) can be formed through gas-phase oxidation and gas-to-particle conversion of directly emitted organic gases, or via aqueous pathways. Globally, SOA comprises the majority of OA, particularly in rural locations away from primary sources (Zhang et al., 2007; Jimenez et al., 2009). However, the processes of formation, chemical transformation, and removal of SOA remain uncertain (Hallquist et al., 2009; Shrivastava et al., 2016).

Hydroxyl radicals (OH), ozone (O₃), and nitrate radicals (NO₃) are the three major oxidants in the atmosphere that react with organic gases to form SOA. The initial steps of oxidation for each oxidant are summarized here according to Atkinson and Arey (2003):

- OH can react via H-abstraction or addition to a C=C double bond, depending on the structure of the organic molecule;
- O₃ generally reacts only with alkenes, adding to a C=C bond to produce a primary ozonide which then decomposes to form a carbonyl plus a Criegee intermediate;
- NO₃ radicals also react by addition to a C=C bond, producing an organic peroxy radical with an adjacent organic nitrate group that will react further. The nitrate functional group formed during the initial NO₃ addition can either remain in the product molecule or decompose to produce NO₂ (g).

Nearly all oxidation pathways in the atmosphere will lead to the production of a peroxy radical (RO₂), which can proceed to react with HO₂, NO₂, NO, another RO₂, or undergo autooxidation (Atkinson, 1997; Orlando and Tyndall, 2012; Crounse et al., 2013). Reaction rate constants and more detailed reaction mechanisms can be found elsewhere (e.g., Atkinson et al., 1982; Atkinson, 1997; Chew et al., 1998; Calvert et al., 2002).

SOA yields from the oxidation of a wide variety of precursor gases by each of these three oxidants have been reported. SOA yields are typically measured from oxidation experiments in large environmental chambers. These yields are evaluated through implementation in regional or global models, which can be compared to

ambient measurements (e.g., Volkamer et al., 2006; Hayes et al., 2015). However, large chamber experiments have been shown to be affected by large losses of semivolatile and low volatility gases (Matsunaga and Ziemann, 2010; Zhang et al., 2014; Krechmer et al., 2015; La et al., 2016; Nah et al., 2016) and particles (Crump and Seinfeld, 1981; McMurry and Rader, 1985; Pierce et al., 2008) to the chamber walls. These artifacts affect the ability to accurately measure SOA yields, and also limit the amount of oxidation that can be achieved in chambers. Large variability in OA concentrations exists between various global OA models, which typically achieve poor agreement and correlation with ambient surface and vertical profile OA concentration measurements (Tsigaridis et al., 2014).

In addition to bulk concentrations, the chemical composition of OA also determines its atmospheric properties. The elemental O:C and H:C ratios of OA can be measured using aerosol mass spectrometry (Aiken et al., 2008; Canagaratna et al., 2015). The O:C and H:C ratios can provide information about the sources and evolution of OA in the atmosphere (Aiken et al., 2008; Heald et al., 2010; Kroll et al., 2011; Ng et al., 2011), and also often correlate with key OA properties such as hygroscopicity, material density, and phase separation (Jimenez et al., 2009; Bertram et al., 2011; Kuwata et al., 2012). Laboratory studies have typically struggled to reproduce the O:C and H:C values found in ambient OA, particularly for the highest O:C values found in remote areas (Aiken et al., 2008; Chen et al., 2015).

While large chambers have been the standard method for studying SOA yields and composition, and are the basis for parameterized yields and oxidation in most models, oxidation flow reactors (OFRs) have recently become a popular alternative approach. OFRs typically have shorter residence times than chambers, which reduces wall contact. Also, ambient air can easily be oxidized in an OFR, while it is difficult and slow to perform such experiments in a large chamber (Tanaka et al., 2003). SOA yields from OH oxidation in OFRs for a variety of individual and mixed precursors have been reported, and generally show that yields in OFRs are similar to chamber yields (Kang et al., 2007, 2011, Lambe et al., 2011, 2015; Li et al., 2013; Bruns et al., 2015)(Kang et al., 2007, 2011, Lambe et al., 2011, 2015; Li et al., 2013; Bruns et al., 2015). Properties related to SOA elemental composition have also been investigated in OFRs (Massoli et al., 2010; Lambe et al., 2011, 2012, 2014; Saukko et al., 2012; Ortega et al., 2013, 2016). However, these studies were limited to laboratory-produced SOA from one or several precursor gases, often at very high concentrations. Several studies have reported on SOA formation from the OH oxidation of ambient air (Ortega et al., 2016; Palm et al., 2016) or emission sources (Cubison et al.,

2011; Keller and Burtscher, 2012; Ortega et al., 2013; Tkacik et al., 2014; Bruns et al., 2015; Karjalainen et al., 2016; Timonen et al., 2016), but SOA from O₃ and NO₃ oxidation of ambient air or direct source emissions has not been studied using an OFR, to our knowledge.

In this study, we oxidized ambient pine forest air with either OH, O₃, or NO₃ in an OFR to investigate how much SOA can be formed from real ambient mixtures of largely biogenic SOA precursor gases, how the SOA precursor concentrations varied with time, and the properties of the SOA formed. The amount of SOA formed from each oxidant was compared to the amount predicted to form from oxidation of the measured ambient VOCs that entered the OFR. We investigated the elemental composition of the SOA that was formed as a function of the amount of oxidant exposure (oxidant concentration multiplied by residence time) in the OFR. The contribution of organic nitrate to SOA formation was also explored and compared to the results with ambient and chamber studies.

2 Experimental methods

2.1 BEACHON-RoMBAS field campaign

The OFR measurements presented here were conducted during July–August 2011 as part of the BEACHON-RoMBAS field campaign (Bio-hydro-atmosphere interactions of Energy, Aerosols, Carbon, H₂O, Organics & Nitrogen – Rocky Mountain Biogenic Aerosol Study; <http://cires.colorado.edu/jimenez-group/wiki/index.php/BEACHON-RoMBAS>). The research site was located in a ponderosa pine forest in a mountain valley at the Manitou Experimental Forest Observatory, near Woodland Park, Colorado (39.10° N, 105.10° W; 2370 m elevation). An overview of previous research at this site, including BEACHON-RoMBAS and prior campaigns, has been presented in detail by Ortega et al. (2014). Here we present a brief summary of research site details that are relevant to this analysis.

VOC concentrations at the site ([quantified using proton-transfer-reaction time-of-flight mass spectrometry; PTR-TOF-MS](#)) varied on a diurnal cycle, dominated by 2-methyl-3-buten-2-ol (MBO) during daytime and monoterpenes (MT) during nighttime. Fry et al. (2013) and Palm et al. (2016) show diurnal cycles of select biogenic and anthropogenic VOCs. VOC measurements from a July–September 2008 campaign at the same site have also been described in Kim et al. (2010). [During BEACHON-RoMBAS, the concentration of](#)

MBO+isoprene ranged from about 1.5 ppb during daytime to 0.3 ppb at nighttime. During BEACHON-RoMBAS, the concentration of MBO+isoprene in the forest canopy ranged from about 2 ppb during daytime to 0.4 ppb at nighttime (see Palm et al., 2016). The ratio of isoprene to MBO at this pine forest site was determined using NO⁺ reagent ion chemical ionization mass spectrometry (Karl et al., 2012) and using GC-MS (Kaser et al., 2013) to be about 21%, indicating the concentration of isoprene at this site was low (<0.3 ppb). MT concentrations in the canopy spanned from 0.14 ppb during the day and 0.5 to 1.1 ppb at night, on average. The Manitou Experimental Forest Observatory site is mainly influenced by biogenic emissions, but occasionally receives airflow from nearby urban areas (Denver metropolitan area and Colorado Springs, 75 and 35 km away from the site respectively), leading to moderate increases in NO_x (up to ~5 ppbv from ~2 ppbv), CO₂ (up to ~140 ppbv from ~100 ppbv), and anthropogenic VOCs (e.g., benzene up to ~50 pptv from ~20 pptv, and toluene up to ~150 pptv from ~50 pptv) during the late afternoon and evening (Fry et al., 2013; Ortega et al., 2014).

2.2 OFR methods

The OFR used in this study was the Potential Aerosol Mass (PAM) flow reactor (Kang et al., 2007, 2011)(Kang et al., 2007, 2011). The PAM reactor is a cylindrical tube 45.7 cm long and 19.7 cm ID with a volume of approximately 13 liters. This type of OFR has been used to study SOA formation and chemistry in a number of previous studies (e.g., Kang et al., 2007, 2011; Massoli et al., 2010; Lambe et al., 2012, 2015; Li et al., 2013; Ortega et al., 2013, 2016; Tkacik et al., 2014; Palm et al., 2016). During BEACHON-RoMBAS, ambient air was sampled through a 14 cm diameter opening on one end of the OFR (with the inlet plate removed to prevent loss of gases/particles on inlet surfaces) through a coarse-grid mesh screen coated with an inert silicon coating (Sulfinert by Silcotek, Bellefonte, PA). The OFR was located on top of the measurement trailer in order to sample ambient air directly without using an inlet. Therefore the temperature and RH inside the OFR were the same as ambient conditions, with the exception of minor heating from the UV lamps mounted inside the OFR (up to ~2°C heating at the highest lamp settings, and ~0.5°C at the settings producing the most SOA; Li et al., 2015). No heating occurred during O₃ or NO₃ modes. Thus RH within the OFR was the same or slightly lower than ambient, depending on the operating mode. The OFR was operated with a residence time in the range of 2–4 min. The residence time distribution in the OFR, modeled using FLUENT for the configuration used in this study (inlet plate removed), is shown in Fig. S1. The modeled residence time distribution is much more homogeneous than has been measured for OFRs operated with an inlet plate (Lambe et al., 2011; Ortega et al.,

2016). However, local winds can result in some variations that are not captured by the FLUENT model. The data were not screened for high local wind speeds. However, periods of high wind speeds were infrequent during the campaign, and the influence of local winds was likely tempered by the fact that the OFR was located within the canopy of the forest. Two OFRs were used simultaneously, with one dedicated to NO₃ oxidation while the other was used for either OH or O₃ oxidation. OH radicals were produced in situ inside the OFR using two different methods, referred to as OFR185 and OFR254 (named according to the wavelength of the highest energy UV light used to generate oxidants within the reactor). These methods have been described in detail previously and showed consistent results (Palm et al., 2016). All results of OH oxidation presented in this paper used the OFR185 method (e.g., Kang et al., 2007, 2011; Massoli et al., 2010; Lambe et al., 2012, 2015; Li et al., 2013; Ortega et al., 2013, 2016; Tkacik et al., 2014; Palm et al., 2016). The gas-phase HO_x/O_x chemistry inside the OFR has also been investigated with kinetic modeling (Li et al., 2015; Peng et al., 2015, 2016). For the wide variety of compounds investigated in Peng et al. (2016), reactions with OH dominated over other possible reactions, including O(¹D), O(³P), O₃, and photolysis at 185 nm or 254 nm, under the conditions of OH oxidation in the OFR during this campaign. During BEACHON-RoMBAS, ambient air was sampled through a 14 cm diameter opening on one end of the OFR (with the inlet plate removed to prevent loss of gases/particles on inlet surfaces) through a coarse-grid mesh screen coated with an inert silicon coating (Sulfinert by Silcotek, Bellefonte, PA). The OFR was operated with a residence time in the range of 2–4 min. The residence time distribution in the OFR, modeled using FLUENT for the configuration used in this study (inlet plate removed), is shown in Fig. S1. The modeled residence time distribution is much more homogeneous than has been measured for OFRs operated with an inlet plate (Lambe et al., 2011; Ortega et al., 2016). However, local winds can result in some variations that are not captured by the FLUENT model. Two OFRs were used simultaneously, with one dedicated to NO₃ oxidation while the other was used for either OH or O₃ oxidation. OH radicals were produced in situ inside the OFR using two different methods, referred to as OFR185 and OFR254 (named according to the wavelength of the highest energy UV light used to generate oxidants within the reactor). These methods have been described in detail previously and showed consistent results (Palm et al., 2016). All results of OH oxidation presented in this paper used the OFR185 method.

NO₃ radicals were generated by thermal decomposition of N₂O₅ (N₂O₅ → NO₂ + NO₃), which was injected into the OFR from a cold trap held in a dry ice + isopropyl alcohol bath. The cold trap was held near -60°C using a temperature controlled copper sleeve immersed in the -78° C bath. A 10–100 sccm flow of zero air eluted N₂O₅ from the trap. This N₂O₅+zero air mixture was injected through an approximately 14 cm diameter ring of 1/8" Teflon tubing with pinholes around the ring mounted just inside the OFR entrance inside the mesh screen. N₂O₅ concentrations were adjusted by changing this flow rate from the N₂O₅ dry ice reservoir. The concentrations of N₂O₅ and NO₃ in both the injection flow and in the output of the OFR were measured using diode laser-based cavity ring-down spectroscopy (CRDS; Wagner et al., 2011). The concentration of NO₂ was measured in the output of the OFR using laser-induced fluorescence (Thornton et al., 2000). The experimental setup for the NO₃-OFR system is illustrated in Fig. S2 and discussed in Sect. S1.

To estimate NO₃ concentrations and exposure in the OFR, the relevant chemistry was modeled using a chemical-kinetic plug-flow model, implemented in the KinSim chemical-kinetic integrator (version 3.10) using Igor Pro 6 (<http://www.igorexchange.com/node/1333>; Wavemetrics, Lake Oswego, OR, USA). A key output of this model was the integrated NO₃ exposure experienced by MT-containing air during the OFR residence time, calculated as the integral of NO₃ concentration over the OFR residence time (in units of molecules cm⁻³ s), and multiplied by the fraction of MT that was estimated to have been mixed with the N₂O₅ flow at each residence time, due to lack of mixing from the small flow rate (see Sect. S1 for more details of the unmixed fraction estimation and parameterization). NO₃ exposure was converted to an equivalent (eq.) atmospheric age by dividing by a typical site-specific nighttime ambient NO₃ concentration, which has been estimated to be on the order of 1 ppt (Fry et al., 2013). This eq. age represents the amount of time the air would have to spend in the atmosphere with 1 ppt NO₃ to experience the same amount of NO₃ exposure as in the OFR. The unit of eq. age is a unit of exposure. When given in units of eq. days, it represents the number of 24 h periods that air would need to spend in an atmosphere containing the stated oxidant concentration in order to achieve the equivalent amount of exposure as in the OFR (which applies for OH and O₃ eq. ages as well). More details about the model can be found in Sect. S1.

The exposure metric for the NO₃-OFR is specific to the site in which it is measured. Fry et al. (2013) estimated the average nighttime NO₃ concentration at this site (approximately 1 pptv) from an average NO₃ production rate and lifetime of approximately 0.03 pptv s⁻¹ and 25 s, respectively. Other sites can have considerably

different production rates for NO₃ and thus very different nighttime exposures. Remote forests, with nighttime NO_x below 50 pptv, could experience NO₃ production rates more than 10 times slower, while forests immediately downwind of urban areas could have NO₃ production rates more than 10 times faster (e.g., outflow from Houston, TX; Brown et al., 2013). Variability in NO₃ production rates and observed NO₃ levels is a common feature of recent field observations (Brown and Stutz, 2012). Estimated eq. NO₃ ages from this study are therefore shown simply for a common metric of comparison for all of the data during this study, interpretable in terms of the average chemistry occurring at the BEACHON site only, and Interpretation of measurements at other sites would need to be adjusted accordingly to compare with other sites' local NO₃ concentrations.

To investigate SOA formation from O₃ oxidation, O₃ was produced external to the OFR by flowing pure dry O₂ gas across two low-pressure mercury UV lamps (BHK, Inc., model no. 82-9304-03). The O₂ was photolyzed by 185 nm light to produce O(³P), which further reacted with O₂ to produce O₃. This O₂+O₃ mixture was injected at 0.5 lpm into the front of the OFR through four ports distributed evenly around and just inside the 14 cm opening. O₃ concentrations were cycled by adjusting the UV lamp intensity (i.e., photon flux) in the O₃ generation setup. O₃ was measured in the output of the OFR using a 2B Technologies Model 205 Monitor. O₃ exposure was calculated by multiplying the measured O₃ concentration in the OFR output by the residence time of the OFR. Loss of injected O₃ to internal OFR walls was not investigated, so the exposure may be slightly underestimated by this method. O₃ exposure was converted to an eq. atmospheric age by dividing by a typical, site-specific, 24 h average, ambient O₃ concentration of 50 ppb. A schematic of the O₃-OFR system is also shown in Fig. S2.

2.3 Particle and gas measurements

Ambient and OFR-oxidized particles were measured with an Aerodyne High-Resolution Time-of-Flight Aerosol Mass Spectrometer (HR-ToF-AMS, referred to here as AMS; DeCarlo et al., 2006; Canagaratna et al., 2007) and a TSI 3936 Scanning Mobility Particle Mobility Analyzer Sizer (SMPS). Details of these measurements have been described previously (Palm et al., 2016). Ambient VOC concentrations were quantified using a PTR-TOF-MS (Kaser et al., 2013). The OFR output was sampled by the PTR-TOF-MS during selected periods only (Aug 4–6, 9–10, and 22–23 for NO₃ oxidation, and Aug. 7–9 and 23–24 for O₃ oxidation; see Palm et al. (2016) for details of sampling VOCs during OH oxidation). The particle mass measurements were corrected for particle losses to

Formatted: Font color: Auto

Formatted: Font color: Auto

Formatted: Font color: Auto

Formatted: Font color: Auto, Pattern: Clear

sampling line walls and at the small particle transmission limit of the AMS aerodynamic lens (combined 2% correction; details of these corrections are the same as in Palm et al., 2016). To account for particle losses to internal OFR surfaces, the particle mass was corrected by the average ratio of ambient particle mass to the particle mass measured through each OFR in the absence of oxidant (1% correction for the O₃ OFR, and 14% for the NO₃ OFR due to a different sampling port with a higher wall surface-area-to-volume ratio).

A correction was also applied to account for any condensable oxidation products (referred to as low-volatility organic compounds; LVOCs) that were formed from gas-phase oxidation in the OFR but condensed on OFR or sampling line walls instead of condensing to form SOA. This is non-atmospheric behavior, due to the short residence time in the OFR and the relatively small aerosol condensational sink in this study. A correction is needed because the dominant fate of such gases in the atmosphere will be condensation to form SOA (lifetime of ~minutes) rather than being lost to any environmental surfaces via dry or wet deposition (lifetime of ~hours to a day; Farmer and Cohen, 2008; Knote et al., 2015; Nguyen et al., 2015). This correction, referred to as the “LVOC fate correction”, was first represented in a model developed in Palm et al. (2016); the full details of the model can be found there. Briefly, the model takes several inputs, including particle condensational sink, OFR residence time, and oxidant concentration. It produces the fractional fates of LVOCs with respect to condensation onto particles, condensation onto OFR walls, further oxidation to give non-condensable molecular fragmentation products, and condensation onto sampling line walls after exiting the back of the OFR. In Palm et al. (2016), the model was verified by quantitatively explaining SO₄ aerosol formation from OH oxidation of ambient SO₂.

The results of the LVOC fate model for the O₃-PAM and NO₃-PAM conditions in this study are shown in Fig. S3. The SOA formation values given in the subsequent analysis are corrected for LVOC fate by dividing the measured SOA formation by the fraction of LVOCs predicted to have condensed to form SOA in the OFR (an average correction of 0.4 μg m⁻³ for both O₃-PAM and NO₃-PAM). These corrected values refer to the amount of SOA that would form from any ambient precursors in the absence of OFR walls and the limited time for condensation within the OFR. LVOCs are assumed not to be lost to fragmentation from excessive O₃ or NO₃ reactions in the gas-phase prior to condensation due to lack of C=C bonds (which is different from the parameterization for OH reactions used in Palm et al., 2016). This assumption is reinforced by the fact that for the highest O₃ and NO₃ eq. ages achieved in this work, no net decrease of OA was observed when SOA-forming

gases were not present (see Sect. 3.2.1 and Fig. 5). If fragmentation reactions in the gas phase (or from heterogeneous oxidation) were important for the range of eq. ages studied here, observations would show a net loss of OA at the highest eq. ages when SOA-forming gases (e.g., MT) were not present.

2.4 Modeling of SOA formation

5 In the analysis in Sect. 3.2.2, the amount of SOA formed by oxidation of ambient air by O₃ or NO₃ in the OFR is compared to the amount predicted to form. This predicted amount was estimated by applying SOA yields to the fraction of measured ambient MT and sesquiterpenes (SQT) concentrations that were predicted to react. Since the ambient VOC measurements were taken above the canopy at a height of 25 m, the concentrations were corrected to reflect in-canopy values that were ingested into the OFR, a technique which has been used

10 previously (Kim et al., 2013; Wolfe et al., 2014; Palm et al., 2016). During this campaign, speciated MT and SQT measurements were not available. When predicting SOA formation in this analysis, we use previous measurements at the same site to approximate that MT consisted of an equal mix of α -pinene, β -pinene, and 3-carene and that SQT was solely isolongifolene (Kim et al., 2010). Numerous chamber studies have reported SOA yields of individual MT from O₃ oxidation (e.g., Ng et al., 2006; Pathak et al., 2007, 2008; Shilling et al., 2008;

15 Zhao et al., 2015) and from NO₃ oxidation (Hallquist et al., 1999; Moldanova and Ljungström, 2000; Spittler et al., 2006; Fry et al., 2009, 2011, 2014; Boyd et al., 2015; Ng et al., 2016). SOA yields from SQT have also been reported for O₃ oxidation (Jaoui et al., 2003, 2013; Ng et al., 2006; Winterhalter et al., 2009; Chen et al., 2012; Tasoglou and Pandis, 2015) and NO₃ oxidation (Fry et al., 2014). In this analysis, the OA concentrations measured after O₃ or NO₃ oxidation ranged from 1–3 $\mu\text{g m}^{-3}$, with few exceptions. For simplicity with this

20 relatively narrow range, the dependence of SOA yields on OA concentrations was not included. Instead, we applied representative SOA yields of 15% for ozonolysis of α -pinene, β -pinene, and 3-carene, and 30% for ozonolysis of isolongifolene. For reaction with NO₃, SOA yields of 4%, 33%, 38%, and 86% were used for α -pinene, β -pinene, 3-carene, and isolongifolene (using β -caryophyllene as a proxy for all SQT; Fry et al., 2014; Kang et al., 2016; Ng et al., 2016). The rate constants used for reaction of α -pinene, β -pinene, 3-carene, and isolongifolene with O₃ and NO₃ were $k_{\text{O}_3} = 8.6 \times 10^{-17}$, 1.5×10^{-17} , 3.6×10^{-17} , and $1.1 \times 10^{-17} \text{ cm}^3 \text{ molec}^{-1} \text{ s}^{-1}$, and $k_{\text{NO}_3} = 6.1 \times 10^{-12}$, 2.5×10^{-12} , 9.5×10^{-12} , and $3.9 \times 10^{-12} \text{ cm}^3 \text{ molec}^{-1} \text{ s}^{-1}$, respectively (Canosa-Mas et al., 1999; Atkinson and Arey, 2003; Richters et al., 2015).

3 Results and discussion

3.1 Modeled vs. measured NO₃ and O₃ exposures

One of the features of the OFR technique is the short residence time required for conducting high time resolution ambient measurements. Combined with the ability to rapidly change the amount of oxidant injected or produced in the OFR, this allows for a wide range of oxidation levels to be studied in a short amount of time (and thus with limited variation of ambient conditions). In this work, the oxidant concentration was changed every 20–30 min, covering a range from no added oxidant to maximum oxidation repeatedly in 2–3 h cycles. In order to interpret the results over the wide range of oxidant exposure, the amount of exposure must be quantified. In Palm et al. (2016), OH exposure was estimated using a model-derived equation (Li et al., 2015; Peng et al., 2015) and calibrated using PTR-TOF-MS measurements of VOC decay in the OFR. In this work, a simple box model was developed and compared with VOC decay measurements to estimate NO₃ and O₃ exposures in the OFR.

The set of reactions and rate constant parameters included in the modeling of NO₃ exposure are shown in Table S1. Figure 1 illustrates the most important mixing ratios and reactive fluxes in the OFR with injected N₂O₅ under typical conditions. Interconversion between N₂O₅ and NO₂ + NO₃ was relatively rapid, which maintained the system near equilibrium at all times. Wall loss of N₂O₅ was estimated to be the main loss of the injected nitrogen-containing species (84%), while reaction of NO₃ with biogenic gases (2%), NO₃ wall losses (14%), and hydrolysis of N₂O₅ on particle surfaces (0.2%) were minor loss pathways. Figure 2a–c compares the N₂O₅, NO₂, and NO₃ mixing ratios measured in the OFR output with those predicted by the model. The model is generally consistent with the measurements. The scatter in the measurements is thought to be due mainly to incomplete and/or variable mixing of the injected N₂O₅ flow into the sampled ambient air (see Sect. S1 for more details), with some contribution from measurement variability at low ambient MT concentrations. The critical output of this model for our application is the prediction of the fraction of MT reacted. Figure 2d shows that the model can reproduce the measured MT decay with an error (average absolute value of modeled minus measured fraction MT remaining) of 11%, providing confirmation that using the model output NO₃ exposure in the subsequent analysis of aerosol mass yields from the OFR is justified. A similar analysis of SQT decay was not possible, because ambient SQT concentrations were too small to accurately measure fractional decays. Also,

MBO did not react substantially with NO_3 in the OFR, consistent with the lifetime for reaction of NO_3 with MBO that is approximately 3 orders of magnitude slower than for reaction with MT (Atkinson and Arey, 2003). This is also representative of the atmosphere, where MBO will overwhelmingly react with OH or O_3 and not NO_3 (Atkinson and Arey, 2003).

5 Unlike NO_3 exposure, the estimation of O_3 exposure ~~didn't~~did not require a detailed chemical model since the O_3 system had no reservoir species analogous to N_2O_5 . O_3 exposure was simply estimated as the measured O_3 concentration in the OFR output multiplied by residence time. To verify this estimate, the measured fraction of MT that reacted in the OFR was compared in Fig. 3 to a model prediction calculated using a simple set of reactions of ozone with the three major MT species (Table S2). The model is consistent with measurements
10 within an error of 9%, and shows that a parameterization for mixing of the O_3 flow into ambient air was not needed. In contrast to the slower 10–100 sccm flow of N_2O_5 , the 0.5 lpm flow of O_2+O_3 appears to have been large enough relative to the total OFR flowrate to result in sufficiently complete mixing. This result suggests that a faster flow of N_2O_5 could be used in future NO_3 oxidation experiments to facilitate better mixing.

Time series examples of measured and modeled MT remaining after OFR oxidation are compared to ambient
15 MT concentrations for both NO_3 and O_3 oxidation in Fig. 4. These examples illustrate the dynamic range from no MT reacted (i.e., when no oxidants were added to the ambient air) to nearly all MT reacted within the 2–3 h cycles for both oxidants. Further examples are shown for NO_3 oxidation in Fig. S6 and for O_3 oxidation in Fig. S7.

3.2 SOA formed from oxidation of ambient air

3.2.1 OA enhancement vs. photochemical age

20 During BEACHON-RoMBAS, ambient air was oxidized by either OH, O_3 , or NO_3 in order to study the amount and properties of SOA that could be formed from ambient precursors. In situ SOA formation from OH oxidation was the subject of a previous manuscript (Palm et al., 2016). Select results are reproduced here as a comparison to SOA formation from O_3 and NO_3 oxidation. Additional new analyses of the chemical composition of SOA formed from OH oxidation is also included along with O_3 and NO_3 oxidation in Sects. 3.3-3.4.

In Palm et al. (2016), SOA formation from OH oxidation in the OFR correlated with ambient MT concentrations (and implicitly with any other gases that correlated with MT, such as SQT and possibly terpene oxidation products). Here, Fig. 5 shows the OA enhancement observed after O₃ and NO₃ oxidation as a function of eq. age in the OFR. Similar to OH oxidation, little SOA formation was observed from O₃ or NO₃ oxidation when ambient MT concentrations were low, regardless of the amount of exposure. When MT concentrations were higher, increasing amounts of SOA were formed with increasing exposure. As seen in Fig. 5 (and in Fig. 6 below), lower eq. NO₃ ages were achieved when MT concentrations were higher, and higher eq. NO₃ ages were achieved when MT concentrations were lower. This was because the higher MT concentrations occurred during nighttime, when lower ambient temperatures shifted the equilibrium towards N₂O₅ and away from NO₂+NO₃ (from the injected N₂O₅), meaning lower NO₃ exposures were realized in the OFR.

Another way to examine the trends in OA enhancement is by separating the results into daytime and nighttime. Due to diurnal cycles in the emission rates (that are strong functions of temperature, and also light for some species), vertical mixing in the boundary layer, and changing rates of ambient oxidation, the concentration of MT (and other SOA precursors) in ambient air showed substantial diurnal cycles (Kim et al., 2010; Fry et al., 2013; Kaser et al., 2013). Ambient air was characterized by higher MBO+isoprene (with ambient OH and O₃ chemistry) during the day and higher MT+SQT (with ambient O₃ and NO₃ chemistry) during the night (Fry et al., 2013). Due to these changes, it might be expected that SOA formation in the OFR would also change diurnally.

OA enhancements vs. eq. age for OH, O₃, and NO₃ oxidation are shown together in Fig. 6, split between daytime (08:00-20:00 LT) and nighttime (20:00-08:00 LT). For all oxidants, more SOA formation was observed during nighttime. This is consistent with the general increase in MT+SQT and SQT (average of 1.1 and 0.04 ppbv in the canopy during nighttime, and 0.4 and 0.03 ppbv during daytime, respectively) and related precursor concentrations in the shallower nighttime boundary layer. This higher SOA formation during nighttime was not a result of larger temperature-dependent partitioning to the particle phase at lower nighttime temperatures, as evidenced by stable values of measured OA enhancement per unit ambient MT (the dominant measured SOA precursor) across the whole range of ambient temperatures (shown in Fig. S8). An exploration of the correlation between maximum SOA formation from each oxidant and all available ambient VOC concentrations is shown in Fig. S9, illustrating that MT are the best tracer of SOA production at this forest site. The maximum amount of SOA formed from OH oxidation was approximately 4 times more than from O₃ or NO₃ oxidation for both

daytime and nighttime over the eq. ages covered in this work. If the gases that formed SOA from each oxidant were the same, then this would require the SOA yields from OH oxidation to be more than 4 times larger than from O₃ or NO₃ oxidation. The references for SOA yields from O₃ and NO₃ oxidation presented herein and for OH oxidation presented in Palm et al. (2016) show this is likely not the case. Instead, one possible explanation for this result could be that a large fraction of SOA-forming gases found in ambient air do not have C=C bonds (e.g., MT oxidation products such as pinonic acid). Such molecules would typically not react appreciably with O₃ or NO₃ over the range of eq. ages achieved in this work, but will still react with OH and may lead to SOA formation. Future O₃ and NO₃ oxidation studies should include higher eq. age ranges in order to investigate if additional SOA could be formed from ambient precursors at higher ages. This concept will be discussed further in Sect.

3.2.2.

Whereas a net loss of OA was observed at >10 eq. days of OH aging due to heterogeneous oxidation (shown in Fig. 7 of Palm et al., 2016), a similar net loss of OA at the highest eq. ages of O₃ and NO₃ oxidation was not observed. Since the highest eq. ages for both O₃ and NO₃ oxidation were approximately 5 days, it is unclear if O₃ or NO₃ heterogeneous oxidation would lead to net loss of ambient OA at substantially higher ages. Future experiments could be designed to achieve higher ages in order to investigate this effect.

3.2.2 Measured vs. predicted OA enhancement

When ambient air is sampled into an OFR, any gases or particles present in that air are subject to oxidation. Measurement of the resultant SOA formation is a top-down measure of the total SOA formation potential of that air as a function of eq. age of oxidation. In other words, an OFR can be used to determine the relative concentrations of SOA-forming gases present in ambient air at any given time. To provide context to the measurements in the OFR, a bottom-up analysis can be carried out by applying laboratory SOA yields to the measured ambient SOA-forming gases that are entering the OFR.

The measured SOA formation after oxidation by O₃ and NO₃ is shown vs. the SOA predicted to form from measured precursor gases in Fig. 7. The measured SOA formation includes all ages greater than 0.7 eq. d for O₃-PAM and greater than 0.3 eq. d for NO₃-PAM, where most or all of the VOCs have reacted. For both oxidants, the data are scattered along the 1:1 line of equal measured and predicted SOA formation. This is in contrast to the analysis for OH oxidation in Palm et al. (2016), where a factor of 4.4 more SOA was formed from OH

oxidation than could be explained by measured VOC precursors. As shown in that analysis, the additional SOA-forming gases in ambient air were likely S/IVOC, a/IVOCs, where the SOA formation from S/IVOCs was 3.4 times larger than the source from VOCs. This conclusion was supported by unspiciated measurements of total S/IVOC concentrations (classified by volatility). SOA yields from S/IVOCs or any other sources are not required to explain SOA formation from O₃ or NO₃. This suggests that the majority of S/IVOCs in this ambient forest air generally did not contain C=C bonds, and therefore did not typically react with O₃ or NO₃ to produce SOA on atmospherically relevant time scales. This is consistent with expectations based on laboratory and ambient studies of MT and SQT oxidation products. Typical oxidation products include compounds such as pinic acid, pinonic acid, pinonaldehyde, caronaldehyde, and nopinone, none of which contain C=C double bonds (e.g., Calogirou et al., 1999b; Yu et al., 1999; Lee et al., 2006). As an example, the reaction rates of pinonaldehyde with OH, O₃, and NO₃ are 3.9×10^{-11} , $<2 \times 10^{-20}$, and $2.0 \times 10^{-14} \text{ cm}^3 \text{ molec}^{-1} \text{ s}^{-1}$, respectively (Atkinson et al., 2006). These rates correspond to eq. lifetimes of 4.7 h, >579 d, and 29 d, respectively, showing that pinonaldehyde will typically only react with OH in the atmosphere or in the OFR under the conditions in this study.

While the measured and predicted SOA formation shown in Fig. 7 are consistent with each other, two main caveats limit the strength of the conclusions that can be drawn from this particular study. First, the amount and dynamic range of SOA formed from O₃ and NO₃ oxidation were relatively small, as were the total ambient aerosol concentrations. This caused the SMPS+AMS measurement noise and variability to be larger relative to the total aerosol measurements than they would be for higher aerosol concentrations. Also, as only a small amount of new SOA was formed, the aerosol condensational sink remained relatively low for all measurements. According to the LVOC fate model, on average only 31% and 36% of LVOCs condensed to form SOA during O₃ and NO₃ oxidation, respectively (see Fig. S3). This required a correction of approximately a factor of 3 to correct measured SOA formation to what would occur in normal atmospheric conditions.

3.3 H:C and O:C ratios of SOA formed from oxidation of ambient air

Analysis of ambient high-resolution AMS spectra can be used to estimate the elemental composition of OA (Aiken et al., 2008; Canagaratna et al., 2015). When SOA is formed in the OFR, the OA that is sampled in the OFR output is a sum of preexisting ambient OA and any SOA produced from oxidation. At sufficiently high eq. ages,

the sampled OA will also include the effects of heterogeneous oxidation. The amount of O, C, and H atoms added by oxidation can be calculated by subtracting the ambient elemental concentrations from those measured after aging. The amounts of each element added by oxidation can be used to determine the O:C and H:C elemental ratios of the SOA that is formed in the OFR.

- 5 The amounts of O and H vs. C added from OH oxidation are shown in Fig. 8. Slopes were fit to the data with positive net addition of C in order to determine the O:C and H:C of the SOA formed for the eq. photochemical age ranges of 0.1–0.4 (avg.=0.18) d, 0.4–1.5 (avg.=0.9) d, 1.5–5 (avg.=2.7) d, and 5–15 (avg.=10) d. The elemental O:C (H:C) ratios of the SOA mass formed in those ranges were 0.55 (1.60), 0.84 (1.44), 1.13 (1.36), and 1.55 (1.22). For data with ages of longer than several eq. days, O was added coincident with loss of C (i.e.,
- 10 negative x-intercept), which is likely due to heterogeneous oxidation leading to fragmentation/evaporation of preexisting OA. This conclusion is reinforced by the evidence that for eq. OH ages greater than several days, heterogeneous oxidation resulted in a net loss of C when ambient MT concentrations were low (Fig. S10), but not for lower eq. ages. Similarly, George and Abbatt (2010) suggested that the lifetime of ambient OA with respect to heterogeneous OH oxidation is approximately two to three days. Therefore, the change in amounts
- 15 of O, C, and H after several eq. days of oxidation will be a mix of heterogeneous change to preexisting OA and addition of new SOA. These effects of heterogeneous oxidation (i.e., x- and y-intercepts) are likely to be approximately the same for all data within each given age range, meaning the slopes fitted above are independent of the heterogeneous processes and contain information about the elemental changes associated with the formation of varying amounts of SOA within each age range.
- 20 Analogous to Fig. 8, the amount of O and H vs. C added from O₃ and NO₃ oxidation are shown in Figs. 9–10. The SOA added from O₃ oxidation had O:C and H:C ratios of 0.50 and 1.61. The SOA added from NO₃ oxidation had O:C and H:C ratios of 0.39 and 1.60. This O:C value of 0.39 for NO₃ oxidation includes only the O atoms that were bound to the C backbone of the organic molecules, and excludes the two O atoms that are bound only to N in the –ONO₂ (nitrate) functional group (Farmer et al., 2010). If all O atoms in the nitrate functional group are
- 25 included, the O:C of this added SOA mass was 0.44. Inclusion of only the carbon-bound oxygen of the nitrate functional group is more reflective of the carbon oxidation state, and is also what is typically reported for AMS O/C measurements (since the organic –NO₂ moiety is measured in the AMS as total nitrate and typically not separated from inorganic nitrate).

Heterogeneous oxidation was not expected to be a factor for the O₃ and NO₃ ages used in this work. This assumption was reinforced by the fact that no net loss of C was observed for these amounts of oxidation, even when ambient MT concentrations (and OA enhancement) were low, as shown in Figs. S11–12. This assumption is also consistent with previous research on lifetimes of OA components with respect to O₃ and NO₃ heterogeneous oxidation. For instance, several aldehydes were found to have a relatively long lifetime equivalent to approximately 2–8 days for NO₃ heterogeneous oxidation when calculated using 1 pptv ambient NO₃ (Iannone et al., 2011). Ng et al. (2016) summarized that reactive uptake of NO₃ into particles is slow for most molecules, with the exception of unsaturated or aromatic molecules, which were unlikely to be major components of the ambient OA in this remote forest (Chan et al., 2016). Although the lifetime of pure oleic acid (which contains a C=C bond) particles with respect to heterogeneous O₃ oxidation can be as short as tens of minutes (Morris et al., 2002), lifetimes for oleic acid in atmospheric particle organic matrices can be tens of hours to days (Rogge et al., 1991; Ziemann, 2005). Furthermore, the uptake coefficients for O₃ to react with saturated molecules are typically 1–2 orders of magnitude slower than for unsaturated molecules (de Gouw and Lovejoy, 1998). In summary, this previous research suggests that heterogeneous oxidation by O₃ or NO₃ may be important at higher eq. ages, but not for those achieved in the present work.

To put the O:C and H:C values of the SOA formed in the OFR in perspective, Van Krevelen diagrams of H:C vs O:C ratios for OA measured after OH, O₃, and NO₃ oxidation are shown compared to concurrent measurements of ambient OA in Fig. 11a–c, and summarized together in Fig. 11d. The effect of heterogeneous OH oxidation on preexisting aerosol is also shown as a line with a slope of -0.58. This line was fitted to the H:C vs. O:C of all OH-aged data where a net loss of C was observed (i.e., SOA formation was not observed and heterogeneous oxidation dominated). Generally speaking, less oxidized (“fresh”) OA will lie in the upper left portion of a Van Krevelen plot, with higher H:C values and lower O:C values. Conversely, more oxidized (“aged”) OA will move towards the lower right, with lower H:C values and higher O:C values (Heald et al., 2010; Ng et al., 2011). Shown in Fig. 11, the SOA formed from O₃, NO₃, and the lowest amount of OH aging (0.1–0.4 eq. days) was found at the upper left of the range occupied by ambient OA. As OH aging increased to higher ranges, the values of H:C decreased and the values of O:C increased, already moving beyond the local ambient range after 0.9 eq. days. At the higher ages, the H:C of the SOA formed lies at higher H:C values than those of the total OA measured after OH aging, which are closer to the trend of heterogeneous oxidation in the Van Krevelen space. This shows

that SOA formed via gas-phase OH oxidation processes in an OFR has a higher H:C than the OA that results from heterogeneous oxidation, while both processes lead to similar increases in O:C. The net movement in the Van Krevelen space can be considered as starting at the ambient H:C and O:C and moving along two vectors: one vector along the heterogeneous oxidation line and another towards the H:C and O:C values of the new SOA formed in the gas phase, where the length of those two vectors are weighted by the amount of OA resulting from each process. When little SOA is formed, the H:C and O:C measured after oxidation lie along the heterogeneous oxidation line. When high amounts of SOA are formed, the H:C and O:C after oxidation shift to higher H:C values, lying closer to the curve defined by the H:C and O:C of SOA mass added in the OFR at the different age ranges (see Fig. S13).

While these two vectors describe the possible oxidation processes in the OFR, there may be other vectors (e.g., from condensed phase chemistry or reactive uptake) occurring in the atmosphere. As documented in Hu et al. (2016), SOA formation processes that require reactive uptake or within-particle non-radical chemistry (such as uptake of isoprene epoxydiols to form IEPOX-SOA) on time scales longer than the several minute residence time in the OFR are not captured with the OFR method used in this work. This is because the rate of reactive uptake and non-radical particle-phase chemistry do not speed up proportionally to increased OH and HO₂ (or O₃ or NO₃). However, to our knowledge the only precursor for which reactive uptake of epoxides has been shown to be a major pathway is isoprene, which was a very minor precursor at this site (Karl et al., 2012). The formation of epoxides during MBO oxidation has been proposed to play a role during BEACHON-RoMBAS (Zhang et al., 2012). However, recent results suggest that formation of epoxides during MBO oxidation is not important in the atmosphere (Knap et al., 2016). Thus, at this time it is not clear whether any important SOA-forming processes in this environment are missed by the OFR setup, and this question should be investigated in future studies.

The H:C of the least oxidized SOA formed in the OFR from all oxidants was near 1.6. As discussed in Palm et al. (2016), SOA formation from OH oxidation in the OFR correlated with MT, and the S/IVOC sources of SOA may have been MT oxidation products or other related biogenic gases. Biogenic terpenes are composed of isoprene units, meaning they all have H:C of 1.6. Therefore, the SOA formed from the lowest eq. ages in the OFR was consistent with oxidation processes that add roughly 4–6 O atoms without removing net H atoms. Addition of –OH or –OOH functional groups after –H abstraction by OH radicals results in addition of O without loss of H, and are consistent with the RO₂+HO₂ reaction conditions that are expected during OH oxidation in the OFR (Kroll

and Seinfeld, 2008; Ortega et al., 2016). OH can also add to a C=C bond, which could lead to addition of H atoms after oxidation. O₃ and NO₃ are expected to react with MT almost exclusively by addition to a C=C bond, which leads to addition of O without initial removal of H atoms (Atkinson and Arey, 2003). However, previous research has shown that many precursor gases, including aromatic molecules with initial H:C close to 1, can form SOA with H:C close to 1.6 (Chen et al., 2011; Chhabra et al., 2011; Canagaratna et al., 2015; Hildebrandt Ruiz et al., 2015). Therefore, H:C alone cannot provide direct evidence about the specific identities of precursor gases in ambient air. The SOA from O₃, NO₃, and 0.1–0.4 eq. days OH aging had H:C values similar to typical semi-volatile oxidized organic aerosol (SV-OOA), while the H:C of SOA from 0.4–1.5 eq. days or longer OH aging resembled low volatility oxidized organic aerosol (LV-OOA); these two types of SOA have been identified in ambient air at many locations (Jimenez et al., 2009; Canagaratna et al., 2015).

The relative time scales of oxidation and condensation in the OFR also need to be considered in order to properly interpret the H:C and O:C of the SOA mass formed in the OFR. In the atmosphere, once a molecule is oxidized to an LVOC that is able to condense onto a particle, lifetimes for condensation onto aerosols are on the order of several minutes (Farmer and Cohen, 2008; Knote et al., 2015; Nguyen et al., 2015). This is typically much shorter than the lifetimes for subsequent reaction with OH, O₃, or NO₃ of tens of minutes to several hours or longer, so condensation will likely occur prior to further oxidation. In OFR oxidation experiments, the lifetime for subsequent oxidation of LVOCs is shortened proportional to the increase in oxidant concentration. However, the condensation lifetime does not scale with oxidant concentration, and remains roughly constant. At sufficiently high oxidant concentrations, LVOCs can be subjected to further oxidation steps that they would not be subjected to in the atmosphere prior to having a chance to condense to form SOA. To compare SOA formation in the OFR vs. ambient air, these relative time scales are considered here as a function of both oxidant type and amount of oxidant exposure.

The lowest range of OH aging for which O:C and H:C values were measured was 0.1–0.4 (avg. 0.18) eq. d, which is 2.4–9.6 (avg. 4.3) eq. h of oxidation. Typical terpenes have lifetimes for reaction with OH on the order of tens of minutes to several hours in the atmosphere (Atkinson and Arey, 2003), which is similar to this lowest eq. age range in the OFR. Typical terpene oxidation products have lifetimes ranging from 3.9 h (caronaldehyde; Alvarado et al., 1998) to 4.7 h (pinonaldehyde; Atkinson et al., 2006) to 11–13 h (nopinone; Atkinson and Aschmann, 1993; Calogirou et al., 1999a) to a computationally estimated 18–21 h (pinic and pinonic acid;

Vereecken and Peeters, 2002). As a rough approximation, this suggests that the SOA formed in the OFR is likely a result of approximately one or at most a few oxidation steps occurring to the molecules that enter the OFR (which may have already experienced one or more oxidation steps in the atmosphere prior to entering the OFR). The aging in this range strikes a balance between achieving enough oxidation to react all incoming precursors at least once while not reacting them an unrealistic number of times in the gas phase before allowing sufficient time for condensation. In the next age range of 0.4–1.5 (avg. 0.9) eq. d of OH aging, in which the maximum OA enhancement occurred, some primary precursors are likely starting to be oxidized multiple times inside the OFR prior to condensation, while some oxidation products will still be oxidized only ~1–2 times. The SOA formed in this range may represent SOA formed from multiple generations of chemistry. At higher ages in the OFR, the aerosol is likely mainly modified by heterogeneous oxidation, with a small contribution from condensation of highly oxidized products. This OA at the highest ages resembles ambient OA found in remote locations (Jimenez et al., 2009; Chen et al., 2015). Indeed, OFRs have previously been used to study heterogeneous oxidation processes (George et al., 2008; Smith et al., 2009).

For O₃ and NO₃ oxidation, the oxidants will react only with C=C double-bond-containing gases. The major MT and SQT species at this field site all contain only a single C=C bond (isoprene and minor MT and SQT species contain two). Subsequent reaction lifetimes of oxidation products with these oxidants will likely be longer than the lifetime for condensation onto particles. For example, the lifetimes for pinonaldehyde with respect to O₃ and NO₃ oxidation are >579 d, and 29 d, respectively (Atkinson et al., 2006). Therefore, we can approximate that multiple generations of oxidation are not dominant for SOA formation when investigating O₃ or NO₃ oxidation in the OFR at this site. This is consistent with previous chamber SOA formation experiments that suggested that first-generation oxidation products dominate SOA formation from O₃ oxidation of a variety of biogenic compounds with a single C=C bond, rather than products of later generations of oxidation (Ng et al., 2006). The SOA formed via O₃ or NO₃ oxidation in the OFR is likely formed from reaction with primary VOCs and a small subset of their reaction products that still contain C=C bonds, such as the α-pinene oxidation product campholenic aldehyde (Kahnt et al., 2014). This SOA should be representative of typical atmospheric SOA formation processes.

3.4 Particulate organic nitrate (pRONO₂) formation from NO₃ oxidation of ambient air

In addition to estimating the elemental composition of OA, the AMS can also be used to estimate the amount of inorganic vs. organic nitrate in submicron aerosols (Farmer et al., 2010; Fry et al., 2013). The ratio of NO_2^+ to NO^+ fragment ions produced by thermal decomposition on the AMS vaporizer and electron impact ionization depends on the type of nitrate. NH_4NO_3 typically produces a ratio of approximately 0.3-1, while particulate organic nitrate (pRONO₂), in which the $-\text{ONO}_2$ functional group is covalently bonded to the carbon backbone (R) through an oxygen atom, typically produces a ratio \sim 2-3 times lower (Fry et al., 2009; Bruns et al., 2010; Farmer et al., 2010; Liu et al., 2012; Day et al., 2017). The measured NO_2^+ to NO^+ ratio is a linear combination of these two chemical components. Using this principle, the NO_3 measured by the AMS was split into the estimated fractions of NH_4NO_3 and pRONO₂ according to the method described in Fry et al. (2013). For the instrument in this work, ratios of 0.3 and 0.13 were used for the NO_2^+ to NO^+ ratios of NH_4NO_3 and pRONO₂, respectively (Fry et al., 2013).

A two-night example of both ambient and NO_3 -radical aged aerosol on Aug. 20–22 is shown in Fig. 12. In ambient air, the majority of NO_3 aerosol was organic. After oxidation in the OFR, different behavior was seen on the two nights shown. On the first night, mainly inorganic nitrate was produced, as evidenced by the higher NO_2^+ to NO^+ ratio, the formation of NH_4 aerosol, and the relatively small amount of SOA formed. On the second night, pRONO₂ was produced, as evidenced by the lower NO_2^+ / NO^+ ratio, a lack of NH_4 aerosol formation, and substantial SOA formation. The organic nitrate formation and SOA formation also roughly tracked the ambient MT concentrations.

These two distinct behaviors in the NO_3 -OFR were likely controlled by ambient RH. There was a competition between thermal dissociation of injected N_2O_5 to produce NO_3+NO_2 (favored at high temperatures and low RH) and the hydrolysis of N_2O_5 on wetted OFR walls to produce HNO_3 (favored at low temperatures and high RH). When hydrolysis occurred rapidly, then there was a sharp decrease in N_2O_5 concentrations. The NO_3 radical concentrations were also greatly reduced, and thus fewer NO_3 radicals were available to react with ambient gases (e.g., MT) to produce pRONO₂. HNO_3 reacted with NH_3 in ambient air or evaporating from OFR surfaces to produce NH_4NO_3 . The results shown in Fig. 12 illustrate this behavior, with NO_3 radical exposure being reduced while NH_4NO_3 was produced during the first night. Despite the presence of similar MT concentrations on both nights, little SOA was produced on the first night. Future applications could include heating of the OFR slightly above ambient temperatures in order to prevent hydrolysis of N_2O_5 on the OFR walls. Inhibiting NH_4NO_3

formation artifacts would be especially critical for data interpretation if measuring aerosol enhancements with only non-chemical instruments such as an SMPS.

Despite this complex chemistry, information about the chemical composition of pRONO₂ formed from real atmospheric precursors can still be derived from times when conditions favored pRONO₂ formation. Shown in Fig. 13 is the mass of organic –ONO₂ added vs. SOA added from oxidation by each of the three oxidants.

Substantial formation of pRONO₂ was observed only for NO₃ radical oxidation, and not for O₃ or OH oxidation. This was expected, since ambient NO_x concentrations were generally low (0.5–4 ppb; Ortega et al., 2014), and the NO₃ oxidation experiment was the only one with an added source of reactive nitrogen. The slopes of Fig. 13 represent the ratio of –ONO₂ to the rest of the organic molecules in pRONO₂. In this study, the slope after NO₃ radical oxidation was 0.10, which is similar to the range of 0.1–0.18 found in previous chamber studies of NO₃ oxidation of terpenes (Fry et al., 2009, 2011; Boyd et al., 2015). To put this in context, if every SOA molecule formed in the OFR contained a single –ONO₂ group, (with its mass of 62 g mol⁻¹), then the molecular mass of the full pRONO₂ molecules would be an average of 620 g mol⁻¹, (giving the slope of 62 g mol⁻¹ / 620 g mol⁻¹ = 0.10 in Fig. 13). Alternatively, if all molecules are assumed to have a mass of 200 or 300 g mol⁻¹, then 32% or 48% of the molecules, respectively, would contain a –ONO₂ functional group (assuming no molecules contain more than one –ONO₂ group). Again, this result is roughly consistent with previous research. For the fraction of OA composed of pRONO₂ in NO₃+β-pinene SOA, Fry et al. (2009) estimated 32–41% (assuming an average molecular weight of 215–231 g mol⁻¹), Fry et al. (2014) estimated 56% (assuming 214 g mol⁻¹), and Boyd et al. (2015) estimated 45–68% (assuming 200–300 g mol⁻¹).

4 Conclusions

In situ SOA formation from ambient pine forest air after oxidation by OH, O₃, or NO₃ radicals was measured using an OFR for the first time. SOA formation from these real ambient mixes of aerosol and SOA precursors was measured semi-continuously, capturing diurnal and daily changes in the relative ambient concentrations of SOA precursor gases. In general, more SOA was formed from the precursors present in nighttime air than in daytime air for all three oxidants. At all times of day, OH oxidation produced approximately 4 times more SOA than O₃ or NO₃ oxidation. The O:C and H:C ratios of the SOA formed by O₃, NO₃, and several eq. hours of OH oxidation was similar to the oxidation levels of ambient OA.

The OFR is a tool that can be used to measure the total SOA formation potential of ambient air at any given time, and how that potential changes with time, whether or not the SOA precursor gases are measured and/or speciated. As discussed in Palm et al. (2016), ambient VOC concentrations alone could not explain the amount of SOA formed in the OFR by OH oxidation. Instead, SOA was likely being formed from S/IVOCs that entered the OFR. In contrast, the quantity of measured VOCs was sufficient to explain the amount of SOA formed from O₃ and NO₃ oxidation; closure between measured and predicted SOA formation in an OFR was achieved. In other words, O₃ and NO₃ oxidation of the ambient S/IVOCs do not appear to produce appreciable amounts of SOA. This suggests that the ambient S/IVOCs tend not to have double bonds.

While this work does not investigate the source of the S/IVOCs, one possibility is that they are oxidation products of primary VOCs (e.g., MT or SQT). The primary VOCs could be emitted upwind of the site, and by the time the molecule enters the OFR, the double bond(s) will have reacted, leaving an oxidation product that reacts further with OH but not O₃ or NO₃. If the lifetime for further reaction of these oxidation products is slower than the lifetime for the double-bond-containing primary emissions, then the oxidation products will build up in the atmosphere. Under this hypothesis, such S/IVOC compounds are not new or unexpected sources of SOA. In most regional and global models, they would already be implicitly accounted for, by tracking the emissions of the primary VOCs which have corresponding overall SOA yields. In this work, we consider only the primary VOCs that are measured to be entering the OFR, not the integrated sum of upwind emissions that were emitted into the air that eventually entering the OFR after some degree of ambient photochemical processing. SOA formation in the OFR takes a snapshot of the atmosphere, which consists of a mix of primary emissions and their oxidation products at various stages of oxidative progress. For this study, those snapshots demonstrate that for OH oxidation, only approximately a quarter of the SOA-forming gases are in the form of primary VOC, while for O₃ and NO₃ oxidation almost all are in the form of primary VOC. It also suggests that for these precursor mixtures, multi-generational chemistry plays a major role in the overall amount of SOA formed from OH oxidation (and much less so for O₃ and NO₃).

If these SOA-forming S/IVOCs do not react with ambient O₃ or NO₃, they will build up in the atmosphere during the night when OH is absent. When the sun rises and OH is produced, a sudden burst of SOA formation might be expected. However, this coincides with dilution of gases and particles due to convective vertical mixing, potentially offsetting such new SOA formation and making it difficult to observe it without detailed chemical

and boundary layer dynamics measurements and/or modeling. These OFR measurements and analysis elucidate the presence and properties of S/IVOCs in the atmosphere, and highlight the need for more measurements and modeling of such gases in order to better understand ambient SOA formation. This work also demonstrates the utility of the OFR as a tool for studying SOA formation from all three major atmospheric oxidants.

5 Acknowledgements

We thank William H. Brune for discussions and contributions including the initial development of the PAM OFR. We thank US NSF grants AGS-1243354 and AGS-1360834, NOAA grant NA13OAR4310063, U.S. DOE ASR Program (Office of Science, BER, DE-SC0011105 & DE-SC0016559), Austrian Science Fund (FWF) project number L518-N20, and the US EPA (STAR 83587701-0) for partial support for this research. BBP acknowledges support from a CIRES Graduate Student Research Fellowship and a US EPA STAR Graduate Fellowship (FP-91761701-0). This work has not been formally reviewed by the US EPA. The views expressed are solely those of the authors, and the US EPA does not endorse any products or commercial services mentioned in this work. LK acknowledges support from DOC-fFORTE-fellowship of the Austrian Academy of Science. The National Center for Atmospheric Research (NCAR) is sponsored by the National Science Foundation. AMO acknowledges a fellowship from the DOE SCGP Fellowship Program (ORAU, ORISE). KJZ was supported by NASA grant NNX09AE12G. We are grateful to Alex Guenther and Jim Smith of NCAR for co-organizing the BEACHON-RoMBAS field campaign, and to the USFS Manitou Experimental Forest Observatory for site support.

References

- Aiken, A. C., DeCarlo, P. F., Kroll, J. H., Worsnop, D. R., Huffman, J. A., Docherty, K. S., Ulbrich, I. M., Mohr, C., Kimmel, J. R., Sueper, D., Sun, Y., Zhang, Q., Trimborn, A., Northway, M., Ziemann, P. J., Canagaratna, M. R., Onasch, T. B., Alfarra, M. R., Prevot, A. S. H., Dommen, J., Duplissy, J., Metzger, A., Baltensperger, U. and Jimenez, J. L.: O/C and OM/OC Ratios of Primary, Secondary, and Ambient Organic Aerosols with High-Resolution Time-of-Flight Aerosol Mass Spectrometry, *Environ. Sci. Technol.*, **42**, 4478–4485, doi:10.1021/es703009q, 2008.
- Alvarado, A., Arey, J. and Atkinson, R.: Kinetics of the Gas-Phase Reactions of OH and NO₃ Radicals and O₃ with the Monoterpene Reaction Products Pinonaldehyde, Caronaldehyde, and Sabinaketone, *J. Atmos. Chem.*, **31**, 281–297, doi:10.1023/A:1006010915971, 1998.
- Atkinson, R.: Gas-Phase Tropospheric Chemistry of Volatile Organic Compounds: 1. Alkanes and Alkenes, *J. Phys. Chem. Ref. Data*, **26**, 215–290, doi:10.1063/1.556012, 1997.
- Atkinson, R. and Arey, J.: Gas-phase tropospheric chemistry of biogenic volatile organic compounds: a review, *Atmos. Environ.*, **37**, 197–219, doi:10.1016/S1352-2310(03)00391-1, 2003.
- Atkinson, R. and Aschmann, S. M.: Atmospheric chemistry of the monoterpene reaction products nopinone, camphenilone, and 4-acetyl-1-methylcyclohexene, *J. Atmos. Chem.*, **16**, 337–348, doi:10.1007/BF01032629, 1993.
- Atkinson, R., Winer, A. M. and Pitts Jr., J.: Rate constants for the gas-phase reactions of O₃ with the natural hydrocarbons isoprene and α and β -pinene, *Atmos. Environ.*, **16**, 1017–1020, 1982.
- Atkinson, R., Baulch, D. L., Cox, R. A., Crowley, J. N., Hampson, R. F., Hynes, R. G., Jenkin, M. E., Rossi, M. J., Troe, J. and IUPAC Subcommittee: Evaluated kinetic and photochemical data for atmospheric chemistry: Volume II - gas phase reactions of organic species, *Atmos. Chem. Phys.*, **6**, 3625–4055, doi:10.5194/acp-6-3625-2006, 2006.
- Bertram, A. K., Martin, S. T., Hanna, S. J., Smith, M. L., Bodsworth, A., Chen, Q., Kuwata, M., Liu, A., You, Y. and Zorn, S. R.: Predicting the relative humidities of liquid-liquid phase separation, efflorescence, and deliquescence of mixed particles of ammonium sulfate, organic material, and water using the organic-to-sulfate mass ratio of the particle and the oxygen-to-carbon ele, *Atmos. Chem. Phys.*, **11**, 10995–11006, doi:10.5194/acp-11-10995-2011, 2011.
- Boyd, C. M., Sanchez, J., Xu, L., Eugene, A. J., Nah, T., Tuet, W. Y., Guzman, M. I. and Ng, N. L.: Secondary organic aerosol formation from the β -pinene+NO₃ system: effect of humidity and peroxy radical fate, *Atmos. Chem. Phys.*, **15**, 7497–7522, doi:10.5194/acp-15-7497-2015, 2015.
- Brown, S. S. and Stutz, J.: Nighttime radical observations and chemistry, *Chem. Soc. Rev.*, **41**, 6405, doi:10.1039/c2cs35181a, 2012.
- Brown, S. S., Dubé, W. P., Bahreini, R., Middlebrook, A. M., Brock, C. A., Warneke, C., de Gouw, J. A., Washenfelder, R. A., Atlas, E., Peischl, J., Ryerson, T. B., Holloway, J. S., Schwarz, J. P., Spackman, R., Trainer, M., Parrish, D. D., Fehshenfeld, F. C. and Ravishankara, A. R.: Biogenic VOC oxidation and organic aerosol formation in an urban nocturnal boundary layer: aircraft vertical profiles in Houston, TX, *Atmos. Chem. Phys.*, **13**, 11317–11337, doi:10.5194/acp-13-11317-2013, 2013.
- Bruns, E. A., Perraud, V., Zelenyuk, A., Ezell, M. J., Johnson, S. N., Yu, Y., Imre, D., Finlayson-Pitts, B. J., Alexander,

- M. L., Bruns, A. E., Perraud, V., Zelenyuk, A., Ezell, M. J., Johnson, S. N., Yu, Y., Imre, D., Finlayson-Pitts, B. J. and Alexander, M. L.: Comparison of FTIR and particle mass spectrometry for the measurement of particulate organic nitrates, *Environ. Sci. Technol.*, 44, 1056–61, doi:10.1021/es9029864, 2010.
- 5 Bruns, E. A., El Haddad, I., Keller, A., Klein, F., Kumar, N. K., Pieber, S. M., Corbin, J. C., Slowik, J. G., Brune, W. H., Baltensperger, U. and Prévôt, A. S. H.: Inter-comparison of laboratory smog chamber and flow reactor systems on organic aerosol yield and composition, *Atmos. Meas. Tech.*, 8, 2315–2332, doi:10.5194/amt-8-2315-2015, 2015.
- 10 Calogirou, A., Jensen, N. R., Nielsen, C. J., Kotzias, D. and Hjorth, J.: Gas-Phase Reactions of Nopinone, 3-Isopropenyl-6-oxo-heptanal, and 5-Methyl-5-vinylnortetrahydrofuran-2-ol with OH, NO₃, and Ozone, *Environ. Sci. Technol.*, 33, 453–460, doi:10.1021/es980530j, 1999a.
- Calogirou, A., Larsen, B. R. and Kotzias, D.: Gas-phase terpene oxidation products: a review, *Atmos. Environ.*, 33, 1423–1439, doi:10.1016/S1352-2310(98)00277-5, 1999b.
- 15 Calvert, J. G., Atkinson, R., Becker, K. H., Kamens, R. M., Seinfeld, J. H., Wallington, T. H. and Yarwood, G.: *The Mechanisms of Atmospheric Oxidation of the Aromatic Hydrocarbons*, Oxford University Press, New York, USA, 2002.
- Canagaratna, M. R., Jayne, J. T., Jimenez, J. L., Allan, J. D., Alfarra, M. R., Zhang, Q., Onasch, T. B., Drewnick, F., Coe, H., Middlebrook, A., Delia, A., Williams, L. R., Trimborn, A. M., Northway, M. J., DeCarlo, P. F., Kolb, C. E., Davidovits, P. and Worsnop, D. R.: Chemical and microphysical characterization of ambient aerosols with the aerodyne aerosol mass spectrometer, *Mass Spectrom. Rev.*, 26, 185–222, doi:10.1002/mas.20115, 2007.
- 20 Canagaratna, M. R., Jimenez, J. L., Kroll, J. H., Chen, Q., Kessler, S. H., Massoli, P., Hildebrandt Ruiz, L., Fortner, E., Williams, L. R., Wilson, K. R., Surratt, J. D., Donahue, N. M., Jayne, J. T. and Worsnop, D. R.: Elemental ratio measurements of organic compounds using aerosol mass spectrometry: characterization, improved calibration, and implications, *Atmos. Chem. Phys.*, 15, 253–272, doi:10.5194/acp-15-253-2015, 2015.
- 25 Canosa-Mas, C. E., King, M. D., Scarr, P. J., Thompson, K. C. and Wayne, R. P.: An experimental study of the gas-phase reactions of the NO₃ radical with three sesquiterpenes: isolongifolene, alloisolongifolene, and α -neoclovene, *Phys. Chem. Chem. Phys.*, 1, 2929–2933, doi:10.1039/a902034i, 1999.
- Chan, A. W. H., Kreisberg, N. M., Hohaus, T., Campuzano-Jost, P., Zhao, Y., Day, D. A., Kaser, L., Karl, T., Hansel, A., Teng, A. P., Ruehl, C. R., Sueper, D. T., Jayne, J. T., Worsnop, D. R., Jimenez, J. L., Hering, S. V. and Goldstein, A. H.: Speciated measurements of semivolatile and intermediate volatility organic compounds (S/IVOCs) in a pine forest during BEACHON-RoMBAS 2011, *Atmos. Chem. Phys.*, 16, 1187–1205, doi:10.5194/acp-16-1187-2016, 2016.
- 30 Chen, Q., Liu, Y., Donahue, N. M., Shilling, J. E. and Martin, S. T.: Particle-phase chemistry of secondary organic material: modeled compared to measured O:C and H:C elemental ratios provide constraints., *Environ. Sci. Technol.*, 45, 4763–70, doi:10.1021/es104398s, 2011.
- 35 Chen, Q., Li, Y. L., McKinney, K. A., Kuwata, M. and Martin, S. T.: Particle mass yield from β -caryophyllene ozonolysis, *Atmos. Chem. Phys.*, 12, 3165–3179, doi:10.5194/acp-12-3165-2012, 2012.
- Chen, Q., Heald, C. L., Jimenez, J. L., Canagaratna, M. R., Zhang, Q., He, L., Huang, X.-F., Campuzano-Jost, P., Palm, B. B., Poulain, L., Kuwata, M., Martin, S. T., Abbatt, J. P. D., Lee, A. K. Y. and Liggio, J.: Elemental composition of organic aerosol: The gap between ambient and laboratory measurements, *Geophys. Res. Lett.*,

42, 4182–4189, doi:10.1002/2015GL063693, 2015.

Chew, A. A., Atkinson, R. and Aschmann, S. M.: Kinetics of the gas-phase reactions of NO₃ radicals with a series of alcohols, glycol ethers, ethers and chloroalkenes, *J. Chem. Soc. Trans.*, 94, 1083–1089, 1998.

5 Chhabra, P. S., Ng, N. L., Canagaratna, M. R., Corrigan, A. L., Russell, L. M., Worsnop, D. R., Flagan, R. C. and Seinfeld, J. H.: Elemental composition and oxidation of chamber organic aerosol, *Atmos. Chem. Phys.*, 11, 8827–8845, doi:10.5194/acp-11-8827-2011, 2011.

Crouse, J. D., Nielsen, L. B., Jørgensen, S., Kjaergaard, H. G. and Wennberg, P. O.: Autoxidation of Organic Compounds in the Atmosphere, *J. Phys. Chem. Lett.*, 4, 3513–3520, doi:10.1021/jz4019207, 2013.

10 Crump, J. G. and Seinfeld, J. H.: Turbulent deposition and gravitational sedimentation of an aerosol in a vessel of arbitrary shape, *J. Aerosol Sci.*, 12, 405–415, doi:10.1016/0021-8502(81)90036-7, 1981.

Cubison, M. J., Ortega, A. M., Hayes, P. L., Farmer, D. K., Day, D., Lechner, M. J., Brune, W. H., Apel, E., Diskin, G. S., Fisher, J. A., Fuelberg, H. E., Hecobian, A., Knapp, D. J., Mikoviny, T., Riemer, D., Sachse, G. W., Sessions, W., Weber, R. J., Weinheimer, A. J., Wisthaler, A. and Jimenez, J. L.: Effects of aging on organic aerosol from open biomass burning smoke in aircraft and laboratory studies, *Atmos. Chem. Phys.*, 11, 12049–12064, doi:10.5194/acp-11-12049-2011, 2011.

15 Day, D. A., Campuzano-Jost, P., Palm, B. B., Hu, W. W., Nault, B. A., Wooldridge, P. J., Cohen, R. C., Docherty, K. S., Huffman, J. A. and Jimenez, J. L.: Evaluation of methods for quantification of bulk particle-phase organic nitrates using real-time aerosol mass spectrometry, *In prep.*, 2017.

20 DeCarlo, P. F., Kimmel, J. R., Trimborn, A., Northway, M. J., Jayne, J. T., Aiken, A. C., Gonin, M., Fuhrer, K., Horvath, T., Docherty, K. S., Worsnop, D. R. and Jimenez, J. L.: Field-Deployable, High-Resolution, Time-of-Flight Aerosol Mass Spectrometer, *Anal. Chem.*, 78, 8281–8289, doi:10.1021/ac061249n, 2006.

Farmer, D. K. and Cohen, R. C.: Observations of HNO₃, ΣAN, ΣPN and NO₂ fluxes: evidence for rapid HO_x chemistry within a pine forest canopy, *Atmos. Chem. Phys.*, 8, 3899–3917, doi:10.5194/acp-8-3899-2008, 2008.

25 Farmer, D. K., Matsunaga, A., Docherty, K. S., Surratt, J. D., Seinfeld, J. H., Ziemann, P. J. and Jimenez, J. L.: Response of an aerosol mass spectrometer to organonitrates and organosulfates and implications for atmospheric chemistry, *P. Natl. Acad. Sci. USA*, 107, 6670–6675, doi:10.1073/pnas.0912340107, 2010.

30 Fry, J. L., Kiendler-Scharr, A., Rollins, A. W., Wooldridge, P. J., Brown, S. S., Fuchs, H., Dubé, W., Mensah, A., dal Maso, M., Tillmann, R., Dorn, H.-P., Brauers, T. and Cohen, R. C.: Organic nitrate and secondary organic aerosol yield from NO₃ oxidation of β-pinene evaluated using a gas-phase kinetics/aerosol partitioning model, *Atmos. Chem. Phys.*, 9, 1431–1449, doi:10.5194/acp-9-1431-2009, 2009.

Fry, J. L., Kiendler-Scharr, A., Rollins, A. W., Brauers, T., Brown, S. S., Dorn, H.-P., Dubé, W. P., Fuchs, H., Mensah, A., Rohrer, F., Tillmann, R., Wahner, A., Wooldridge, P. J., Cohen, R. C. and Dube, W.: SOA from limonene: role of NO₃ in its generation and degradation, *Atmos. Chem. Phys.*, 11, 3879–3894, doi:doi:10.5194/acp-11-3879-2011, 2011.

35 Fry, J. L., Draper, D. C., Zarzana, K. J., Campuzano-Jost, P., Day, D. A., Jimenez, J. L., Brown, S. S., Cohen, R. C., Kaser, L., Hansel, A., Cappellin, L., Karl, T., Hodzic Roux, A., Turnipseed, A., Cantrell, C., Lefer, B. L. and Grossberg, N.: Observations of gas- and aerosol-phase organic nitrates at BEACHON-RoMBAS 2011, *Atmos. Chem. Phys.*, 13, 8585–8605, doi:10.5194/acp-13-8585-2013, 2013.

- Fry, J. L., Draper, D. C., Barsanti, K. C., Smith, J. N., Ortega, J., Winkler, P. M., Lawler, M. J., Brown, S. S., Edwards, P. M., Cohen, R. C. and Lee, L.: Secondary Organic Aerosol Formation and Organic Nitrate Yield from NO₃ Oxidation of Biogenic Hydrocarbons, *Environ. Sci. Technol.*, 48, 11944–11953, doi:10.1021/es502204x, 2014.
- George, I. J. and Abbatt, J. P. D.: Heterogeneous oxidation of atmospheric aerosol particles by gas-phase radicals., *Nat. Chem.*, 2, 713–22, doi:10.1038/nchem.806, 2010.
- George, I. J., Slowik, J. and Abbatt, J. P. D.: Chemical aging of ambient organic aerosol from heterogeneous reaction with hydroxyl radicals, *Geophys. Res. Lett.*, 35, L13811, doi:10.1029/2008GL033884, 2008.
- de Gouw, J. A. and Lovejoy, E. R.: Reactive uptake of ozone by liquid organic compounds, *Geophys. Res. Lett.*, 25, 931–934, doi:10.1029/98GL00515, 1998.
- Hallquist, M., Wängberg, I., Ljungström, E., Barnes, I. and Becker, K.-H.: Aerosol and product yields from NO₃ radical-initiated oxidation of selected monoterpenes, *Environ. Sci. Technol.*, 33, 553–559, doi:10.1021/es980292s, 1999.
- Hallquist, M., Wenger, J. C., Baltensperger, U., Rudich, Y., Simpson, D., Claeys, M., Dommen, J., Donahue, N. M., George, C., Goldstein, A. H., Hamilton, J. F., Herrmann, H., Hoffmann, T., Iinuma, Y., Jang, M., Jenkin, M. E., Jimenez, J. L., Kiendler-Scharr, A., Maenhaut, W., McFiggans, G., Mentel, T. F., Monod, A., Prévôt, A. S. H., Seinfeld, J. H., Surratt, J. D., Szmigielski, R. and Wildt, J.: The formation, properties and impact of secondary organic aerosol: current and emerging issues, *Atmos. Chem. Phys.*, 9, 5155–5236, doi:10.5194/acp-9-5155-2009, 2009.
- Hayes, P. L., Carlton, A. G., Baker, K. R., Ahmadov, R., Washenfelder, R. A., Alvarez, S., Rappenglück, B., Gilman, J. B., Kuster, W. C., de Gouw, J. A., Zotter, P., Prévôt, A. S. H., Szidat, S., Kleindienst, T. E., Offenberg, J. H., Ma, P. K. and Jimenez, J. L.: Modeling the formation and aging of secondary organic aerosols in Los Angeles during CalNex 2010, *Atmos. Chem. Phys.*, 15, 5773–5801, doi:10.5194/acp-15-5773-2015, 2015.
- Heald, C. L., Kroll, J. H., Jimenez, J. L., Docherty, K. S., DeCarlo, P. F., Aiken, A. C., Chen, Q., Martin, S. T., Farmer, D. K. and Artaxo, P.: A simplified description of the evolution of organic aerosol composition in the atmosphere, *Geophys. Res. Lett.*, 37, L08803, doi:10.1029/2010gl042737, 2010.
- Hildebrandt Ruiz, L., Paciga, A. L., Cerully, K. M., Nenes, A., Donahue, N. M. and Pandis, S. N.: Formation and aging of secondary organic aerosol from toluene: changes in chemical composition, volatility, and hygroscopicity, *Atmos. Chem. Phys.*, 15, 8301–8313, doi:10.5194/acp-15-8301-2015, 2015.
- [Hu, W., Palm, B. B., Day, D. A., Campuzano-Jost, P., Krechmer, J. E., Peng, Z., de Sá, S. S., Martin, S. T., Alexander, M. L., Baumann, K., Hacker, L., Kiendler-Scharr, A., Koss, A. R., de Gouw, J. A., Goldstein, A. H., Seco, R., Sjostedt, S. J., Park, J.-H., Guenther, A. B., Kim, S., Canonaco, F., Prévôt, A. S. H., Brune, W. H. and Jimenez, J. L.: Volatility and lifetime against OH heterogeneous reaction of ambient isoprene-epoxydiols-derived secondary organic aerosol \(IEPOX-SOA\), *Atmos. Chem. Phys.*, 16, 11563–11580, doi:10.5194/acp-16-11563-2016, 2016.](#)
- Iannone, R., Xiao, S. and Bertram, A. K.: Potentially important nighttime heterogeneous chemistry: NO₃ with aldehydes and N₂O₅ with alcohols, *Phys. Chem. Chem. Phys.*, 13, 10214, doi:10.1039/c1cp20294d, 2011.
- Jaoui, M., Leungsakul, S. and Kamens, R. M.: Gas and Particle Products Distribution from the Reaction of β-Caryophyllene with Ozone, *J. Atmos. Chem.*, 45, 261–287, doi:10.1023/A:1024263430285, 2003.
- Jaoui, M., Kleindienst, T. E., Docherty, K. S., Lewandowski, M. and Offenberg, J. H.: Secondary organic aerosol formation from the oxidation of a series of sesquiterpenes: α-cedrene, β-caryophyllene, α-humulene and α-

farnesene with O₃, OH and NO₃ radicals, *Environ. Chem.*, 10, 178, doi:10.1071/EN13025, 2013.

Jimenez, J. L., Canagaratna, M. R., Donahue, N. M., Prevot, A. S. H., Zhang, Q., Kroll, J. H., DeCarlo, P. F., Allan, J. D., Coe, H., Ng, N. L., Aiken, A. C., Docherty, K. S., Ulbrich, I. M., Grieshop, A. P., Robinson, A. L., Duplissy, J., Smith, J. D., Wilson, K. R., Lanz, V. A., Hueglin, C., Sun, Y. L., Tian, J., Laaksonen, A., Raatikainen, T., Rautiainen, J., Vaattovaara, P., Ehn, M., Kulmala, M., Tomlinson, J. M., Collins, D. R., Cubison, M. J., Dunlea, J., Huffman, J. A., Onasch, T. B., Alfarra, M. R., Williams, P. I., Bower, K., Kondo, Y., Schneider, J., Drewnick, F., Borrmann, S., Weimer, S., Demerjian, K., Salcedo, D., Cottrell, L., Griffin, R., Takami, A., Miyoshi, T., Hatakeyama, S., Shimojo, A., Sun, J. Y., Zhang, Y. M., Dzepina, K., Kimmel, J. R., Sueper, D., Jayne, J. T., Herndon, S. C., Trimborn, A. M., Williams, L. R., Wood, E. C., Middlebrook, A. M., Kolb, C. E., Baltensperger, U. and Worsnop, D. R.: Evolution of Organic Aerosols in the Atmosphere, *Science*, 326, 1525–1529, doi:10.1126/science.1180353, 2009.

Kahnt, A., Iinuma, Y., Mutzel, A., Böge, O., Claeys, M. and Herrmann, H.: Campholenic aldehyde ozonolysis: a mechanism leading to specific biogenic secondary organic aerosol constituents, *Atmos. Chem. Phys.*, 14, 719–736, doi:10.5194/acp-14-719-2014, 2014.

Kang, E., Root, M. J., Toohey, D. W. and Brune, W. H.: Introducing the concept of Potential Aerosol Mass (PAM), *Atmos. Chem. Phys.*, 7, 5727–5744, doi:10.5194/acp-7-5727-2007, 2007.

Kang, E., Toohey, D. W. and Brune, W. H.: Dependence of SOA oxidation on organic aerosol mass concentration and OH exposure: experimental PAM chamber studies, *Atmos. Chem. Phys.*, 11, 1837–1852, doi:10.5194/acp-11-1837-2011, 2011.

Kang, H., Day, D. A., Krechmer, J. E., Ayres, B. R., Keehan, N. I., Thompson, S. L., Hu, W., Campuzano-Jost, P., Schroder, J. C., Stark, H., Ranney, A. P., Ziemann, P. J., Zarzana, K. J., Wild, R. J., Dube, W. P., Brown, S. S., Fry, J. L. and Jimenez, J. L.: A33E-0280: Secondary organic aerosol mass yields from the dark NO₃ oxidation of α -pinene and Δ -carene: effect of RO₂ radical fate, in American Geophysical Union Fall Meeting, 2016.

Karjalainen, P., Timonen, H., Saukko, E., Kuuluvainen, H., Saarikoski, S., Aakko-Saksa, P., Murtonen, T., Bloss, M., Dal Maso, M., Simonen, P., Ahlberg, E., Svenningsson, B., Brune, W. H., Hillamo, R., Keskinen, J. and Rönkkö, T.: Time-resolved characterization of primary particle emissions and secondary particle formation from a modern gasoline passenger car, *Atmos. Chem. Phys.*, 16, 8559–8570, doi:10.5194/acp-16-8559-2016, 2016.

Karl, T., Hansel, A., Cappellin, L., Kaser, L., Herdinger-Blatt, I. and Jud, W.: Selective measurements of isoprene and 2-methyl-3-buten-2-ol based on NO⁺ ionization mass spectrometry, *Atmos. Chem. Phys.*, 12, 11877–11884, doi:10.5194/acp-12-11877-2012, 2012.

Kaser, L., Karl, T., Schnitzhofer, R., Graus, M., Herdinger-Blatt, I. S., DiGangi, J. P., Sive, B., Turnipseed, A., Hornbrook, R. S., Zheng, W., Flocke, F. M., Guenther, A., Keutsch, F. N., Apel, E. and Hansel, A.: Comparison of different real time VOC measurement techniques in a ponderosa pine forest, *Atmos. Chem. Phys.*, 13, 2893–2906, doi:10.5194/acp-13-2893-2013, 2013.

Keller, A. and Burtscher, H.: A continuous photo-oxidation flow reactor for a defined measurement of the SOA formation potential of wood burning emissions, *J. Aerosol Sci.*, 49, 9–20, doi:10.1016/j.jaerosci.2012.02.007, 2012.

Kim, S., Karl, T., Guenther, A., Tyndall, G., Orlando, J., Harley, P., Rasmussen, R. and Apel, E.: Emissions and ambient distributions of Biogenic Volatile Organic Compounds (BVOC) in a ponderosa pine ecosystem: interpretation of PTR-MS mass spectra, *Atmos. Chem. Phys.*, 10, 1759–1771, doi:10.5194/acp-10-1759-2010,

2010.

Kim, S., Wolfe, G. M., Mauldin, L., Cantrell, C., Guenther, A., Karl, T., Turnipseed, A., Greenberg, J., Hall, S. R., Ullmann, K., Apel, E., Hornbrook, R., Kajii, Y., Nakashima, Y., Keutsch, F. N., DiGangi, J. P., Henry, S. B., Kaser, L., Schnitzhofer, R., Graus, M., Hansel, A., Zheng, W. and Flocke, F. F.: Evaluation of HO_x sources and cycling using measurement-constrained model calculations in a 2-methyl-3-butene-2-ol (MBO) and monoterpene (MT) dominated ecosystem, *Atmos. Chem. Phys.*, 13, 2031–2044, doi:10.5194/acp-13-2031-2013, 2013.

[Knap, H. C., Schmidt, J. A. and Jørgensen, S.: Hydrogen shift reactions in four methyl-buten-ol \(MBO\) peroxy radicals and their impact on the atmosphere, *Atmos. Environ.*, 147, 79–87, doi:10.1016/j.atmosenv.2016.09.064, 2016.](#)

Knote, C., Hodzic, A. and Jimenez, J. L.: The effect of dry and wet deposition of condensable vapors on secondary organic aerosols concentrations over the continental US, *Atmos. Chem. Phys.*, 15, 1–18, doi:10.5194/acp-15-1-2015, 2015.

Krechmer, J. E., Coggon, M. M., Massoli, P., Nguyen, T. B., Crouse, J. D., Hu, W., Day, D. A., Tyndall, G. S., Henze, D. K., Rivera-Rios, J. C., Nowak, J. B., Kimmel, J. R., Mauldin, R. L., Stark, H., Jayne, J. T., Sipilä, M., Junninen, H., Clair, J. M. St., Zhang, X., Feiner, P. A., Zhang, L., Miller, D. O., Brune, W. H., Keutsch, F. N., Wennberg, P. O., Seinfeld, J. H., Worsnop, D. R., Jimenez, J. L. and Canagaratna, M. R.: Formation of Low Volatility Organic Compounds and Secondary Organic Aerosol from Isoprene Hydroxyhydroperoxide Low-NO Oxidation, *Environ. Sci. Technol.*, 49, 10330–10339, doi:10.1021/acs.est.5b02031, 2015.

Kroll, J. H. and Seinfeld, J. H.: Chemistry of secondary organic aerosol: Formation and evolution of low-volatility organics in the atmosphere, *Atmos. Environ.*, 42, 3593–3624, doi:10.1016/j.atmosenv.2008.01.003, 2008.

Kroll, J. H., Donahue, N. M., Jimenez, J. L., Kessler, S. H., Canagaratna, M. R., Wilson, K. R., Altieri, K. E., Mazzoleni, L. R., Wozniak, A. S., Bluhm, H., Mysak, E. R., Smith, J. D., Kolb, C. E. and Worsnop, D. R.: Carbon oxidation state as a metric for describing the chemistry of atmospheric organic aerosol., *Nat. Chem.*, 3, 133–9, doi:10.1038/nchem.948, 2011.

Kuwata, M., Zorn, S. R. and Martin, S. T.: Using elemental ratios to predict the density of organic material composed of carbon, hydrogen, and oxygen., *Environ. Sci. Technol.*, 46, 787–94, doi:10.1021/es202525q, 2012.

La, Y. S., Camredon, M., Ziemann, P. J., Valorso, R., Matsunaga, A., Lannuque, V., Lee-Taylor, J., Hodzic, A., Madronich, S. and Aumont, B.: Impact of chamber wall loss of gaseous organic compounds on secondary organic aerosol formation: explicit modeling of SOA formation from alkane and alkene oxidation, *Atmos. Chem. Phys.*, 16, 1417–1431, doi:10.5194/acp-16-1417-2016, 2016.

Lambe, A. T., Onasch, T. B., Massoli, P., Croasdale, D. R., Wright, J. P., Ahern, A. T., Williams, L. R., Worsnop, D. R., Brune, W. H. and Davidovits, P.: Laboratory studies of the chemical composition and cloud condensation nuclei (CCN) activity of secondary organic aerosol (SOA) and oxidized primary organic aerosol (OPOA), *Atmos. Chem. Phys.*, 11, 8913–8928, doi:10.5194/acp-11-8913-2011, 2011.

Lambe, A. T., Onasch, T. B., Croasdale, D. R., Wright, J. P., Martin, A. T., Franklin, J. P., Massoli, P., Kroll, J. H., Canagaratna, M. R., Brune, W. H., Worsnop, D. R. and Davidovits, P.: Transitions from Functionalization to Fragmentation Reactions of Laboratory Secondary Organic Aerosol (SOA) Generated from the OH Oxidation of Alkane Precursors, *Environ. Sci. Technol.*, 46, 5430–5437, doi:10.1021/es300274t, 2012.

Lambe, A. T., Ahern, A. T., Wright, J. P., Croasdale, D. R., Davidovits, P. and Onasch, T. B.: Oxidative aging and

- cloud condensation nuclei activation of laboratory combustion soot, *J. Aerosol Sci.*, **79**, 31–39, doi:10.1016/j.jaerosci.2014.10.001, 2014.
- Lambe, A. T., Chhabra, P. S., Onasch, T. B., Brune, W. H., Hunter, J. F., Kroll, J. H., Cummings, M. J., Brogan, J. F., Parmar, Y., Worsnop, D. R., Kolb, C. E. and Davidovits, P.: Effect of oxidant concentration, exposure time, and seed particles on secondary organic aerosol chemical composition and yield, *Atmos. Chem. Phys.*, **15**, 3063–3075, doi:10.5194/acp-15-3063-2015, 2015.
- Lee, A., Goldstein, A. H., Kroll, J. H., Ng, N. L., Varutbangkul, V., Flagan, R. C. and Seinfeld, J. H.: Gas-phase products and secondary aerosol yields from the photooxidation of 16 different terpenes, *J. Geophys. Res.*, **111**, D17305, doi:10.1029/2006JD007050, 2006.
- Li, R., Palm, B. B., Borbon, A., Graus, M., Warneke, C., Ortega, A. M., Day, D. A., Brune, W. H., Jimenez, J. L., de Gouw, J. A. and Brune, B.: Laboratory studies on secondary organic aerosol formation from crude oil vapors., *Environ. Sci. Technol.*, **47**, 12566–74, doi:10.1021/es402265y, 2013.
- Li, R., Palm, B. B., Ortega, A. M., Hlywiak, J., Hu, W., Peng, Z., Day, D. A., Knote, C., Brune, W. H., de Gouw, J. A. and Jimenez, J. L.: Modeling the Radical Chemistry in an Oxidation Flow Reactor: Radical Formation and Recycling, Sensitivities, and the OH Exposure Estimation Equation, *J. Phys. Chem. A*, **119**, 4418–4432, doi:10.1021/jp509534k, 2015.
- Liu, S., Shilling, J. E., Song, C., Hiranuma, N., Zaveri, R. A. and Russell, L. M.: Hydrolysis of Organonitrate Functional Groups in Aerosol Particles, *Aerosol Sci. Technol.*, **46**, 1359–1369, doi:10.1080/02786826.2012.716175, 2012.
- Massoli, P., Lambe, A. T., Ahern, A. T., Williams, L. R., Ehn, M., Mikkilä, J., Canagaratna, M. R., Brune, W. H., Onasch, T. B., Jayne, J. T., Petäjä, T., Kulmala, M., Laaksonen, A., Kolb, C. E., Davidovits, P. and Worsnop, D. R.: Relationship between aerosol oxidation level and hygroscopic properties of laboratory generated secondary organic aerosol (SOA) particles, *Geophys. Res. Lett.*, **37**, L24801, doi:10.1029/2010GL045258, 2010.
- Matsunaga, A. and Ziemann, P. J.: Gas-Wall Partitioning of Organic Compounds in a Teflon Film Chamber and Potential Effects on Reaction Product and Aerosol Yield Measurements, *Aerosol Sci. Technol.*, **44**, 881–892, doi:10.1080/02786826.2010.501044, 2010.
- McMurry, P. H. and Rader, D. J.: Aerosol Wall Losses in Electrically Charged Chambers, *Aerosol Sci. Technol.*, **4**, 249–268, doi:10.1080/02786828508959054, 1985.
- Moldanova, J. and Ljungström, E.: Modeling of particle formation from NO₃ oxidation of selected monoterpenes, *J. Aerosol Sci.*, **31**, 1317–1333, doi:10.1016/S0021-8502(00)00041-0, 2000.
- Morris, J. W., Davidovits, P., Jayne, J. T., Jimenez, J. L., Shi, Q., Kolb, C. E., Worsnop, D. R., Barney, W. S. and Cass, G.: Kinetics of submicron oleic acid aerosols with ozone: A novel aerosol mass spectrometric technique, *Geophys. Res. Lett.*, **29**, 71-1-71–4, doi:10.1029/2002GL014692, 2002.
- Myhre, G., Shindell, D., Bréon, F.-M., Collins, W., Fuglestvedt, J., Huang, J., Koch, D., Lamarque, J.-F., Lee, D., Mendoza, B., Nakajima, T., Robock, A., Stephens, G., Takemura, T. and Zhang, H.: Anthropogenic and Natural Radiative Forcing, in *Climate Change 2013: The Physical Science Basis. Contribution of Working Group I to the Fifth Assessment Report of the Intergovernmental Panel on Climate Change*, edited by Stocker, T. F., Qin, D., Plattner, G.-K., Tignor, M., Allen, S. K., Boschung, J., Nauels, A., Xia, Y., Bex, V., and Midgley, P. M., Cambridge University Press, Cambridge, UK, New York, NY, USA, 659–740, 2013.

- Nah, T., McVay, R. C., Zhang, X., Boyd, C. M., Seinfeld, J. H. and Ng, N. L.: Influence of seed aerosol surface area and oxidation rate on vapor wall deposition and SOA mass yields: a case study with α -pinene ozonolysis, *Atmos. Chem. Phys.*, **16**, 9361–9379, doi:10.5194/acp-16-9361-2016, 2016.
- 5 Ng, N. L., Kroll, J. H., Keywood, M. D., Bahreini, R., Varutbangkul, V., Flagan, R. C., Seinfeld, J. H., Lee, A. and Goldstein, A. H.: Contribution of first- versus second-generation products to secondary organic aerosols formed in the oxidation of biogenic hydrocarbons, *Environ. Sci. Technol.*, **40**, 2283–2297, doi:10.1021/es052269u, 2006.
- Ng, N. L., Canagaratna, M. R., Jimenez, J. L., Chhabra, P. S., Seinfeld, J. H. and Worsnop, D. R.: Changes in organic aerosol composition with aging inferred from aerosol mass spectra, *Atmos. Chem. Phys.*, **11**, 6465–6474, doi:10.5194/acp-11-6465-2011, 2011.
- 10 Ng, N. L., Brown, S. S., Archibald, A. T., Atlas, E., Cohen, R. C., Crowley, J. N., Day, D. A., Donahue, N. M., Fry, J. L., Fuchs, H., Griffin, R. J., Guzman, M. I., Hermann, H., Hodzic, A., Iinuma, Y., Jimenez, J. L., Kiendler-Scharr, A., Lee, B. H., Luecken, D. J., Mao, J., McLaren, R., Mutzel, A., Osthoff, H. D., Ouyang, B., Picquet-Varrault, B., Platt, U., Pye, H. O. T., Rudich, Y., Schwantes, R. H., Shiraiwa, M., Stutz, J., Thornton, J. A., Tilgner, A., Williams, B. J. and Zaveri, R. A.: Nitrate radicals and biogenic volatile organic compounds: oxidation, mechanisms and organic aerosol, *Atmos. Chem. Phys. Discuss.*, **1**–111, doi:10.5194/acp-2016-734, 2016.
- 15 Nguyen, T. B., Crounse, J. D., Teng, A. P., St. Clair, J. M., Paulot, F., Wolfe, G. M. and Wennberg, P. O.: Rapid deposition of oxidized biogenic compounds to a temperate forest, *P. Natl. Acad. Sci. USA*, **112**, E392–E401, doi:10.1073/pnas.1418702112, 2015.
- Orlando, J. J. and Tyndall, G. S.: Laboratory studies of organic peroxy radical chemistry: an overview with emphasis on recent issues of atmospheric significance, *Chem. Soc. Rev.*, **41**, 6294, doi:10.1039/c2cs35166h, 2012.
- Ortega, A. M., Day, D. A., Cubison, M. J., Brune, W. H., Bon, D., de Gouw, J. A. and Jimenez, J. L.: Secondary organic aerosol formation and primary organic aerosol oxidation from biomass-burning smoke in a flow reactor during FLAME-3, *Atmos. Chem. Phys.*, **13**, 11551–11571, doi:10.5194/acp-13-11551-2013, 2013.
- 25 Ortega, A. M., Hayes, P. L., Peng, Z., Palm, B. B., Hu, W., Day, D. A., Li, R., Cubison, M. J., Brune, W. H., Graus, M., Warneke, C., Gilman, J. B., Kuster, W. C., de Gouw, J., Gutiérrez-Montes, C. and Jimenez, J. L.: Real-time measurements of secondary organic aerosol formation and aging from ambient air in an oxidation flow reactor in the Los Angeles area, *Atmos. Chem. Phys.*, **16**, 7411–7433, doi:10.5194/acp-16-7411-2016, 2016.
- 30 Ortega, J., Turnipseed, A., Guenther, A. B., Karl, T. G., Day, D. A., Gochis, D., Huffman, J. A., Prenni, A. J., Levin, E. J. T., Kreidenweis, S. M., DeMott, P. J., Tobo, Y., Patton, E. G., Hodzic, A., Cui, Y. Y., Harley, P. C., Hornbrook, R. S., Apel, E. C., Monson, R. K., Eller, A. S. D., Greenberg, J. P., Barth, M. C., Campuzano-Jost, P., Palm, B. B., Jimenez, J. L., Aiken, A. C., Dubey, M. K., Geron, C., Offenberg, J., Ryan, M. G., Fornwalt, P. J., Pryor, S. C., Keutsch, F. N., DiGangi, J. P., Chan, A. W. H., Goldstein, A. H., Wolfe, G. M., Kim, S., Kaser, L., Schnitzhofer, R., Hansel, A., Cantrell, C. A., Mauldin, R. L. and Smith, J. N.: Overview of the Manitou Experimental Forest
- 35 Observatory: site description and selected science results from 2008 to 2013, *Atmos. Chem. Phys.*, **14**, 6345–6367, doi:10.5194/acp-14-6345-2014, 2014.
- Palm, B. B., Campuzano-Jost, P., Ortega, A. M., Day, D. A., Kaser, L., Jud, W., Karl, T., Hansel, A., Hunter, J. F., Cross, E. S., Kroll, J. H., Peng, Z., Brune, W. H. and Jimenez, J. L.: In situ secondary organic aerosol formation from ambient pine forest air using an oxidation flow reactor, *Atmos. Chem. Phys.*, **16**, 2943–2970, doi:10.5194/acp-16-2943-2016, 2016.
- 40

- Pathak, R., Donahue, N. M. and Pandis, S. N.: Ozonolysis of β -Pinene: Temperature Dependence of Secondary Organic Aerosol Mass Fraction, *Environ. Sci. Technol.*, 42, 5081–5086, doi:10.1021/es070721z, 2008.
- Pathak, R. K., Presto, A. A., Lane, T. E., Stanier, C. O., Donahue, N. M. and Pandis, S. N.: Ozonolysis of α -pinene: parameterization of secondary organic aerosol mass fraction, *Atmos. Chem. Phys.*, 7, 3811–3821, doi:10.5194/acp-7-3811-2007, 2007.
- Peng, Z., Day, D. A., Stark, H., Li, R., Lee-Taylor, J., Palm, B. B., Brune, W. H. and Jimenez, J. L.: HO_x radical chemistry in oxidation flow reactors with low-pressure mercury lamps systematically examined by modeling, *Atmos. Meas. Tech.*, 8, 4863–4890, doi:10.5194/amt-8-4863-2015, 2015.
- Peng, Z., Day, D. A., Ortega, A. M., Palm, B. B., Hu, W., Stark, H., Li, R., Tsigaridis, K., Brune, W. H. and Jimenez, J. L.: Non-OH chemistry in oxidation flow reactors for the study of atmospheric chemistry systematically examined by modeling, *Atmos. Chem. Phys.*, 16, 4283–4305, doi:10.5194/acp-16-4283-2016, 2016.
- Pierce, J. R., Engelhart, G. J., Hildebrandt, L., Weitkamp, E. A., Pathak, R. K., Donahue, N. M., Robinson, A. L., Adams, P. J. and Pandis, S. N.: Constraining Particle Evolution from Wall Losses, Coagulation, and Condensation-Evaporation in Smog-Chamber Experiments: Optimal Estimation Based on Size Distribution Measurements, *Aerosol Sci. Technol.*, 42, 1001–1015, doi:10.1080/02786820802389251, 2008.
- Pope, C. A. and Dockery, D. W.: Health Effects of Fine Particulate Air Pollution: Lines that Connect, *J. Air Waste Manage. Assoc.*, 56, 709–742, doi:10.1080/10473289.2006.10464485, 2006.
- Richters, S., Herrmann, H. and Berndt, T.: Gas-phase rate coefficients of the reaction of ozone with four sesquiterpenes at 295 ± 2 K, *Phys. Chem. Chem. Phys.*, 17, 11658–11669, doi:10.1039/C4CP05542J, 2015.
- Rogge, W. F., Hildemann, L. M., Mazurek, M. A., Cass, G. R. and Simoneit, B. R. T.: Sources of fine organic aerosol. 1. Charbroilers and meat cooking operations, *Environ. Sci. Technol.*, 25, 1112–1125, doi:10.1021/es00018a015, 1991.
- Saukko, E., Lambe, A. T., Massoli, P., Koop, T., Wright, J. P., Croasdale, D. R., Pedernera, D. A., Onasch, T. B., Laaksonen, A., Davidovits, P., Worsnop, D. R. and Virtanen, A.: Humidity-dependent phase state of SOA particles from biogenic and anthropogenic precursors, *Atmos. Chem. Phys.*, 12, 7517–7529, doi:10.5194/acp-12-7517-2012, 2012.
- Shilling, J. E., Chen, Q., King, S. M., Rosenoern, T., Kroll, J. H., Worsnop, D. R., McKinney, K. A. and Martin, S. T.: Particle mass yield in secondary organic aerosol formed by the dark ozonolysis of α -pinene, *Atmos. Chem. Phys.*, 8, 2073–2088, doi:10.5194/acp-8-2073-2008, 2008.
- Shrivastava, M., Thornton, J., Cappa, C., Fan, J., Goldstein, A., Guenther, A., Jimenez, J. L., Kuang, C., Laskin, A., Martin, S., Ng, N. L., Petaja, T., Pierce, J., Rasch, P., Roldin, P., Seinfeld, J., Shilling, J., Smith, J., Volkamer, R., Wang, J., Worsnop, D., Zaveri, R., Zelenyuk, A. and Zhang, Q.: Recent advances in understanding secondary organic aerosols: implications for global climate forcing, *Rev. Geophys.*, submitted, 2016.
- Smith, J. D., Kroll, J. H., Cappa, C. D., Che, D. L., Liu, C. L., Ahmed, M., Leone, S. R., Worsnop, D. R. and Wilson, K. R.: The heterogeneous reaction of hydroxyl radicals with sub-micron squalane particles: a model system for understanding the oxidative aging of ambient aerosols, *Atmos. Chem. Phys.*, 9, 3209–3222, doi:10.5194/acp-9-3209-2009, 2009.
- Spittler, M., Barnes, I., Bejan, I., Brockmann, K. J., Benter, T. and Wirtz, K.: Reactions of NO₃ radicals with limonene and α -pinene: Product and SOA formation, *Atmos. Environ.*, 40, 116–127,

doi:10.1016/j.atmosenv.2005.09.093, 2006.

Tanaka, P. L., Allen, D. T. and Mullins, C. B.: An environmental chamber investigation of chlorine-enhanced ozone formation in Houston, Texas, *J. Geophys. Res.*, **108**, 4576, doi:10.1029/2002JD003314, 2003.

5 Tasoglou, A. and Pandis, S. N.: Formation and chemical aging of secondary organic aerosol during the β -caryophyllene oxidation, *Atmos. Chem. Phys.*, **15**, 6035–6046, doi:10.5194/acp-15-6035-2015, 2015.

Thornton, J. A., Wooldridge, P. J. and Cohen, R. C.: Atmospheric NO_2 : In Situ Laser-Induced Fluorescence Detection at Parts per Trillion Mixing Ratios, *Anal. Chem.*, **72**, 528–539, doi:10.1021/ac9908905, 2000.

10 Timonen, H., Karjalainen, P., Saukko, E., Saarikoski, S., Aakko-Saksa, P., Simonen, P., Murtonen, T., Dal Maso, M., Kuuluvainen, H., Ahlberg, E., Svenningsson, B., Pagels, J., Brune, W. H., Keskinen, J., Worsnop, D. R., Hillamo, R. and Rönkkö, T.: Influence of fuel ethanol content on primary emissions and secondary aerosol formation potential for a modern flex-fuel gasoline vehicle, *Atmos. Chem. Phys. Discuss.*, 1–28, doi:10.5194/acp-2016-579, 2016.

15 Tkacik, D. S., Lambe, A. T., Jathar, S., Li, X., Presto, A. A., Zhao, Y., Blake, D., Meinardi, S., Jayne, J. T., Croteau, P. L. and Robinson, A. L.: Secondary Organic Aerosol Formation from in-Use Motor Vehicle Emissions Using a Potential Aerosol Mass Reactor, *Environ. Sci. Technol.*, **48**, 11235–11242, doi:10.1021/es502239v, 2014.

20 Tsigaridis, K., Daskalakis, N., Kanakidou, M., Adams, P. J., Artaxo, P., Bahadur, R., Balkanski, Y., Bauer, S. E., Bellouin, N., Benedetti, A., Bergman, T., Berntsen, T. K., Beukes, J. P., Bian, H., Carslaw, K. S., Chin, M., Curci, G., Diehl, T., Easter, R. C., Ghan, S. J., Gong, S. L., Hodzic, A., Hoyle, C. R., Iversen, T., Jathar, S., Jimenez, J. L., Kaiser, J. W., Kirkevåg, A., Koch, D., Kokkola, H., Lee, Y. H., Lin, G., Liu, X., Luo, G., Ma, X., Mann, G. W., Mihalopoulos, N., Morcrette, J.-J., Müller, J.-F., Myhre, G., Myriokefalitakis, S., Ng, N. L., O'Donnell, D., Penner, J. E., Pozzoli, L., Pringle, K. J., Russell, L. M., Schulz, M., Sciare, J., Seland, Ø., Shindell, D. T., Sillman, S., Skeie, R. B., Spracklen, D., Stavrakou, T., Steenrod, S. D., Takemura, T., Tiitta, P., Tilmes, S., Tost, H., van Noije, T., van Zyl, P. G., von Salzen, K., Yu, F., Wang, Z., Wang, Z., Zaveri, R. A., Zhang, H., Zhang, K., Zhang, Q. and Zhang, X.: The AeroCom evaluation and intercomparison of organic aerosol in global models, *Atmos. Chem. Phys.*, **14**, 10845–10895, doi:10.5194/acp-14-10845-2014, 2014.

25 Vereecken, L. and Peeters, J.: Enhanced H-atom abstraction from pinonaldehyde, pinonic acid, pinic acid, and related compounds: theoretical study of C–H bond strengths, *Phys. Chem. Chem. Phys.*, **4**, 467–472, doi:10.1039/b109370c, 2002.

30 Volkamer, R., Jimenez, J. L., San Martini, F., Dzepina, K., Zhang, Q., Salcedo, D., Molina, L. T., Worsnop, D. R. and Molina, M. J.: Secondary organic aerosol formation from anthropogenic air pollution: Rapid and higher than expected, *Geophys. Res. Lett.*, **33**, L17811, doi:10.1029/2006GL026899, 2006.

Wagner, N. L., Dubé, W. P., Washenfelder, R. A., Young, C. J., Pollack, I. B., Ryerson, T. B. and Brown, S. S.: Diode laser-based cavity ring-down instrument for NO_3 , N_2O_5 , NO , NO_2 and O_3 from aircraft, *Atmos. Meas. Tech.*, **4**, 1227–1240, doi:10.5194/amt-4-1227-2011, 2011.

35 Winterhalter, R., Herrmann, F., Kanawati, B., Nguyen, T. L., Peeters, J., Vereecken, L. and Moortgat, G. K.: The gas-phase ozonolysis of β -caryophyllene ($\text{C}_{15}\text{H}_{24}$). Part I: an experimental study, *Phys. Chem. Chem. Phys.*, **11**, 4152, doi:10.1039/b817824k, 2009.

Wolfe, G. M., Cantrell, C., Kim, S., Mauldin III, R. L., Karl, T., Harley, P., Turnipseed, A., Zheng, W., Flocke, F., Apel, E. C., Hornbrook, R. S., Hall, S. R., Ullmann, K., Henry, S. B., DiGangi, J. P., Boyle, E. S., Kaser, L., Schnitzhofer, R.,

Hansel, A., Graus, M., Nakashima, Y., Kajii, Y., Guenther, A. and Keutsch, F. N.: Missing peroxy radical sources within a summertime ponderosa pine forest, *Atmos. Chem. Phys.*, 14, 4715–4732, doi:10.5194/acp-14-4715-2014, 2014.

5 Yu, J., Griffin, R. J., Cocker, D. R., Flagan, R. C., Seinfeld, J. H. and Blanchard, P.: Observation of gaseous and particulate products of monoterpene oxidation in forest atmospheres, *Geophys. Res. Lett.*, 26, 1145–1148, doi:10.1029/1999GL900169, 1999.

10 Zhang, Q., Jimenez, J. L., Canagaratna, M. R., Allan, J. D., Coe, H., Ulbrich, I., Alfarra, M. R., Takami, A., Middlebrook, A. M., Sun, Y. L., Dzepina, K., Dunlea, E., Docherty, K., DeCarlo, P. F., Salcedo, D., Onasch, T., Jayne, J. T., Miyoshi, T., Shimojo, A., Hatakeyama, S., Takegawa, N., Kondo, Y., Schneider, J., Drewnick, F., Borrmann, S., Weimer, S., Demerjian, K., Williams, P., Bower, K., Bahreini, R., Cottrell, L., Griffin, R. J., Rautiainen, J., Sun, J. Y., Zhang, Y. M. and Worsnop, D. R.: Ubiquity and dominance of oxygenated species in organic aerosols in anthropogenically influenced Northern Hemisphere midlatitudes, *Geophys. Res. Lett.*, 34, L13801, doi:10.1029/2007GL029979, 2007. H., Worton, D. R., Lewandowski, M., Ortega, J., Rubitschun, C. L., Park, J.-H., Kristensen, K., Campuzano-Jost, P., Day, D. A., Jimenez, J. L., Jaoui, M., Offenberg, J. H., Kleindienst, T. E., Gilman, J., Kuster, W. C., de Gouw, J., Park, C., Schade, G. W., Frossard, A. A., Russell, L., Kaser, L., Jud, W., Hansel, A., Cappellin, L., Karl, T., Glasius, M., Guenther, A., Goldstein, A. H., Seinfeld, J. H., Gold, A., Kamens, R. M. and Surratt, J. D.: Organosulfates as Tracers for Secondary Organic Aerosol (SOA) Formation from 2-Methyl-3-Buten-2-ol (MBO) in the Atmosphere, *Environ. Sci. Technol.*, 46, 9437–9446, doi:10.1021/es301648z, 2012.

15 Zhang, Q., Jimenez, J. L., Canagaratna, M. R., Allan, J. D., Coe, H., Ulbrich, I., Alfarra, M. R., Takami, A., Middlebrook, A. M., Sun, Y. L., Dzepina, K., Dunlea, E., Docherty, K., DeCarlo, P. F., Salcedo, D., Onasch, T., Jayne, J. T., Miyoshi, T., Shimojo, A., Hatakeyama, S., Takegawa, N., Kondo, Y., Schneider, J., Drewnick, F., Borrmann, S., Weimer, S., Demerjian, K., Williams, P., Bower, K., Bahreini, R., Cottrell, L., Griffin, R. J., Rautiainen, J., Sun, J. Y., Zhang, Y. M. and Worsnop, D. R.: Ubiquity and dominance of oxygenated species in organic aerosols in anthropogenically-influenced Northern Hemisphere midlatitudes, *Geophys. Res. Lett.*, 34, L13801, doi:10.1029/2007GL029979, 2007.

20 Zhang, X., Cappa, C. D., Jathar, S. H., McVay, R. C., Ensberg, J. J., Kleeman, M. J. and Seinfeld, J. H.: Influence of vapor wall loss in laboratory chambers on yields of secondary organic aerosol, *P. Natl. Acad. Sci. USA*, 111, 5802–7, doi:10.1073/pnas.1404727111, 2014.

30 Zhao, D. F., Kaminski, M., Schlag, P., Fuchs, H., Acir, I.-H., Bohn, B., Häsel, R., Kiendler-Scharr, A., Rohrer, F., Tillmann, R., Wang, M. J., Wegener, R., Wildt, J., Wahner, A. and Mentel, T. F.: Secondary organic aerosol formation from hydroxyl radical oxidation and ozonolysis of monoterpenes, *Atmos. Chem. Phys.*, 15, 991–1012, doi:10.5194/acp-15-991-2015, 2015.

Ziemann, P. J.: Aerosol products, mechanisms, and kinetics of heterogeneous reactions of ozone with oleic acid in pure and mixed particles, *Faraday Discuss.*, 130, 469, doi:10.1039/b417502f, 2005.

35

Figures

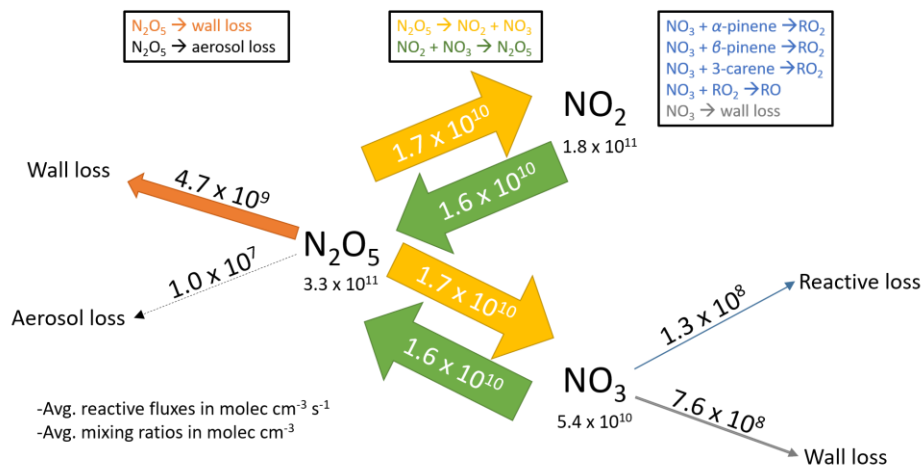
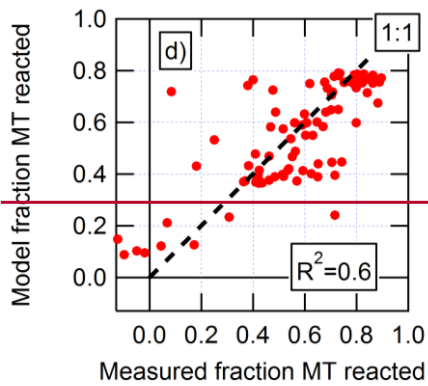
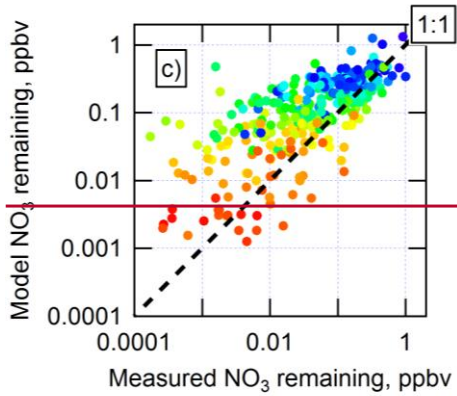
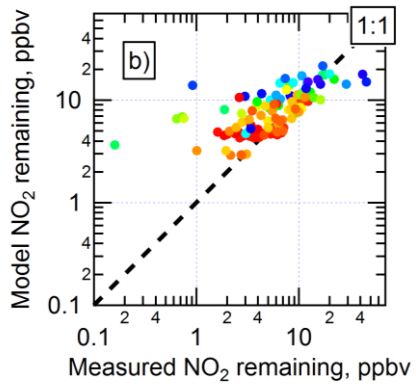
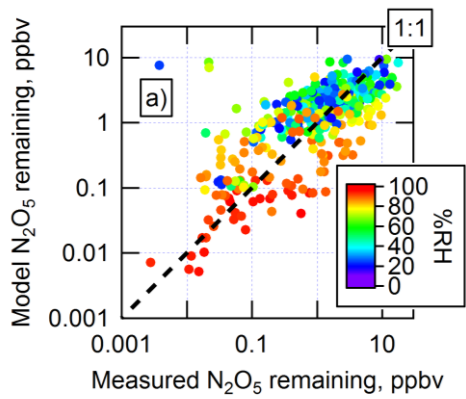


Fig. 1. Typical average mixing ratios and reactive fluxes for the major reactions in the NO₃-OFR when injecting N₂O₅ to investigate SOA formation from NO₃ oxidation. These reactive fluxes resulted from running the model with inputs of 25°C, 50% RH, 50 ppb O₃, 2 ppb NO₂, 1.5 ppb NO₃, 50 ppb N₂O₅, 0.75 ppb total MT, and a rate constant for N₂O₅ uptake to aerosol surfaces of $3 \times 10^{-5} \text{ s}^{-1}$. Reaction arrow widths are sized relative to their average reactive fluxes. Reactions that were included in the model (shown in Table S1) but with smaller average rates are not shown here.

5



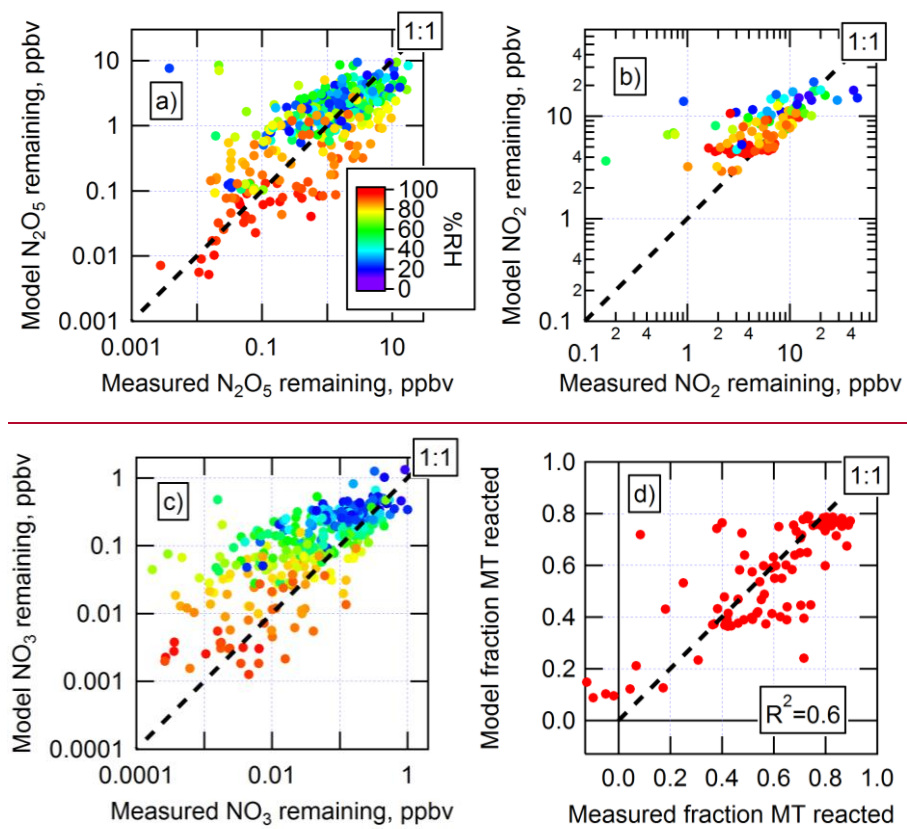


Fig. 2. Modeled vs. measured a) N_2O_5 , b) NO_2 , c) NO_3 , and d) fraction of ambient MT reacted with NO_3 in the output of the NO_3 -OFR.

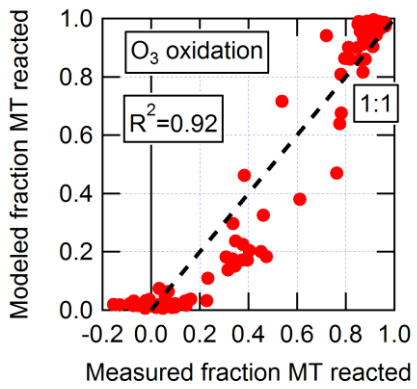
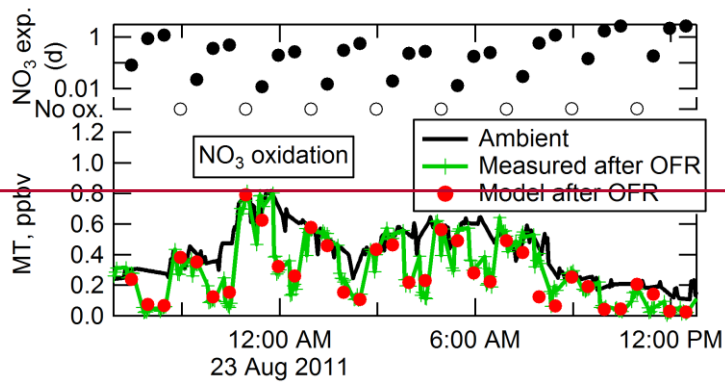
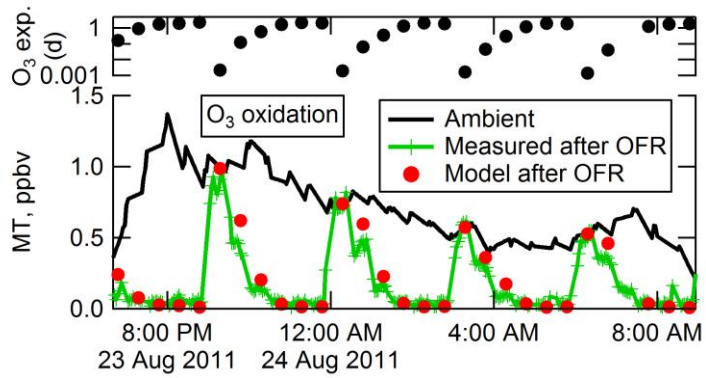


Fig. 3. Modeled vs. measured fraction MT reacted by O₃ oxidation in the O₃-OFR.



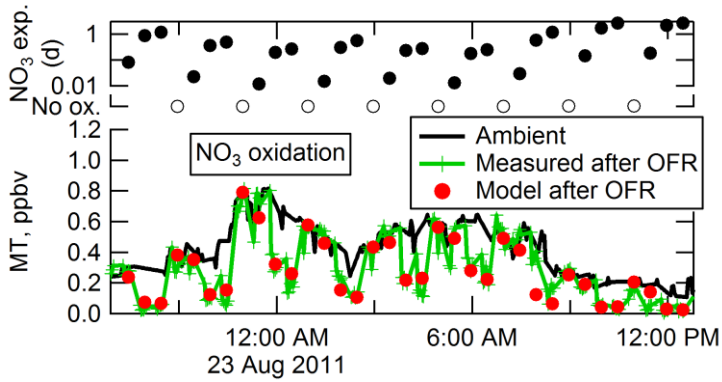
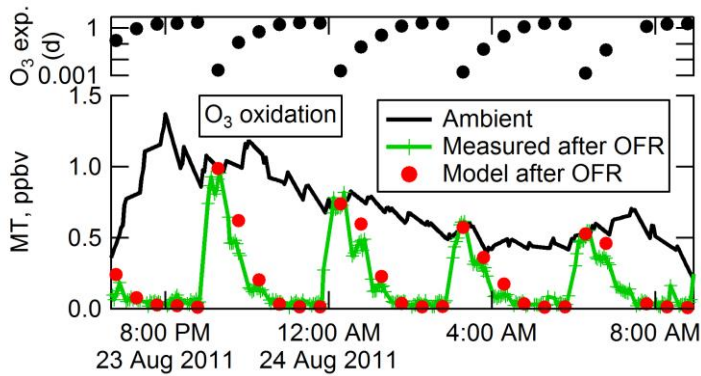


Fig. 4. Ambient, measured remaining, and modeled remaining MT from O₃ oxidation on Aug. 23–24 (top) and NO₃ oxidation on Aug. 22–23 (bottom) in the OFR. Modeled O₃ and NO₃ exposures are also shown. The amount of oxidation was cycled from no added oxidant (no MT reacted) to maximum oxidation (most or all MT reacted) in repeated 2–3 h cycles.

5

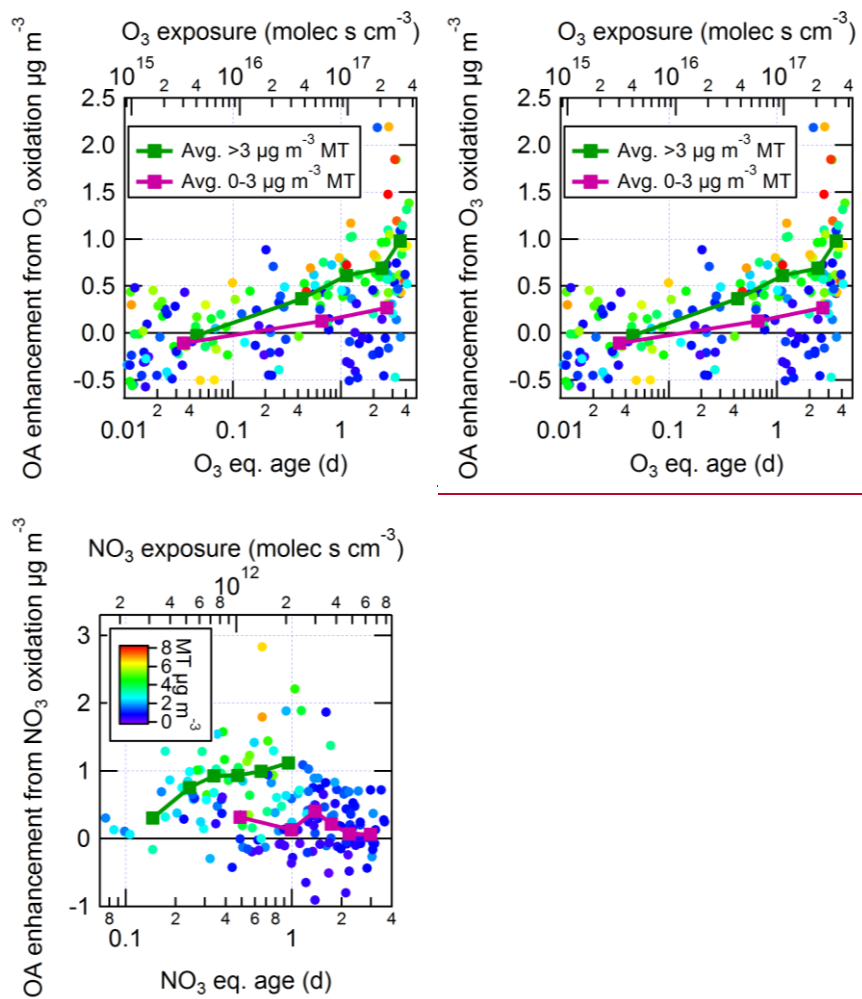
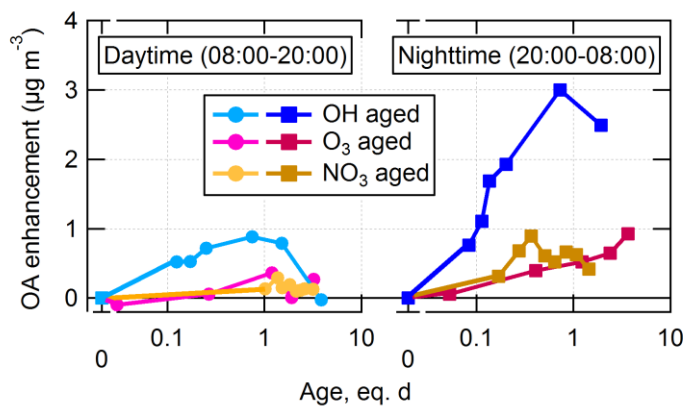


Fig. 5. OA enhancement from oxidation of ambient air by O₃ (left) and NO₃ (right) as a function of oxidant exposure. Data are colored by ambient in-canopy MT concentrations and include the LVOC fate correction.

5 Binned averages for times when ambient MT concentrations were either below or above 3 µg m⁻³ (0.66 ppb) are

also shown, illustrating the positive relationship between OA enhancement and MT concentrations at the higher oxidant concentrations.



(1 eq. d = 1.5×10^6 molec d cm⁻³ OH, 50 ppbv d O₃, or 1 pptv d NO₃ exposure)

Fig. 6. OA enhancement vs. age in eq. d for OH, O₃, and NO₃ oxidation, separated into daytime (08:00–20:00 LT) and nighttime (20:00–08:00 LT) data. All data is LVOC fate corrected. OH oxidation produced several-fold more OA enhancement than O₃ and NO₃ oxidation. OH-aged OA enhancement data is taken from Palm et al. (2016), and shows data only for <5 eq. d aging where the LVOC fate correction could be applied.

5

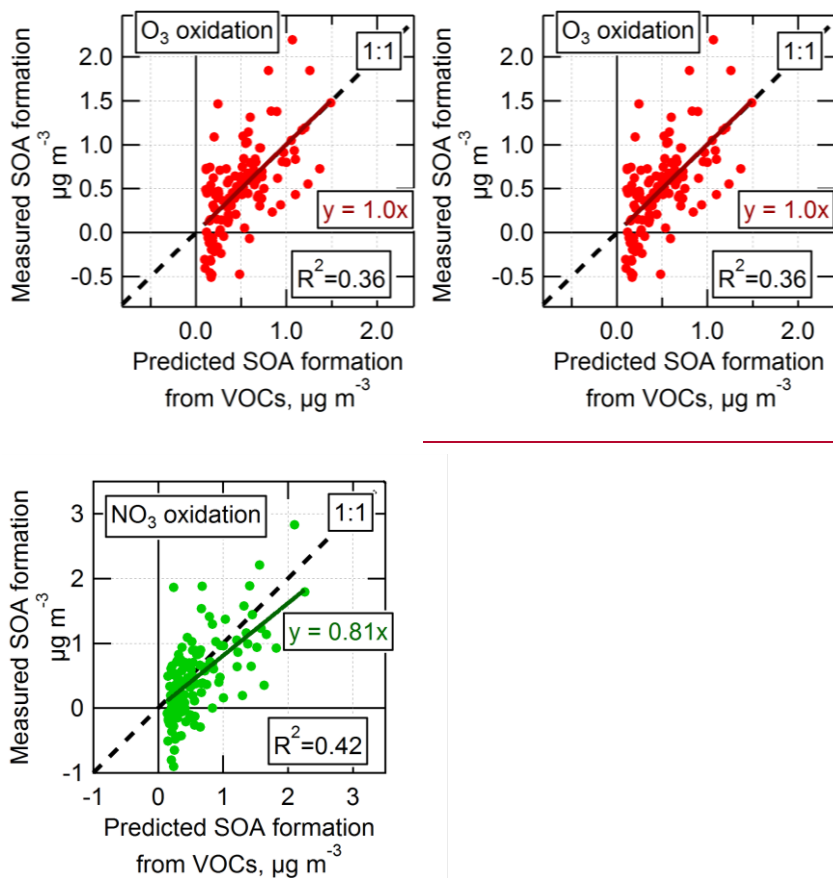


Fig. 7. Measured vs. predicted SOA formation for O₃ and NO₃ oxidation in an OFR. The measured SOA formation includes the LVOC fate correction, and includes all ages greater than 0.7 eq. d for O₃-PAM and greater than 0.3 eq. d for NO₃-PAM. Predicted SOA formation was estimated by applying published chamber SOA yields to the mass of VOCs predicted by the model to be oxidized in the OFR (see Sect. 2.3 for details).

5

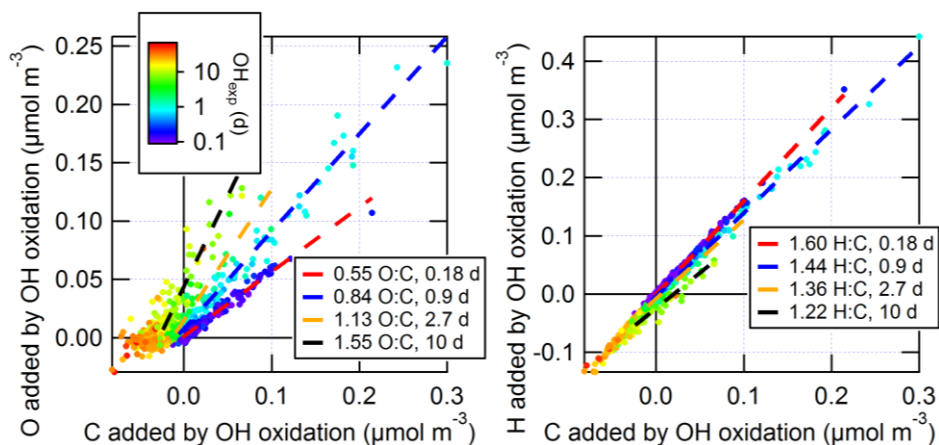


Fig. 8. Scatter plots of $\mu\text{mol m}^{-3}$ O and $\mu\text{mol m}^{-3}$ H added per $\mu\text{mol m}^{-3}$ C added from OH oxidation of ambient air in the OFR. Slopes are fit to the photochemical age ranges of 0.1–0.4 (avg.=0.18) d, 0.4–1.5 (avg.=0.9) d, 1.5–5 (avg.=2.7) d, and 5–15 (avg.=10) d, showing that the atomic O:C(H:C) ratios of the SOA mass formed in those ranges were 0.55 (1.60), 0.84 (1.44), 1.13 (1.36), and 1.55 (1.22), respectively. At higher ages, heterogeneous oxidation led to loss of C and H and little to no loss of O.

5

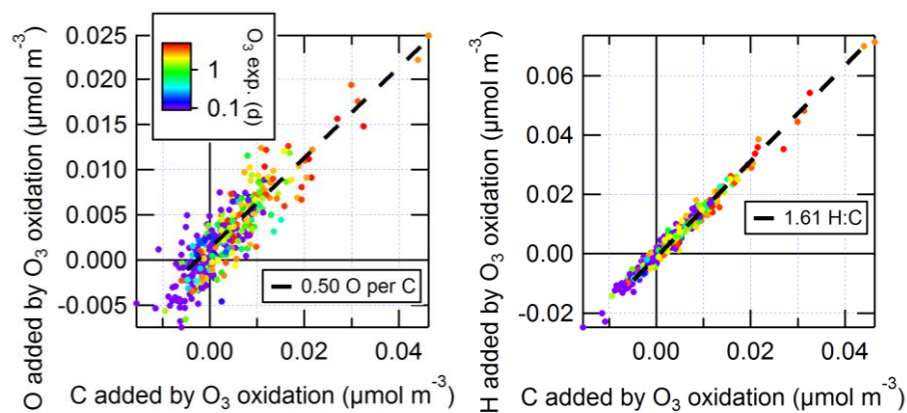


Fig. 9. Scatter plots of $\mu\text{mol m}^{-3}$ O and $\mu\text{mol m}^{-3}$ H added per $\mu\text{mol m}^{-3}$ C added from O₃ oxidation of ambient air in the OFR. Data are colored by eq. d of O₃ exposure. The slopes show that the atomic O:C (H:C) ratio of the SOA mass formed was 0.50 (1.61). The slopes did not change with increasing photochemical age.

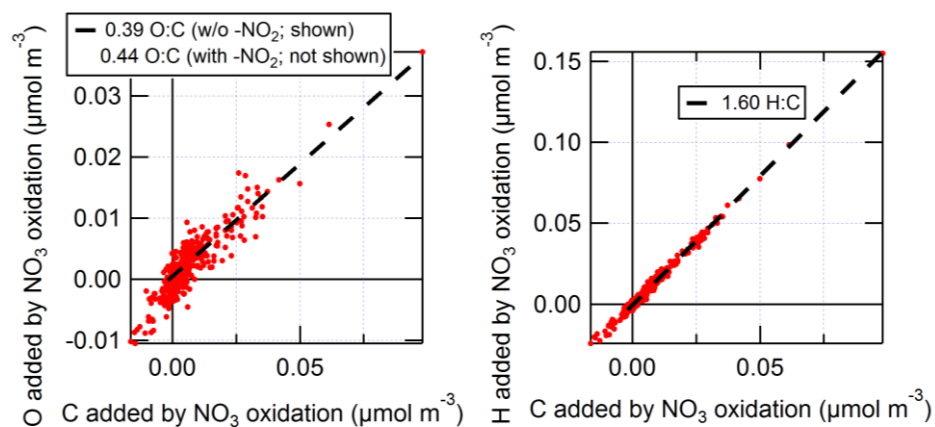


Fig. 10. Scatter plots of $\mu\text{mol m}^{-3}$ O and $\mu\text{mol m}^{-3}$ H added per $\mu\text{mol m}^{-3}$ C added from NO_3 oxidation of ambient air in the OFR. The amount of O added is shown without including the O from the $-\text{NO}_2$ group, since those O atoms do not affect the oxidation state of C. The slopes show that the atomic O:C(H:C) ratio of the SOA mass formed was 0.39 (1.60). The slopes did not change with increasing NO_3 exposure. Contrary to Figs. 8–9, data are not colored by NO_3 exposure. The ranges of NO_3 exposure achieved during daytime vs. nighttime were unequal (Figs. 5-6, S12), obscuring any trend of OA enhancement vs. eq. age.

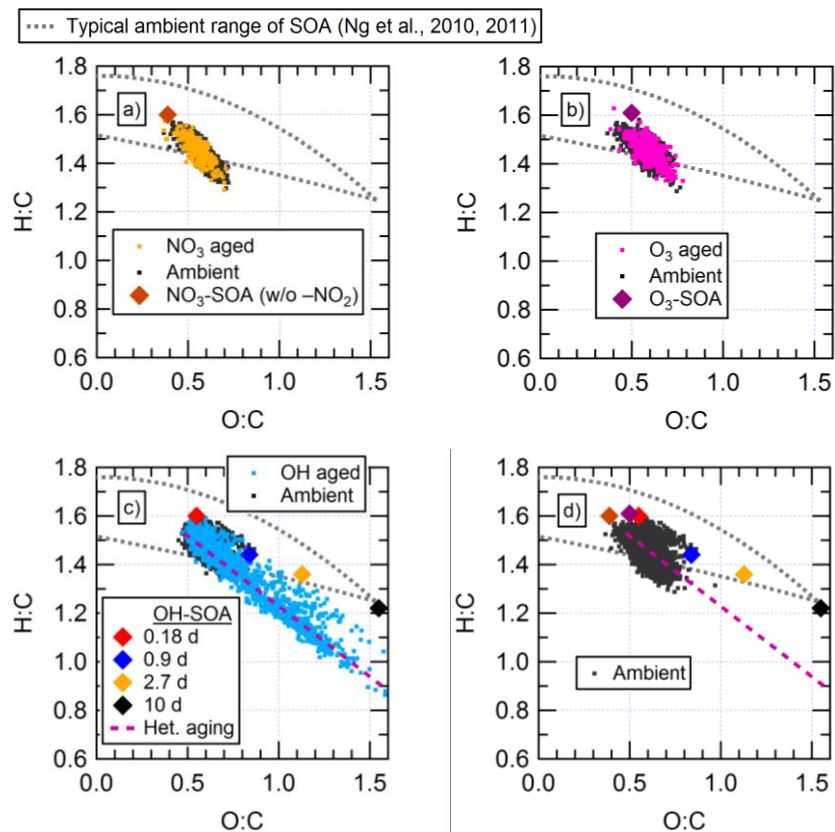


Fig. 11. Van Krevelen diagrams of H:C vs. O:C ratios of OA after oxidation by a) NO_3 , b) O_3 , and c) OH along with concurrent ambient ratios. The H:C and O:C ratios of the new SOA mass formed in the OFR (i.e., the slopes from Figs. 8–10) are shown for each oxidant (diamonds), and are summarized in d) compared with all ambient measurements. For data where no net C addition was observed after OH oxidation, the slope along which heterogeneous OH oxidation transforms the ambient OA is shown (purple dashed line).

5

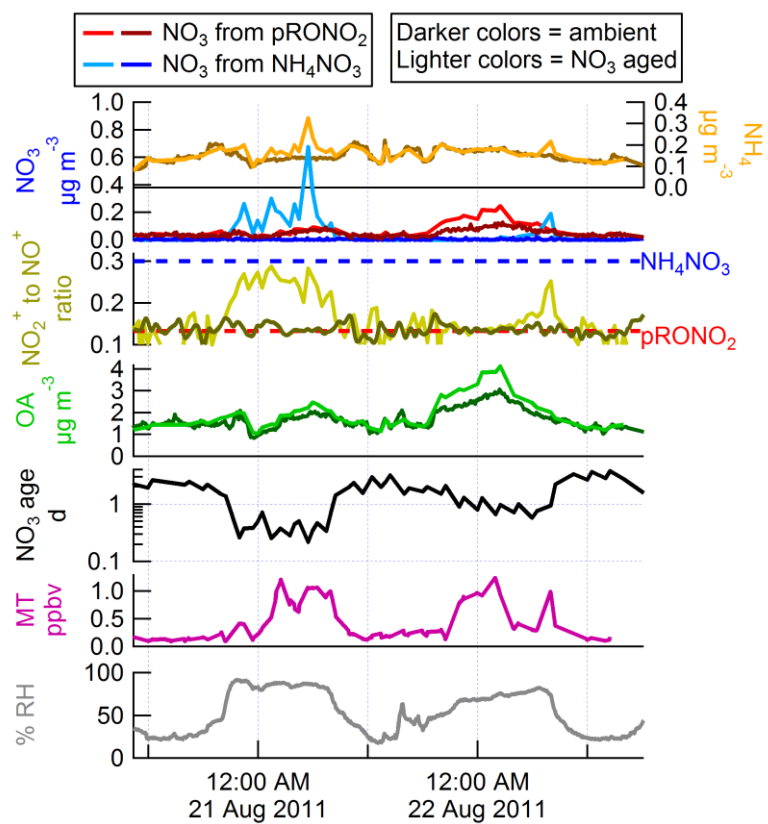


Fig. 12. Example time series of OA, NH₄, and NO₃ (split into pRONO₂ and NH₄NO₃) aerosol measurements after NO₃ oxidation in the OFR, compared to ambient aerosol, NO₂⁺ to NO⁺ ratio, model-derived eq. age of NO₃ oxidation, MT concentration, and RH measurements. Production of both NH₄NO₃ and pRONO₂ was observed at different times, which appears to depend on changes in experimental conditions.

5

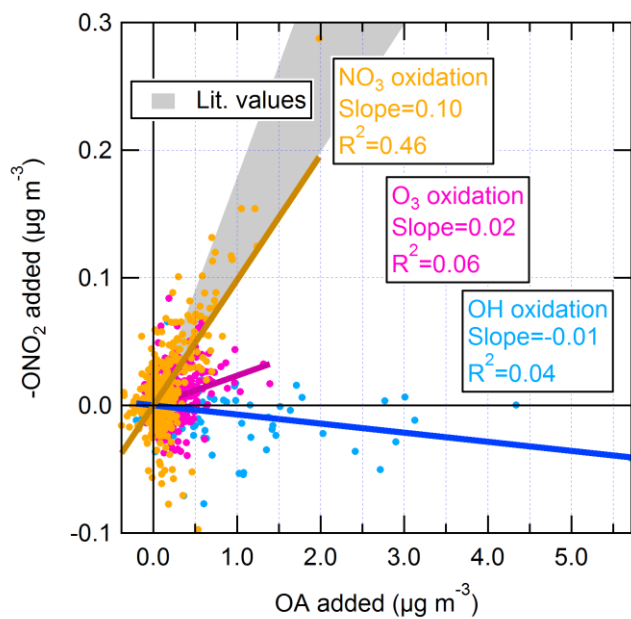


Fig. 13. Organic $-\text{ONO}_2$ mass added vs. OA added from OH, O_3 , and NO_3 oxidation in an OFR. No pRONO_2 formation was observed (or expected) from OH or O_3 oxidation under the experimental conditions. The slope of 0.10 from NO_3 oxidation is consistent with previous chamber measurements (shown in grey), which range from approximately 0.1–0.18 (Fry et al., 2009, 2011; Boyd et al., 2015).

5

Supplemental Information for:

Secondary organic aerosol formation from in situ OH, O₃, and NO₃ oxidation of ambient forest air in an oxidation flow reactor

Brett B. Palm^{1,2}, Pedro Campuzano Jost^{1,2}, Amber M. Ortega^{1,3,4}, Douglas A. Day^{1,2}, Juliane L. Fry¹, Steven S. Brown^{2,5}, Kyle J. Zarzana^{1,2,6}, William Dube^{1,5}, Nicholas L. Wagner^{1,5}, Danielle C. Draper^{4,6}, Lisa Kaser⁶, Werner Jud^{7,8}, Thomas Karl⁸, Armin Hansel⁷, Cándido Gutiérrez-Montes⁹, and Jose L. Jimenez^{1,2}

¹Cooperative Institute for Research in Environmental Sciences, University of Colorado, USA;

²Department of Chemistry and Biochemistry, University of Colorado, USA;

³Department of Atmospheric and Oceanic Science, University of Colorado, USA;

⁴Department of Chemistry, Reed College, USA;

⁵NOAA Earth System Research Laboratory, Chemical Sciences Division, Boulder, CO, USA

⁶National Center for Atmospheric Research, USA;

⁷Institute of Ion Physics and Applied Physics, University of Innsbruck, Austria;

⁸Institute of Atmospheric and Cryospheric Sciences, University of Innsbruck, Austria;

⁹Departamento de Ingeniería, Mecánica y Minería, Universidad de Jaén, Jaén, Spain

^{*}Now at Air Pollution Control Division, Colorado Department of Public Health and Environment, Denver, CO, USA

[#]Now at NOAA Earth System Research Laboratory, Chemical Sciences Division, Boulder, CO, USA

[†]Now at Department of Chemistry, University of California, Irvine, USA

^ΔNow at Research Unit Environmental Simulation (EUS), Institute of Biochemical Plant Pathology (BIOP), Helmholtz Zentrum München GmbH, Germany

S1 NO₃ oxidant modeling

To estimate NO₃ exposure in the OFR when injecting N₂O₅, the KinSim chemical-kinetic integrator (version 3.10) was used. Table S1 contains the reactions and rate constant parameters implemented in the model. The model was run with a residence time calculated from the total measured flow in the OFR (between 150 and 240 s). The model was run using this research site's ambient pressure of 770 mbar, and was initialized with measurements of ambient temperature, RH, O₃ concentrations, monoterpene (MT) concentrations, a constant 0.15 ppb NO, and injected NO₂, NO₃, and N₂O₅ concentrations for each data point. The N₂O₅ wall loss rate constant k_{wall} , shown in Fig. S4a, was empirically determined to have a base value of 0.014 s⁻¹ (lifetime of 71 s) using the measured N₂O₅ difference between the injection flow and OFR output concentrations while injecting N₂O₅ into dry zero air in the reactor. Using measurements when injecting into ambient air, an empirical increase in this wall loss rate was required when RH was greater than 80% in order to reproduce the concentrations of N₂O₅ injected and remaining in the OFR output (see Fig. 2a). Figure S4b shows the modeled vs. measured N₂O₅ remaining, illustrating the need for the increasing wall loss rate at high RH. The base wall loss rate of 0.014 s⁻¹ is several times faster than

35 the wall loss rate of 0.0025 s^{-1} estimated in Palm et al. (2016) for condensable organic gases (LVOCs)
36 produced by oxidation in the OFR. This empirical result may be a consequence of the N_2O_5 flow being
37 injected through a Teflon ring that was mounted close to the OFR wall, increasing the effective surface-
38 area-to-volume ratio experienced by the injected N_2O_5 . Injection near the wall may also have been the
39 cause for the relatively large increase in wall loss rate at high RH. The N_2O_5 wall loss rate also implicitly
40 includes any losses on the sampling line walls after the OFR, which also had higher surface-area-to-
41 volume ratios that would likely lead to larger apparent loss rates. The NO_3 wall loss rate was assumed to
42 be equal to the N_2O_5 wall loss rate (and has little effect on the key model outputs). The rate constant for
43 reactive uptake of N_2O_5 onto particulate water surfaces, k_{aer} , is shown as a function of RH in Fig. S5. It
44 was calculated using the measured ambient aerosol condensational sink using the same method
45 described for condensation of LVOCs onto aerosols in Palm et al (2016), except using an organic-mass-
46 fraction-corrected uptake efficiency $\gamma(\text{N}_2\text{O}_5)$ from Gaston et al. (2014). This heterogeneous uptake was
47 typically several orders of magnitude slower than the wall loss rate, and was therefore a minor loss
48 pathway for N_2O_5 .

49 Time constraints prevented the full characterization of the flow characteristics of the experimental
50 setup during the field measurements. Instead, PTR-TOF-MS measurements of the decay of ambient MT
51 in the OFR were used to parameterize the mixing process. With relatively robust constraints provided by
52 measurements of N_2O_5 , NO_2 , and NO_3 , the model results make it clear that a well-mixed OFR would
53 contain more than enough NO_3 to react virtually all ambient biogenic gases, if gases were immediately
54 well-mixed. However, the PTR-TOF-MS measurements verified that substantial amounts of MT often
55 remained in the OFR output. Incomplete mixing of the injected N_2O_5 was the most likely explanation for
56 this observation. A parameterization for the time constant needed for mixing of the injected N_2O_5 flow
57 with ambient air at the entrance of the OFR was added to the model to provide an effective empirical
58 mixing time scale of 100 s. This parameterization for mixing has the same effect as the high wall loss
59 rates of N_2O_5 , which is to decrease the concentrations of oxidant experienced by MT inside the reactor.
60 The true time scale of mixing and wall loss rate may be somewhat different, but the model results
61 presented herein suggest the values used in this work capture the net behavior satisfactorily. The time
62 series of measured and modeled MT decay are shown in Fig. S6–7, which are in addition to the example
63 given in Fig. 4.

64 **References**

- 65 Atkinson, R. and Arey, J.: Gas-phase tropospheric chemistry of biogenic volatile organic compounds: a
66 review, *Atmos. Environ.*, 37, 197–219, doi:10.1016/S1352-2310(03)00391-1, 2003.
- 67 Atkinson, R., Baulch, D. L., Cox, R. A., Crowley, J. N., Hampson, R. F., Hynes, R. G., Jenkin, M. E., Rossi, M.
68 J. and Troe, J.: Evaluated kinetic and photochemical data for atmospheric chemistry: Volume I - gas
69 phase reactions of O_x, HO_x, NO_x and SO_x species, *Atmos. Chem. Phys.*, 4, 1461–1738, doi:10.5194/acp-4-
70 1461-2004, 2004.
- 71 Atkinson, R., Baulch, D. L., Cox, R. A., Crowley, J. N., Hampson, R. F., Hynes, R. G., Jenkin, M. E., Rossi, M.
72 J., Troe, J. and IUPAC Subcommittee: Evaluated kinetic and photochemical data for atmospheric
73 chemistry: Volume II - gas phase reactions of organic species, *Atmos. Chem. Phys.*, 6, 3625–4055,
74 doi:10.5194/acp-6-3625-2006, 2006.
- 75 Gaston, C. J., Thornton, J. A. and Ng, N. L.: Reactive uptake of N₂O₅ to internally mixed inorganic and
76 organic particles: the role of organic carbon oxidation state and inferred organic phase separations,
77 *Atmos. Chem. Phys.*, 14, 5693–5707, doi:10.5194/acp-14-5693-2014, 2014.
- 78 Lambe, A. T., Ahern, A. T., Williams, L. R., Slowik, J. G., Wong, J. P. S., Abbatt, J. P. D., Brune, W. H., Ng, N.
79 L., Wright, J. P., Croasdale, D. R., Worsnop, D. R., Davidovits, P. and Onasch, T. B.: Characterization of
80 aerosol photooxidation flow reactors: heterogeneous oxidation, secondary organic aerosol formation
81 and cloud condensation nuclei activity measurements, *Atmos. Meas. Tech.*, 4, 445–461,
82 doi:10.5194/amt-4-445-2011, 2011.
- 83 Palm, B. B., Campuzano-Jost, P., Ortega, A. M., Day, D. A., Kaser, L., Jud, W., Karl, T., Hansel, A., Hunter, J.
84 F., Cross, E. S., Kroll, J. H., Peng, Z., Brune, W. H. and Jimenez, J. L.: In situ secondary organic aerosol
85 formation from ambient pine forest air using an oxidation flow reactor, *Atmos. Chem. Phys.*, 16, 2943–
86 2970, doi:10.5194/acp-16-2943-2016, 2016.
- 87 Sander, S. P., Abbatt, J. P. D., Barker, J. R., Burkholder, J. B., Friedl, R. R., Golden, D. M., Huie, R. E., Kolb,
88 C. E., Kurylo, M. J., Moortgat, G. K., Orkin, V. L. and Wine, P. H.: Chemical Kinetics and Photochemical
89 Data for Use in Atmospheric Studies Evaluation Number 17, JPL Publ. 10-6, Jet Propulsion Laboratory,
90 California Institute of Technology, Pasadena, CA, USA, 2011.

91

92 **Tables**

93 **Table S1.** List of reactions and parameters used in modeling of the oxidant chemistry in the OFR when performing NO₃ oxidation. The rate
 94 constants are calculated using the modified Arrhenius equation $k = A \cdot \left(\frac{T(K)}{300}\right)^{-n} \cdot e^{-\frac{E}{RT(K)}}$ with pressure dependence as described in Sect. 2 of
 95 JPL (Sander et al., 2011). Parameter values are from JPL, with exceptions noted.

Reactant 1	Reactant 2	Product 1	Product 2	Product 3	A _∞	E _∞ /R	n _∞	A ₀	E ₀ /R	n ₀
NO	O ₃	NO ₂	O ₂		3e-12	1500	0	0	0	0
NO ₂	O ₃	NO ₃	O ₂		1.2e-13	2450	0	0	0	0
N ₂ O ₅		NO ₂	NO ₃		9.7e+14 ¹	11080	-0.1	0.0013	11000	3.5
N ₂ O ₅		Wall loss			k_{wall}^2	0	0	0	0	0
NO ₃		Wall loss			k_{wall}^2	0	0	0	0	0
NO ₃	α-pinene	RO ₂			1.2e-12 ¹	-490	0	0	0	0
NO ₃	3-carene	RO ₂			9.1e-12 ¹	0	0	0	0	0
NO ₃	β-pinene	RO ₂			2.5e-12 ¹	0	0	0	0	0
N ₂ O ₅	H ₂ O(g)	HNO ₃	HNO ₃		1e-22	0	0	0	0	0
N ₂ O ₅	H ₂ O(aerosol)	HNO ₃	HNO ₃		k_{aer}^2	0	0	0	0	0
NO	NO ₃	NO ₂	NO ₂		1.8e-11	-110	0	0	0	0
NO ₂	NO ₃	NO	NO ₂	O ₂	4.5e-14	1260	0	0	0	0
NO ₃	NO ₃	NO ₂	NO ₂	O ₂	8.5e-13	2450	0	0	0	0
NO ₂	NO ₃	N ₂ O ₅			1.9e-12 ¹	0	-0.2	3.6e-30	0	4.1
NO ₃	RO ₂	RO			1.5e-12	0	0	0	0	0
MT mixing source		α-pinene	3-carene	β-pinene	0.01 ²	0	0	0	0	0

96 ¹Parameter values taken from IUPAC (Atkinson et al., 2004, 2006)

97 ²See Sect. S1 for parameter details

Reactant_1	Reactant_2	Product_1	A	E	n
O ₃	α -pinene	Products	9.05×10^{-46}	640	0
O ₃	β -pinene	Products	1.25×10^{-45}	1270	0
O ₃	3-carene	Products	4.8×10^{-47}	0	0

Table S2. List of reactions and parameters used in modeling of the oxidant chemistry in the OFR when performing O₃ oxidation. The rate constants are calculated using the modified Arrhenius equation $k =$

$$A \cdot \left(\frac{T(K)}{300}\right)^{-n} \cdot e^{-\frac{E}{T(K)}}$$

Parameter values are from IUPAC (Atkinson et al., 2006).

98
99
100
101
102
103
104

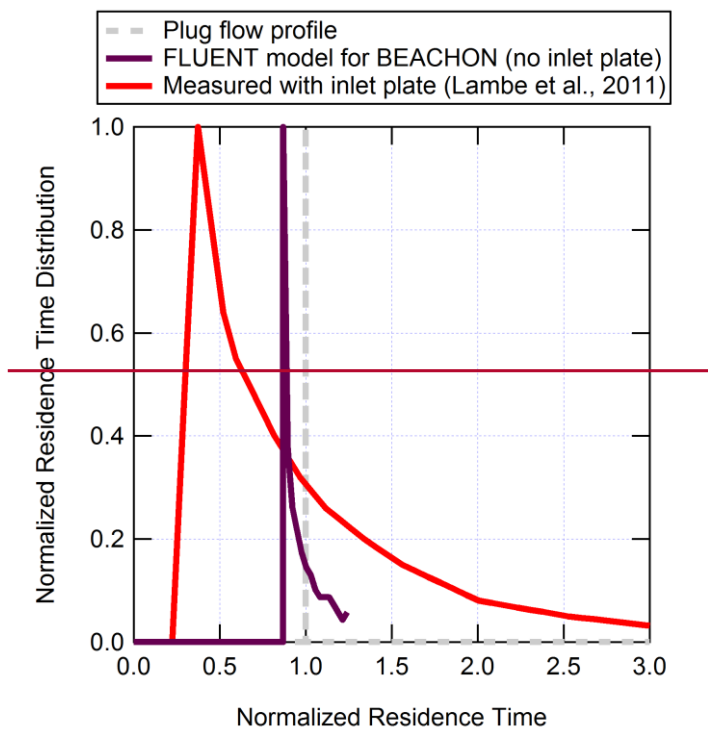
Formatted: Position: Horizontal: Left, Relative to: Column, Vertical: In line, Relative to: Margin, Horizontal: 0", Wrap Around

Formatted Table

Formatted: Position: Horizontal: Left, Relative to: Column, Vertical: In line, Relative to: Margin, Horizontal: 0", Wrap Around

Formatted: Position: Horizontal: Left, Relative to: Column, Vertical: In line, Relative to: Margin, Horizontal: 0", Wrap Around

Formatted: Position: Horizontal: Left, Relative to: Column, Vertical: In line, Relative to: Margin, Horizontal: 0", Wrap Around

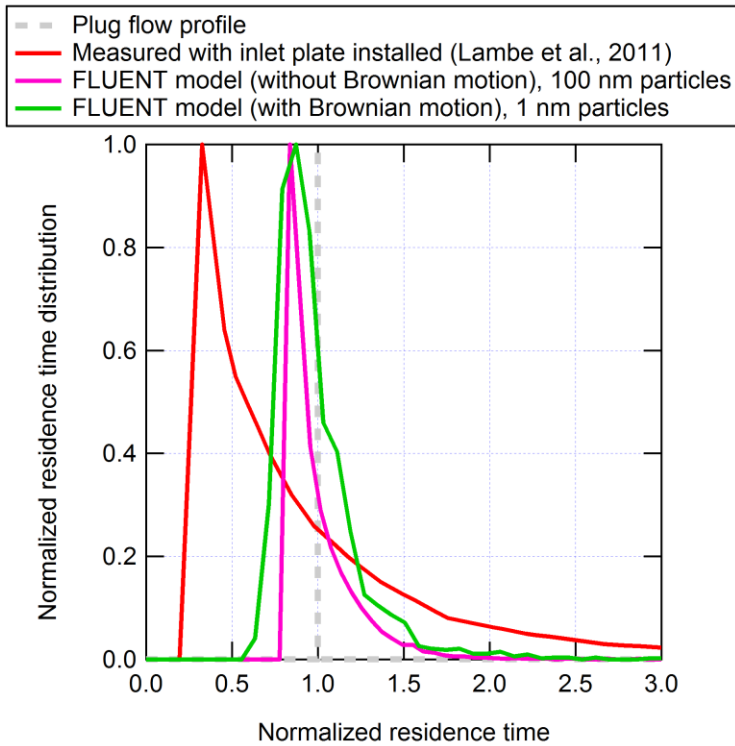


105

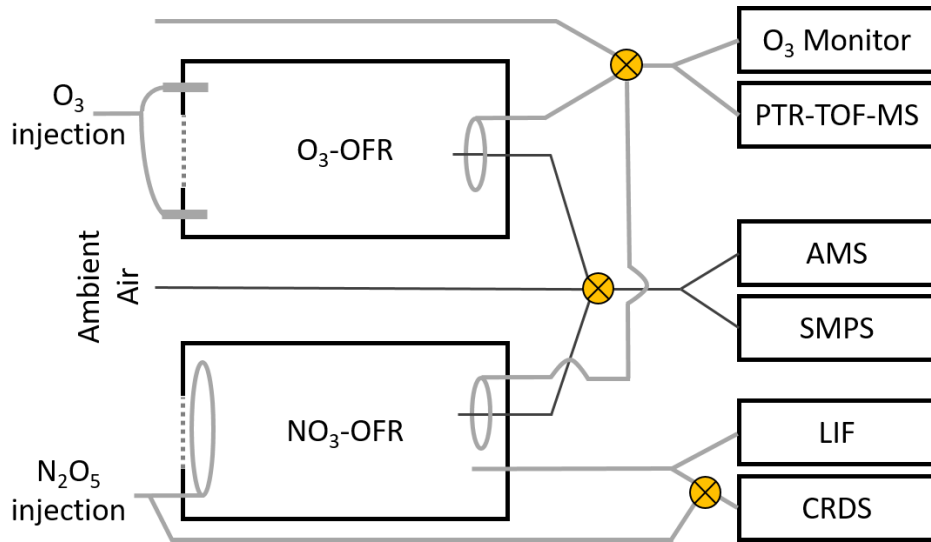
Reactant 1	Reactant 2	Product 1	A	E	n
O_2	α -pinene	Products	8.05×10^{-16}	640	0
O_2	β -pinene	Products	1.35×10^{-15}	1270	0
O_2	3-carene	Products	4.8×10^{-17}	0	0

106

- Formatted: Position: Horizontal: Left, Relative to: Column, Vertical: In line, Relative to: Margin, Horizontal: 0", Wrap Around
- Formatted Table
- Formatted: Position: Horizontal: Left, Relative to: Column, Vertical: In line, Relative to: Margin, Horizontal: 0", Wrap Around
- Formatted: Position: Horizontal: Left, Relative to: Column, Vertical: In line, Relative to: Margin, Horizontal: 0", Wrap Around
- Formatted: Position: Horizontal: Left, Relative to: Column, Vertical: In line, Relative to: Margin, Horizontal: 0", Wrap Around

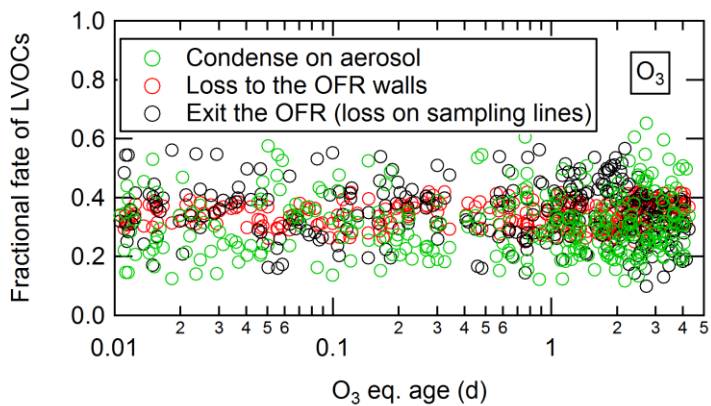


107
 108 **Fig. S1.** Normalized residence time distributions in the OFR as a function of normalized residence time (1
 109 = avg. residence time of each distribution). The FLUENT model was used to calculate ~~the~~ residence
 110 ~~times~~ times for 1 nm particles (with Brownian motion) and 100 nm particles (without Brownian motion)
 111 for the OFR configuration without the inlet plate to represent conditions used during BEACHON-
 112 RoMBAS. ~~This distribution is~~ These distributions are compared to the bis(2-ethylhexyl) sebacate (BES)
 113 particle residence time distribution measured with the inlet plate ~~on~~ installed in Lambe et al. (2011) and
 114 to the ideal plug flow distribution (where all particles have equal residence time calculated as the OFR
 115 volume divided by the total flow rate through the OFR). The residence time distribution without the
 116 inlet plate is much narrower than with the plate and is close to plug flow, ~~though~~ although local winds
 117 ~~will~~ may at times create a broader distribution than the model shows.

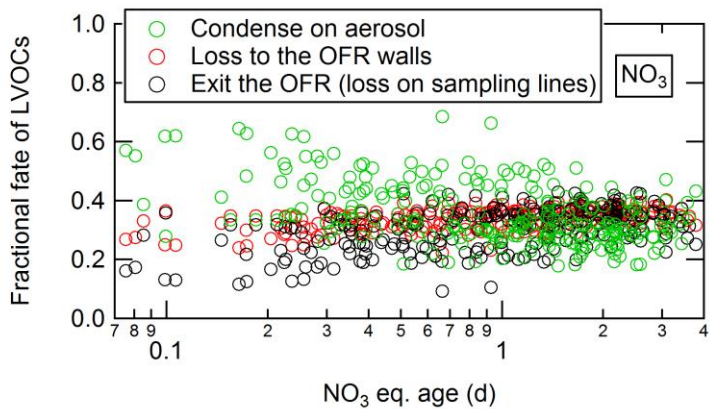


118

119 **Fig. S2.** Schematic of experimental setup of NO_3 -OFR and O_3 -OFR experiments.



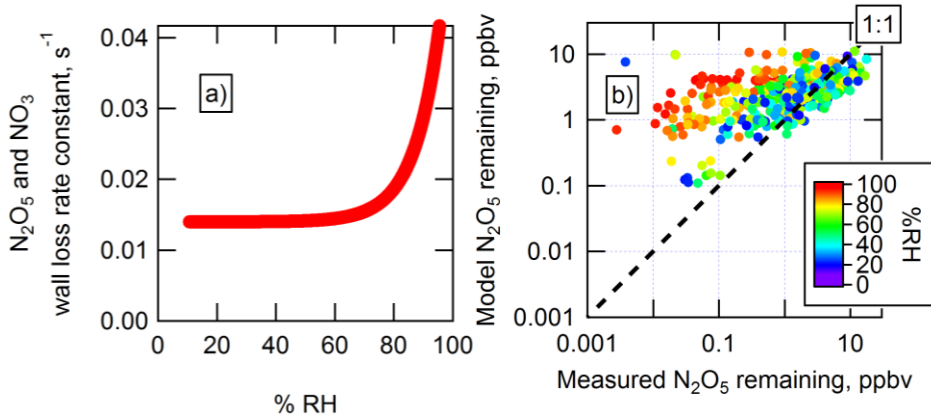
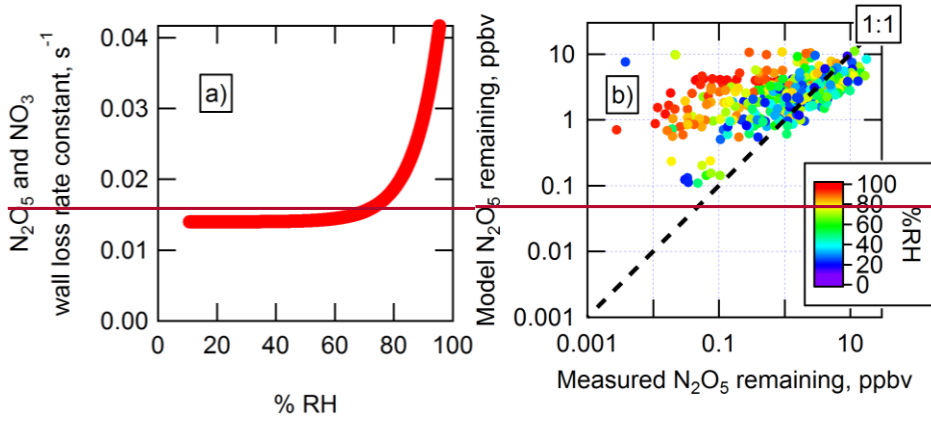
120



121

122 **Fig. S3. Fractional/Modeled fractional** fates of condensable low-volatility organic compounds (LVOCs)
 123 produced in the OFR, as a function of eq. age for O₃ oxidation (top) and NO₃ oxidation (bottom). For O₃
 124 oxidation, on average 31% of LVOCs condensed onto particles, 34% condensed on OFR walls, and 35%
 125 exited the OFR to condense on sampling line walls. For NO₃ oxidation, on average 36% of LVOCs
 126 condensed onto particles, 34% condensed on OFR walls, and 30% exited the OFR to condense on
 127 sampling line walls.

128

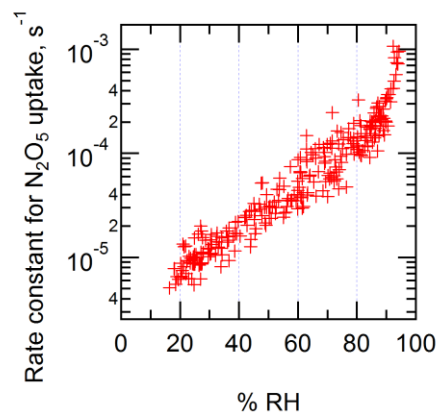


131 **Fig. S4.** a) The wall loss rate constant of N_2O_5 and NO_3 vs. %RH, determined empirically in order to
 132 achieve agreement between modeled and measured N_2O_5 concentrations (Fig. 2a). b) Modeled vs.
 133 measured N_2O_5 remaining (analogous to Fig. 2a), shown if the N_2O_5 and NO_3 wall loss rate was assumed
 134 to be a constant $0.014\ s^{-1}$ at all %RH.

129

130

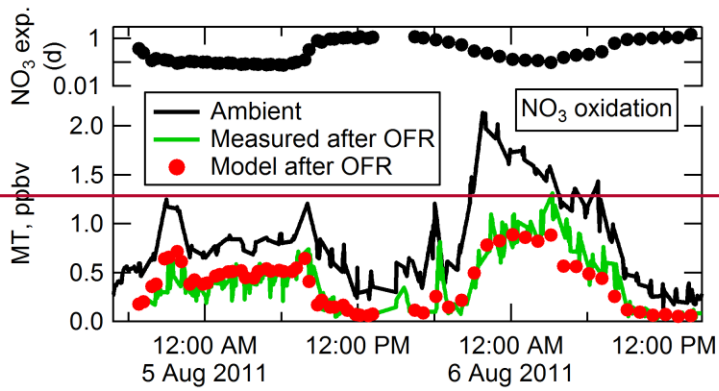
135



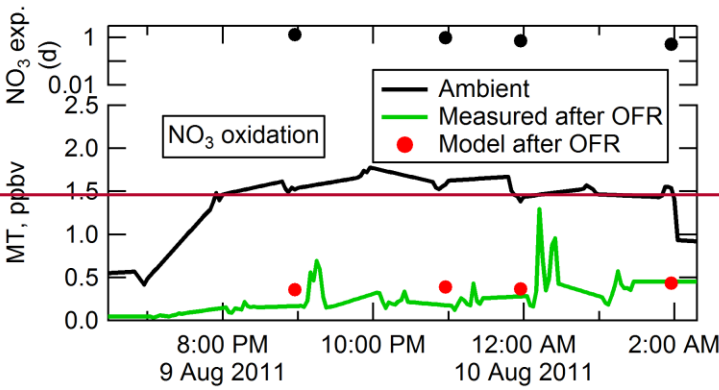
136

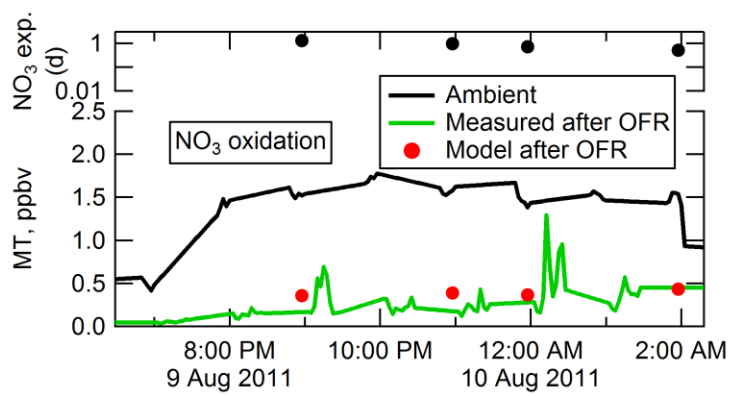
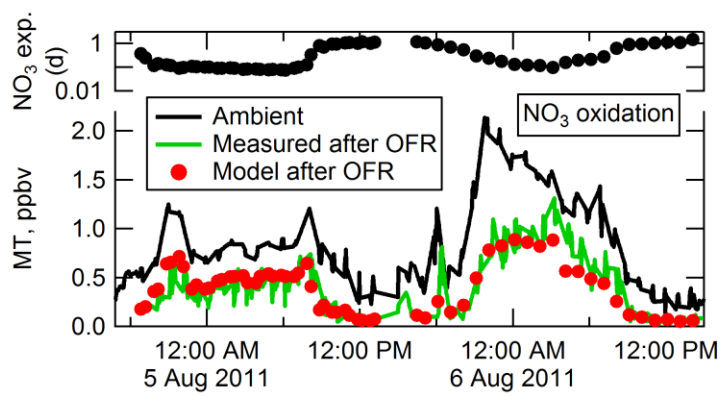
137 **Fig. S5.** Calculated rate constant for reactive uptake of N_2O_5 onto particles, as a function of RH. The rate
138 constant was calculated using the same method for condensation of gases onto aerosols described in
139 Palm et al (2016), using the measured ambient aerosol condensational sink and using an organic-mass-
140 fraction-corrected uptake efficiency $\gamma(N_2O_5)$ from Gaston et al. (2014).

141



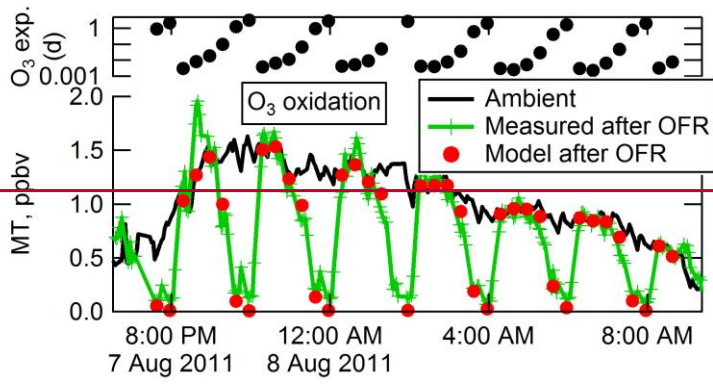
142



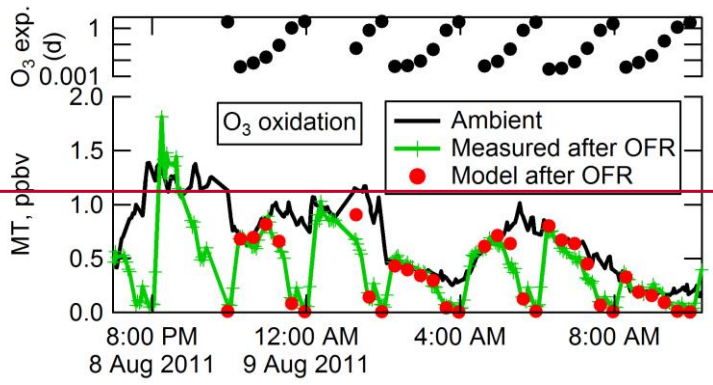


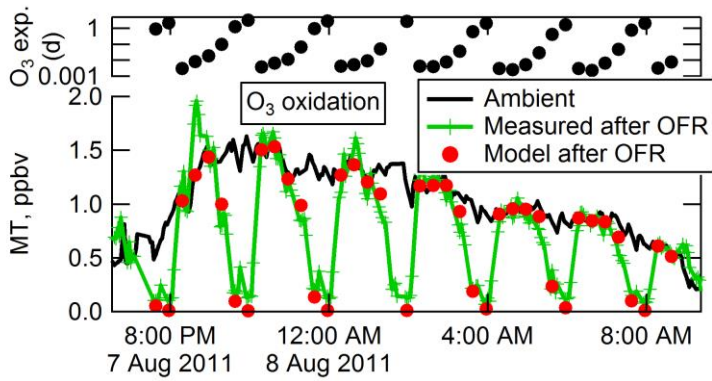
145 **Fig. S6.** Ambient, measured remaining, and modeled remaining MT from NO_3 oxidation in the OFR on
 146 Aug. 4–6 and Aug. 9–10, along with modeled NO_3 exposure (d). For these examples, the amount of
 147 injected N_2O_5 was held roughly constant- (with a higher constant value injected on Aug. 9–10).

148

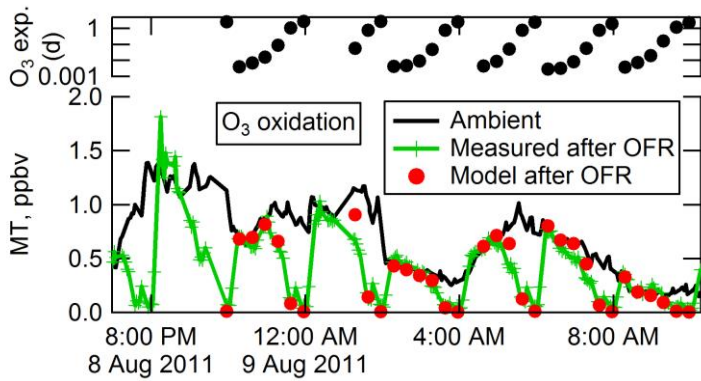


149





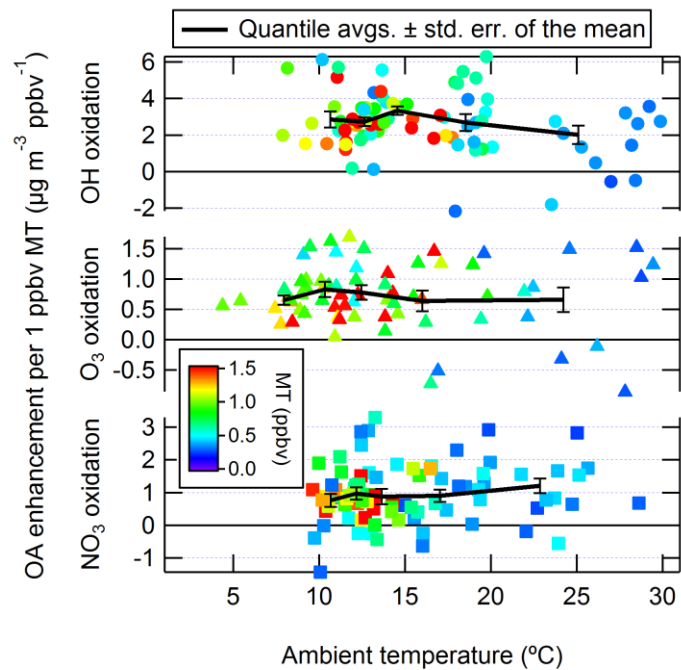
150



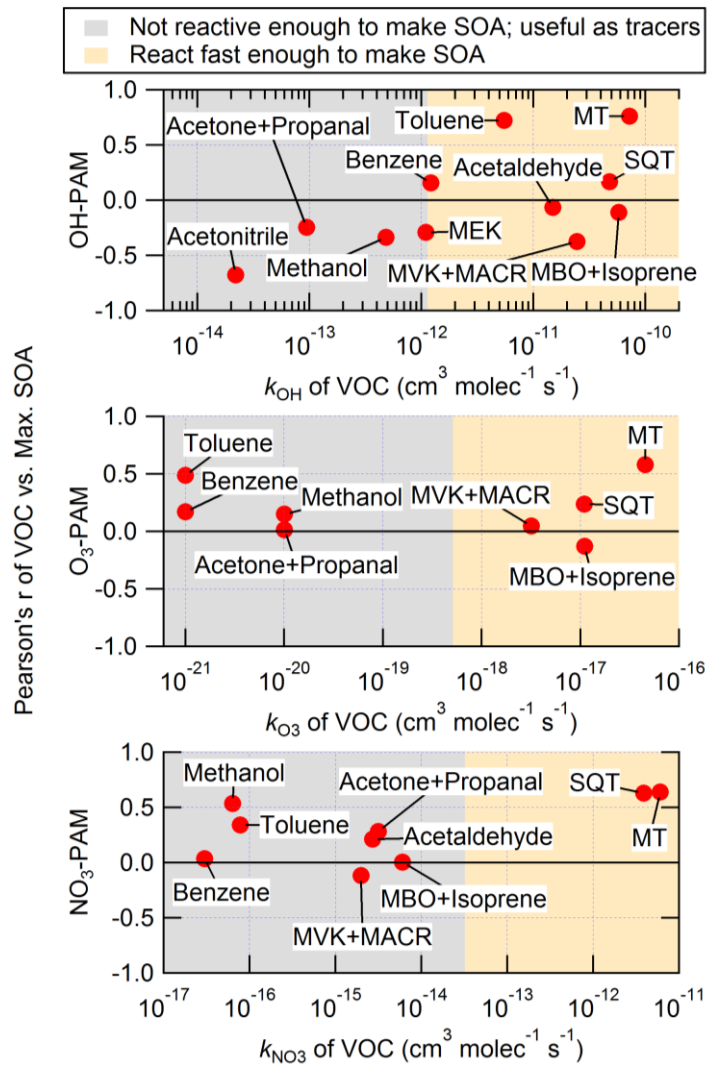
151

152 **Fig. S7.** Ambient, measured remaining, and modeled remaining MT from O₃ oxidation in the OFR on Aug.
 153 7–8 and Aug. 8–9, along with modeled O₃ exposure (d₊). The amount of oxidation was cycled from no
 154 added oxidant (no MT reacted) to maximum oxidation (most or all MT reacted) in repeated 2–3 h cycles.
 155 Note that the ambient MT were sampled through a separate inlet within the canopy, several meters
 156 from the OFR. Short periods of higher MT concentrations measured through the OFR (at low O₃
 157 exposures) may be due to spatial heterogeneity in ambient MT concentrations within the canopy.

158

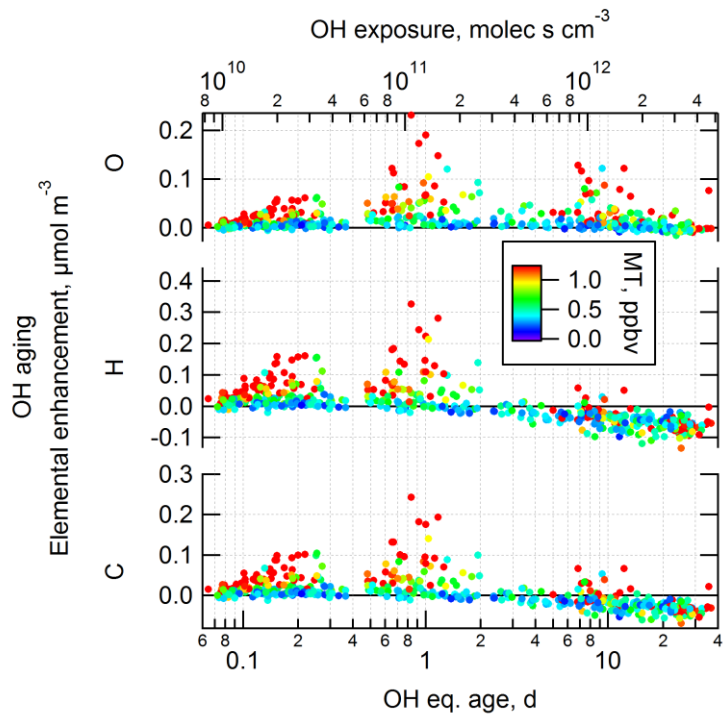


159
 160 **Fig. S8.** OA enhancement per ppbv ambient MT for OH, O₃ and NO₃ oxidation in the OFR as a function of
 161 ambient temperature. Enhancement is defined as the difference between the concentrations measured
 162 after oxidation and in ambient air, where positive enhancements signify formation in the OFR. Data are
 163 colored by ambient in-canopy MT concentrations, and include the LVOC fate correction. Quantile
 164 averages of OA enhancement per ppbv MT are shown for each oxidant, with error bars corresponding to
 165 the standard error of the mean of each quantile.
 166

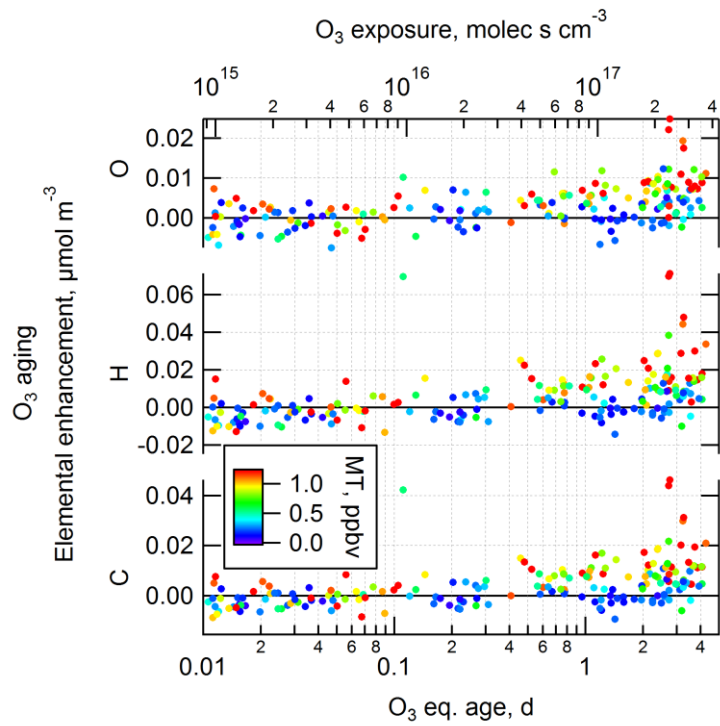


167

168 **Fig. S9.** Pearson's r for the correlation between maximum SOA formation for each oxidant and the
 169 available ambient VOC concentrations. Maximum SOA formation is defined as the ranges of 0.4–1.5 eq.
 170 d for OH-PAM, 0.7–5 eq. d for O₃-PAM, 0.3–4 eq. d for NO₃-PAM. Reaction rate constants are taken from
 171 Atkinson and Arey (2003) and the IUPAC database (Atkinson et al., 2006)(Atkinson et al., 2006). The
 172 orange colored background denotes rate constants that are fast enough so that $\geq 20\%$ of the VOC can
 173 react to form SOA under the conditions of maximum SOA formation in the OFR for each oxidant. In
 174 contrast, the grey background shows rate constants where the molecules do not react in the OFR and
 175 cannot contribute to SOA formation, but could be useful as tracers.

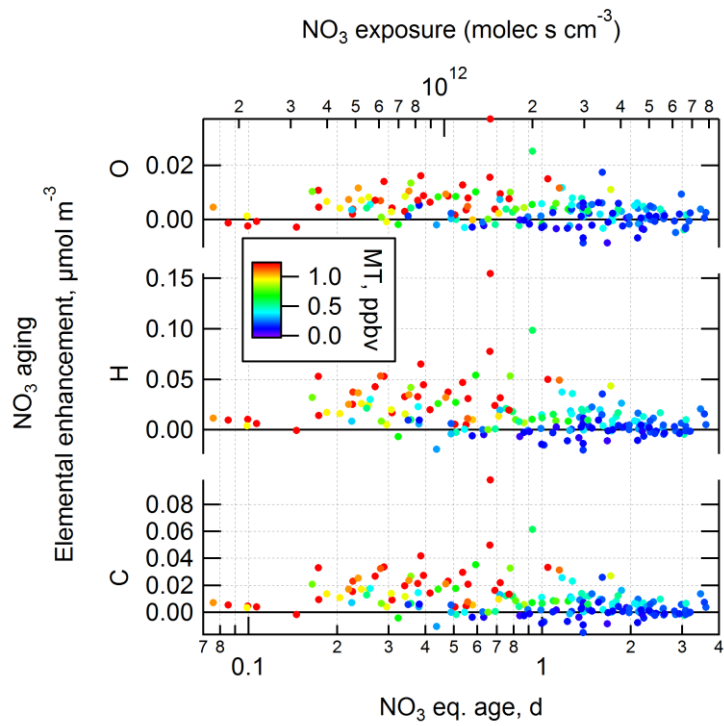


176
 177 **Fig. S10.** Elemental C, H, and O enhancements due to OH aging in the OFR, as a function of eq. OH age
 178 and exposure. Enhancement is defined as the difference between the concentrations measured after
 179 oxidation and in ambient air, where positive enhancements signify formation in the OFR. Data are
 180 colored by ambient in-canopy MT concentrations, and do not include the LVOC fate correction.
 181

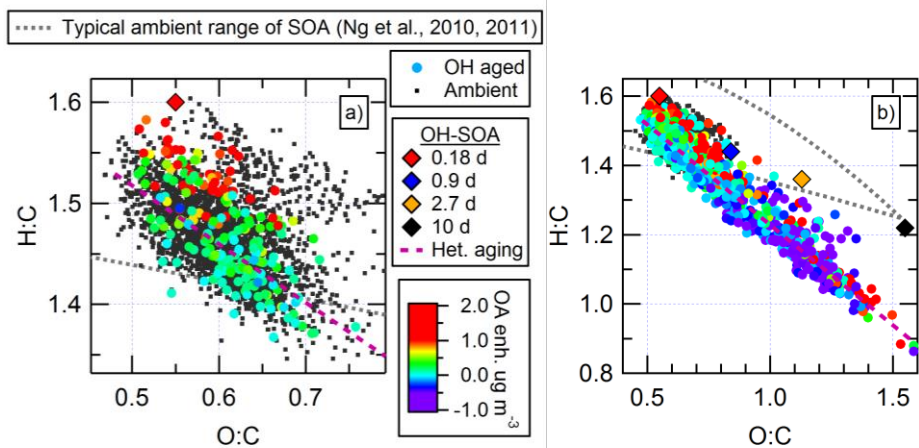


182
 183 **Fig. S11.** Elemental C, H, and O enhancements due to O₃ aging in the OFR, as a function of eq. O₃ age and
 184 exposure. Enhancement is defined as the difference between the concentrations measured after
 185 oxidation and in ambient air, where positive enhancements signify formation in the OFR. Data are
 186 colored by ambient in-canopy MT concentrations, and do not include the LVOC fate correction.

187
 188



189
 190 **Fig. S12.** Elemental C, H, and O enhancements due to NO₃ aging in the OFR, as a function of eq. NO₃ age
 191 and exposure. Enhancement is defined as the difference between the concentrations measured after
 192 oxidation and in ambient air, where positive enhancements signify formation in the OFR. Data are
 193 colored by ambient in-canopy MT concentrations, and do not include the LVOC fate correction.
 194



195
 196 **Fig. S13.** Van Krevelen diagrams of H:C vs. O:C ratios of OA after OH oxidation of ambient air in an OFR,
 197 along with values for ambient OA. OH aged data are colored by the amount of OA enhancement
 198 observed after oxidation. The H:C and O:C ratios of the new SOA mass formed in the OFR (i.e., the slopes
 199 from Fig. 8) are shown (diamonds; see Fig. 11). For data where no net C addition was observed after OH
 200 oxidation, the slope along which heterogeneous OH oxidation transforms the ambient OA is shown
 201 (purple dashed line). Panel a) shows only data in the eq. range of 0.1–0.4 (avg.=0.18) d, while panel b)
 202 shows all data.

203